



TECHNISCHE
UNIVERSITÄT
WIEN
Vienna University of Technology

Dissertation

Airborne laser scanning terrain and land cover models as basis for hydrological and hydraulic studies

ausgeführt zum Zwecke der Erlangung des akademischen Grades eines
Doktors der Naturwissenschaften
(Doktor rerum naturalium)

unter der Leitung von

Univ.Prof. Dipl.-Ing Dr.techn Wolfgang Wagner
Forschungsgruppen Photogrammetrie & Fernerkundung
E120

Univ.Prof. Dipl.-Ing Dr.techn Günter Blöschl
Centre for Water Resource Systems (CWRS)
E006

eingereicht an der Technischen Universität Wien
Fakultät für Mathematik und Geoinformation

als Beitrag zum
Vienna Doctoral Programme on Water Resource Systems

von
Mag. Michael Vetter
0317610
Kaiser-Franz-Josef-Straße 24
6890 Lustenau

Wien, Mai 2013



TECHNISCHE
UNIVERSITÄT
WIEN
Vienna University of Technology

Dissertation

Airborne laser scanning terrain and land cover models as basis for hydrological and hydraulic studies

submitted for the academic degree of
Doctor of Natural Sciences
(Doctor rerum naturalium)

supervised by

Univ.Prof. Dipl.-Ing Dr.techn Wolfgang Wagner
Research Groups Photogrammetry & Remote Sensing
E120

Univ.Prof. Dipl.-Ing Dr.techn Günter Blöschl
Centre for Water Resource Systems (CWRS)
E006

submitted at the Vienna University of Technology
Faculty of Mathematics and Geoinformation

as part of the
Vienna Doctoral Programme on Water Resource Systems

by
Mag. Michael Vetter
0317610
Kaiser-Franz-Josef-Straße 24
6890 Lustenau

Vienna, May 2013

Declaration

Hiermit erkläre ich, dass ich diese Arbeit selbständig verfasst habe, dass ich die verwendeten Quellen und Hilfsmittel vollständig angegeben habe und dass ich die Stellen der Arbeit, einschließlich Tabellen, Karten und Abbildungen, die anderen Werken oder dem Internet im Wortlaut oder dem Sinn nach entnommen sind, auf jeden Fall unter Angabe der Quelle als Entlehnung kenntlich gemacht habe.

I declare that all the material presented in this thesis is my own work and have not been written, entirely or partly, by any other person. I also declare that any external information published, including texts, tables, maps and figures, are cited if they are used literally or analogously.

Vienna, May 2013

'Es ist nicht genug zu wissen - man muss auch anwenden. Es ist nicht genug zu
wollen - man muss auch tun.'

'Knowing is not enough, we must apply. Willing is not enough, we must do'

Johann Wolfgang von Goethe

Acknowledgements

I would like to thank...

... my supervisors, DI Dr. Wolfgang Wagner and Prof. DI Dr. Günter Blöschl for discussions, inspirations and guidance.

... the 'Centre for Water Resource Systems of the Vienna University of Technology' and the 'Vienna Doctoral Programme on Water Resource Systems' for the research network.

... the financial support from the Austrian Science Funds (FWF) as part of the Vienna Doctoral Programme on Water Resource Systems (DK-plus W1219-N22).

... the Federal State of Vorarlberg and the City of Vienna for providing the laser scanning data for my research.

... my family and all my friends for constant motivation.

... my fiancée for supporting me during the years of hurrying from one deadline to the next.

... my co-authors for the great teamwork and support.

Special thanks to Bernhard Höfle, Gottfried Mandlbürger and Martin Rutzinger for endless hours of fruitful discussions, shared thoughts and the motivation to go continue my studies.

Michael Vetter
Vienna
May, 2013

Abstract

In recent years, Airborne Laser Scanning (ALS) has become the state-of-the-art technique for topographic data acquisition. Most ALS sensors record the reflected laser beam with X,Y,Z coordinates and the signal amplitude (also referred to as intensity) as a three-dimensional point cloud. One or more echoes, or even the full-waveform can be recorded per laser shot, depending on the scanner type.

Most applications in hydrology or hydraulics use Digital Surface Models (DSMs) or Digital Terrain Models (DTMs) in gridded raster formats generated from a 3D ALS point cloud. To compute those models, the point cloud is filtered and classified in ground, vegetation or building and other object classes. Those elevation models are regularly used for drainage network delineation, volume estimation of the water body, calculation of flow velocity or inundated areas, flood simulations and many more. The analysis is often based on the original DTM without any modifications. This thesis presents methods generating specific parameters from ALS data i.e. improved DTMs or generating input parameters from ALS for special tasks in the hydro-related context. In this thesis the hydro-related context is mentioned as the topics which are in the scientific field of hydrology and hydrodynamic-numerical modeling based on ALS data. The main goal is to show the capability of using high-resolution DTMs from ALS in hydraulic and hydrological studies.

The high level of topographic details is the main advantage using ALS data, which also causes many problems in different hydrological and hydraulic applications. So, the detailed topographic information can have a negative impact on the quality of hydrological and hydraulic applications. Besides the high level of geometric details, the intensity values as well as the full vertical point distribution within the 3D point cloud is available. It is shown, based on selected applications, how to minimize the negative effects of topographic details and how to extract specific parameters for hydrological and hydraulic purposes directly from ALS data by using geoinformation and remote sensing methods. Those applications are embedded in a workflow including the following parts: 1) drainage network delineation, 2) water surface classification, 3) river bed modeling and 4) hydraulic

roughness estimation. The main focus is on improving existing methods to extract hydraulic and hydrological features from the ALS data with a high level of automatization.

The first part deals with Laser Remote Sensing technology in general. Besides the measurement principles, different laser platforms and common gridded derivatives are presented. Finally, recent technology trends are discussed.

Within the first methodological chapter a workflow to optimize a 1m-DTM for drainage network delineation is presented. A 1m-DTM is normally not used as basis for flow accumulation methods because of the high amount of included terrain details and the potential of wrong deflection of the drainage delineation algorithms along road edges. Mostly coarse DTMs, smoothed by using average filters, are used. Where detailed topographic features and roads are removed by the DTM smoothing. Therefore, the 1m spatial resolution of the ALS DTM is no longer available for the drainage delineation. By removing anthropogenic structures, mainly roads, a conditioned DTM is produced without the negative influences of the roads from the original 1m-DTM on the flow accumulation. The resulting drainage network computed on the conditioned 1m-DTM show an increase in delineation accuracy of up to 9% in correctness and completeness compared to the original 1m-DTM or a coarse resolution 5m-DTM as basis for flow accumulation.

The second methodological chapter is about the delineation of water surface areas using ALS geometric and radiometric data derived from the point cloud. Because of the interaction of the laser signal at a specific wavelength and the water surface, the capability to identify areas containing water is very high. These water surface areas are used for land cover classification or generating proper geometry data for hydrodynamic-numerical models. The extent of the water surface is used to replace the water surface with river bed geometry or for hydraulic friction parameter allocation.

Based on the water surface extent a river bed modeling method is presented in the next chapter. An additional raster based water surface delineation procedure has been developed. By combining the existing water surface with terrestrially measured cross section data, a river bed model is created, which is finally integrated into the existing DTM. The main aim of this chapter is to create a DTM of the watercourse, including the river bed model, which can be used as basis for hydrodynamic-numerical modeling and for change detection between two major flood events. The advantage of the DTM with an integrated river bed is that the relevant elevation data of the flood plains are used from the dense and accurate

original DTM and the river bed is an interpolated DTM from cross sections. If the distance between the cross sections is large, the river bed model is of poor quality, because of the linear interpolation of the cross sections.

In the final methodological part a point cloud based method for estimating hydraulic roughness coefficients is presented. Based on the geometry of the 3D point cloud, vertical structures of the vegetation are analyzed and classified into different land cover classes, which are transformed to Manning's n values. The advantages of the presented method are that the data analysis is fully automatic, reproducible and fast. Finally, the geometry used as elevation input for a 2D hydrodynamic-numerical model and the roughness parameters are measured at one single point in time and calculated from the same data source. Therefore, it is possible to create a hydrodynamic-numerical model exactly from the time of ALS data acquisition with all relevant geometry and roughness parameters.

Kurzfassung

Seit einigen Jahren wird Airborne Laser Scanning (ALS) als Methode zur Erfassung von topographischen Daten herangezogen. Die meisten ALS Sensoren nehmen neben den X,Y,Z Koordinaten auch die Signalamplitude (auch Intensität genannt) als Dreidimensionale Punktwolke auf, wobei zwischen single, multiple-echos und fullwave-form Aufnahmesystemen unterschieden werden kann.

Für Anwendungen im Bereich der Hydrologie oder der Hydraulik werden meist Digitale Oberflächenmodelle (DOM) oder Digitale Geländemodelle (DGM) in Rasterformat verwendet, welche aus der 3D Punktwolke abgeleitet werden. Diese Modelle werden durch Filterung und Klassifikation der Punktwolke in Boden-, Vegetations- oder Gebäude- und andere Klassen berechnet. Meist werden Geländemodelle zur Berechnung von Gerinnenetzwerken, Volumensabschätzungen von Wasserkörpern, der Berechnung von Überflutungsflächen und der Fließgeschwindigkeiten in hydrodynamisch-numerischen Modellen herangezogen. Diese Analysen basieren zum größten Teil auf den originalen Geländemodellen, die nicht speziell optimiert wurden. In der vorliegenden Dissertation werden Methoden zur Verbesserung von DGMen sowie der Generierung von Inputparametern für hydro-relevante Fragestellungen vorgestellt und diskutiert. Das Ziel der Dissertation ist es, das vorhandene Potential von hochauflösenden ALS Daten für hydrologische und hydraulische Studien aufzuzeigen und nutzbar zu machen.

Der Vorteil von räumlich hoch auflösenden ALS Daten gegenüber räumlich geringaufgelösten topographischen Daten, ist der hohe Detailgrad an Geländeinformationen, wobei dieser bei hydrologischen und hydraulischen Fragestellungen oft auch negative Auswirkungen hat. Neben der hohen Detailgenauigkeit der topographischen Informationen beinhalten ALS Daten zusätzlich die Intensitätsinformation und verfügen zudem über eine gute vertikale Verteilung der Messungen. Anhand von ausgewählten Anwendungen wird gezeigt, wie solche negativen Geländeeinflüsse minimiert werden können und wie aus den ALS Daten Objekte aber auch spezielle Parameter für hydraulische und hydrologische Fragestellungen berechnet werden können. Diese Anwendungen sind, 1)

Gerinnenetzwerkableitung, 2) Wasseroberflächenklassifikation, 3) Flusssohleninterpolation und 4) hydraulische Rauigkeitsbestimmung. Das Hauptaugenmerk der Arbeit liegt auf der Verbesserung bestehender Methoden zur Generierung hydrologischer und hydraulischer Merkmale aus ALS Daten bei maximaler Automation.

Einleitend wird auf die aktuelle Situation im Bereich Laser Fernerkundung eingegangen. Dabei werden neben der Aufnahmeprinzipien die verschiedene Sensorplattformen und die abgeleiteten Rastermodelle vorgestellt. Zudem wird auf aktuelle technologische Trends eingegangen.

Im ersten Methodenteil der Dissertation wird ein Ansatz vorgestellt, bei dem ein 1m-DGM für die Ableitung von Gerinnenetzwerken optimiert wird. Normalerweise werden nur selten 1m-DGMe für die Ableitung von Gerinnenetzwerken, basierend auf Fließakkumulationmethoden, herangezogen, da der hohe Detailgrad der topographischen Informationen sowie die im Geländemodell enthaltenen Straßen einen negativen Einfluss haben. Meist werden räumlich gering aufgelöste Geländemodelle verwendet, bei denen Straßen und topographische Kleinstrukturen durch eine Glättung (zB. low pass filter) eliminiert werden. Dabei geht gleichzeitig der hohe Detailgrad und die hohe räumliche Auflösung verloren, welche schließlich nicht mehr für die Gerinneberechnung vorhanden sind. Durch eliminieren der anthropogenen Strukturen, hauptsächlich der Straßen, kann ein optimiertes DGM erstellt werden, bei dem die negativen Einflüsse der Straßen auf die Fließakkumulationmethoden minimiert werden. Der Ergebnisvergleich zwischen Netzwerken, die auf dem optimierten 1m-DGM und denen, die auf dem original 1m-DGM, einem 5m optimierten oder einem geglätteten 5m-DGM basieren, zeigen eine Verbesserung von rund 9% bei der Vollständigkeit bzw. Genauigkeit.

Im zweiten methodischen Teil wird ein punktwolkenbasierter Ansatz zur Wasseroberflächenklassifikation basierend auf Geometrie- und Radiometriedaten erläutert. Durch die Interaktion des Laserstrahls einer bestimmten Wellenlänge mit der Wasseroberfläche können ALS Intensitätsdaten optimal zur Detektion von Wasseroberflächen eingesetzt werden. Wasseroberflächen sind vor allem in der Erstellung von Landbedeckungskarten aber auch für die Berechnung von hydrodynamisch-numerischen Modellen wichtig. Die genaue Lage der Wasserfläche nimmt bei der hydrodynamisch-numerischen Berechnung einen hohen Stellenwert ein, da diese für die Integration von Flusssohlenmodellen aber auch für die Zuweisung von Rauigkeitsparametern verwendet wird.

Weiters wird, ausgehend von der Wasseroberfläche, ein Flusssohlenmodell errechnet. Zudem wird eine zusätzliche Methode zur Wasseroberflächenableitung basierend auf Rasterdaten vorgestellt. Durch die Kombination von Wasseroberfläche und terrestrisch-gemessenen Flussquerprofilen wird ein Flussbettmodell berechnet, das mit dem bestehenden DGM vereinigt wird. Das neu berechnete DGM mit der integrierten Flusssohle kann für hydrodynamisch-numerische Modellierungen aber auch für die Berechnung von Flusssohlenveränderungen zwischen zwei Hochwasserereignissen herangezogen werden. Die Vorteile der Methode sind, dass die hochauflösenden Geländedaten aus dem ALS erhalten und mit dem Flusssohlenmodell ergänzt werden. Die Qualität des abgeleiteten Flusssohlenmodells hängt dabei primär von den Abständen der verwendeten Flussquerprofile ab.

Im letzten Methodenteil wird ein punktwolkenbasierter Ansatz zur hydraulischen Rauigkeitsbestimmung vorgestellt. Ausgehend von Geometriedaten der 3D Punktwolke werden die vertikalen Strukturen der Vegetation analysiert und verschiedene Landbedeckungsklassen berechnet, welchen schließlich Manning's n Werte zugewiesen werden. Die Vorteile dieser Methode sind die vollautomatisierte Analyse, die hohe Reproduzierbarkeit der Ergebnisse sowie die kurze Rechenzeit. Mit dieser Methode wird ermöglicht, dass die Geometrie und die Rauigkeitsdaten von ein und derselben Befliegung abgeleitet werden und beide als Input für hydrodynamisch-numerische Modellierungen dienen können. Daher kann sichergestellt werden, dass alle Inputdaten (Geometrie und Rauigkeiten) von exakt einem Zeitpunkt stammen, was bis dato nicht der Fall gewesen ist.

Contents

Acknowledgements	i
Abstract	iii
Kurzfassung	vii
List of Figures	xv
List of Tables	xvii
1 Introduction	1
1.1 Motivation	2
1.2 Research aims	3
1.3 Thesis outline	4
1.3.1 Vienna Doctoral Programme on Water Resource Systems . .	4
1.3.2 Structure	5
1.3.3 Selected publications	7
1.3.4 Additional publications	8
2 LiDAR background and terminology	11
2.1 LiDAR technology	12
2.2 ALS data and derivatives	16
2.3 Recent trends in LiDAR technology	18
3 Conditioning of high resolution airborne laser scanning data for drainage network delineation	21
3.1 Introduction	22
3.2 Objectives	23
3.3 Test site and data	24
3.4 Methods	26
3.5 Results	28
3.5.1 DTM conditioning	28
3.5.2 Drainage derivation	29
3.5.3 Accuracy of the derived drainage network	30

3.6	Discussion	31
3.7	Conclusion	35
3.8	Acknowledgments	36
4	Water classification using 3D airborne laser scanning point clouds	37
4.1	Introduction	38
4.2	Background	40
4.2.1	Interaction of near infrared laser light with water	40
4.2.2	Related work	40
4.3	Test sites and data	42
4.3.1	Test sites	42
4.3.2	Reference data production	43
4.4	Water surface classification	44
4.4.1	Amplitude correction and radiometric adjustment	44
4.4.2	Laser shot dropout modeling	46
4.4.3	Data exploration	47
4.4.4	Threshold based classification	51
4.5	Results	51
4.6	Discussion	52
4.7	Conclusion	54
4.8	Acknowledgments	54
5	Estimating changes of riverine landscapes and riverbeds by using airborne LiDAR data and river cross-sections	55
5.1	Introduction	56
5.2	Test site and data	59
5.3	Methods	62
5.3.1	Water surface delineation	62
5.3.2	Centerline computation	63
5.3.3	Three-dimensional riverbed point cloud generation	63
5.3.4	DBM generation	64
5.4	Results	64
5.5	Discussion	67
5.6	Conclusions and Outlook	68
5.7	Acknowledgements	71
6	Vertical vegetation structure analysis and hydraulic roughness determination using dense ALS point cloud data – a voxel based approach	73
6.1	Introduction	74

6.2	Background	75
6.2.1	Vegetation structure and surface roughness	75
6.2.2	LiDAR used in hydraulics and hydrology	76
6.3	Method	78
6.3.1	General concept	78
6.3.2	Cell-level	80
6.3.3	Voxel-level	80
6.3.4	Connection-level	80
6.3.5	Hydraulic roughness classification	81
6.4	Results and discussion	81
6.5	Conclusions and future work	83
6.6	Acknowledgements	84
7	Synthesis and conclusions	85
7.1	Synthesis and major findings	86
7.1.1	Drainage network delineation	86
7.1.2	Water surface mapping	88
7.1.3	River bed modeling	89
7.1.4	Hydraulic roughness estimation	90
7.1.5	Ongoing work	90
7.2	Conclusion	92
7.3	Future work	93
7.4	Final paragraph	93
	Bibliography	95
	Curriculum vitae	113

List of Figures

1.1	Relations between the different thesis chapters	5
2.1	Principle of LiDAR distance measurement	13
2.2	ALS-platform, scan pattern, GPS, INU	14
2.3	Discrete echo recording vs. full-waveform	15
2.4	Point cloud, DTM, DSM and DIM	17
3.1	Test site (Bregenzerwald, Vorarlberg, Austria)	25
3.2	Workflow	27
3.3	Difference plot between original and conditioned 1m-DTM	29
3.4	Drainage network based on original and conditioned DTMs (1m, 5m)	30
3.5	Results of drainage network delineation	32
4.1	Water surface classification workflow	44
4.2	Radiometric adjustment	45
4.3	Corrected vs. radiometric adjusted amplitude values	46
4.4	Dropout modeling schema	46
4.5	Terrestrial orthophoto with measured water-land boundary	47
4.6	Relation between angle and corrected amplitude values on water	48
4.7	Profile through a watercourse	49
4.8	Standard deviation of height and amplitude density ratio	50
4.9	Pre-classification at the Venter Ache	51
4.10	Classification results, Bregenzer Ache, Venter Ache	52
4.11	Classification results, Hintereisfernerbach	53
5.1	River bed modeling test site	60
5.2	Used digital models	61
5.3	Workflow of the DBM derivation method	61
5.4	Steps of the 3D-riverbed point cloud calculation	64
5.5	DIMs and WEPs	65
5.6	Plots through cross-section No. 1 and No. 4 (at locations in Fig. 5.1)	66
5.7	Difference-models and plots through the river	69
6.1	Basic concept	79
6.2	Schema of the cell-, voxel- and connection-level	80

6.3	Traditionally derived Manning's values vs. the ALS derived values	82
6.4	Depth of inundated area and difference model from 2D simulation	82

List of Tables

3.1	Cumulative length of networks	32
3.2	Error assessment (completeness, correctness and quality)	32
3.3	Additional error assessment	34
4.1	Flight data and test sites	43
6.1	Rule-base for hydraulic roughness classification	82

CHAPTER



Introduction

1.1 Motivation

Water resource management and flood protection play an important role in human activities. On the one hand the availability of water influence the settlement strategies and the size of an urban settlement. On the other hand the frequency and magnitude of flood events are the main limitations for the spread of human settlements. Therefore, the management of water resources and the reduction of potential flood damages have been in focus of research for a long time (Hubbart, 2008). Nowadays, an increasing use of remote sensing data can be observed due to data's accuracy, the spatial and temporal resolution and the use of data from different sensors like RADAR, LiDAR or images used in studies, related to water resources management and flood protection (Wagner et al., 2011). By the use of remote sensing technologies, like Airborne Laser Scanning (ALS), Terrestrial Laser Scanning (TLS), airborne or space borne imagery and other Earth Observation techniques, the ability of solving water related questions is nowadays more sophisticated than in the past. Available data from different sensors reach the level of 1m spatial resolution or even less, a temporal resolution of several hours and a high spectral resolution. At the same time the methods and algorithms for data processing have become more robust and sophisticated, while the quality of mapping and classification results have increased with a little time delay regarding to data amount

and quality (Wagner et al., 2011). Due to these facts, the adaptation of existing methods or the conditioning of the input data have to be applied to gain accurate and proper modeling results (Ericum et al., 2010; Höfle and Rutzinger, 2011). The importance of using the best available resolution of the data, which are then specially modified for an applications, is crucial (Mandlbürger et al., 2009).

Due to the large number of floods in the last years, which caused tremendous damages to human properties, damage and risk reduction strategies have become an important field of research (EEA, 2010). Remote sensing data and methods are used in many different scientific fields (e.g. Höfle and Rutzinger, 2011; Hohenthal et al., 2011; Abermann et al., 2010; Hyyppä et al., 2004). Airborne laser scanning point clouds and derived products are available on local and regional scale with high spatial resolution. In this thesis the term 'high resolution' is used synonymously for a cell size of 1x1 m or the ALS point cloud, which exhibiting a point density of more than 1 *point/m*². The importance to provide strategies to increase feature delineation accuracy using high resolution spatial data like ALS as input is becoming increasingly evident (Li and Wong, 2010; Sofia et al., 2011; Wichmann et al., 2008). Area-wide and country-wide ALS data with high spatial resolution have already been available in many European countries (Mandlbürger et al., 2010a). The high spatial

resolution causes manifold challenges in data processing and analysis using existing hydraulic and hydrological algorithms (Mandlbürger et al., 2009, 2011b). Most of the hydro-related methods were created to use low spatial resolution topographic data. Two strategies can be figured out in order to overcome this problem. Firstly, the algorithms which are used in the specific applications can be changed to handle the full spatial resolution of the input ALS data. Secondly, the ALS data themselves can individually be adapted for the very special applications and the used algorithms.

The motivation behind this thesis is to show the advantages of using the full spatial resolution and the radiometric capacity of the ALS data to maintain an increase in the accuracy of hydrological and hydraulic study results by using ALS data as input. It will be demonstrated that spatial resolution and the radiometric information of ALS data can be used to achieve more accurate results in the scientific field of hydrology and hydraulics by conditioning the input data and by extracting relevant features directly from the ALS data.

1.2 Research aims

The aim of this research is to explore and use the full potential of the ALS data within hydro-related studies, which have been done very rarely

for hydraulic or hydrological applications so far. The whole capability of ALS data are the high spatial resolution and the provided radiometric information (Mallet and Bretar, 2009; Wagner, 2010). At first the main focus is the use of the highest available spatial resolution as well as the backscattered information (referred to as intensity or amplitude) to increase the accuracy of water related studies. To achieve this goal, geoinformation methods are used to improve ALS based elevation and point cloud data to gain more accurate results (Mandlbürger et al., 2009; Cobby et al., 2003; Hollaus et al., 2005).

By presenting four different methods, which are from the hydrological and hydraulic field, the potential of using high resolution ALS data as input is demonstrated. It is figured out that the use of ALS data in hydro-related studies improves the results significantly. The focus is on creating different methods, which can be used in a workflow to improve the capability of using ALS data in hydro-related studies. Therefore, the methods are developed in a way that the output layer of one method can be used as input for an other part of the workflow (cf. Fig. 1.1). This thesis investigates the use of ALS data in combination with methods from geoinformatics to increase the capability for information extraction (DTM or point cloud) and hydro-related applications.

Some methods presented in this the-

sis are more generic and can also be used for other applications outside the hydrological or hydraulic field. Some methods are specially designed to calculate features in the domain of hydro sciences. But all in all the combination of the presented methods is the essential part of this thesis and shows the

ability to improve the quality of hydrological or hydrodynamic modeling results.

The main goals can be divided and summarized into the four main chapters of this thesis, focusing on:

1. improving terrain models (DTMs) for drainage delineation by conditioning the DTM, where anthropogenic structures, like roads, are strictly removed from the DTM before deriving drainage networks.
2. introducing a point cloud based method for water surface classification integrating geometry and backscattered intensity information of the original 3D ALS point cloud.
3. developing an approach to interpolated the river bed from terrestrially measured data, which can be integrated into the DTM to quantify changes of the river bed between major flood events or which can be used as improved data source for hydraulic modeling.
4. presenting a point cloud based method for vertical vegetation classification, which is used for hydraulic friction coefficient determination using the geometric information of the laser data.

1.3 Thesis outline

1.3.1 Vienna Doctoral Programme on Water Resource Systems

This PhD thesis is written within the context of the 'Vienna Doctoral Programme on Water Resource Systems (DK-Plus)' located at the 'Vienna University of Technology, Austria'. This interdisciplinary program focuses on the research of complex water resource systems. The doctoral program is funded by the Austrian Science Funds FWF (DK-plus W1219-N22)

and has been designed to run from 2009 to 2021 involving about 70 PhD students.

Two institutes, 'Research Groups Photogrammetry & Remote Sensing, Department of Geodesy and Geoinformation' and the 'CWRS - Centre for Water Resource Systems' from the 'Vienna University of Technology', have been involved in supervising this thesis.

The supervisors are Prof. Wolfgang Wagner (Research Groups Photogrammetry & Remote Sensing) and Prof. Günter Blöschl head of the 'Department

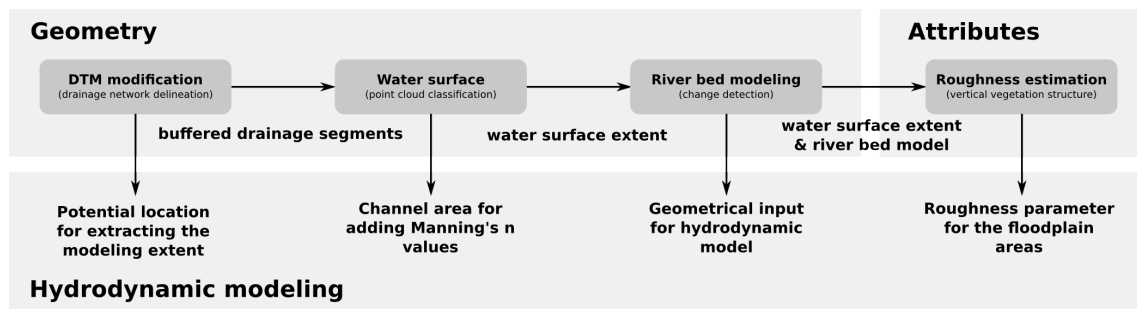


Figure 1.1: Overall context of the different thesis chapters and relations to each other

of Hydrology and Water Resources Management', director of the 'Centre for Water Resource Systems', chair of the 'Vienna Doctoral Programme on Water Resource Systems' and president of the 'European Geosciences Union, EGU'.

1.3.2 Structure

This cumulative thesis comprises three peer-review journal papers (chapter 3, 4, 5) and one peer-reviewed conference proceeding paper (chapter 6).

The thesis structure is as follows:

In chapter 2 a general overview about LiDAR (ALS and TLS) techniques and methods is presented. A technical overview about data acquisition and processing is given. Besides the point cloud processing, the relevant derivatives are described in detail. Finally, an outlook on recent trends in

data acquisition and processing is presented. The chapter is related to Wagner et al. (2011), where a short version of the presented chapter is published.

The first methodological part of this thesis is chapter 3, relating to Vetter and Mandlbürger (2013). This chapter deals with the conditioning of high resolution DTMs derived from ALS data for drainage network delineation. A workflow is presented in which the influences of roads on the drainage network delineation is minimized and the accuracy of the derived network is maximized. This is done by recalculating the DTM along streets and replacing the original slope with a so-called 'near-natural slope', which corresponds to the original slope before the road construction works. A comparison of network delineation results is done for networks derived from four different DTM-variations (conditioned 1m & 5m-DTM and original 1m & smoothed 5m-DTM). The network delineation results show an increase in

correctness and completeness using the conditioned 1m-DTM instead of the original 1m-DTM, the smoothed 5m-DTM or the conditioned 5m-DTM. The results can be used to improve existing river data sets and for further calculations in which the potential locations of streams are needed as a priori information.

In chapter 4, a method to delineate water surface areas using ALS geometry and intensity values is presented. This chapter relates to Vetter et al. (2009b) where a point cloud based method (threshold based classification) including a radiometric adjustment of multi-temporal data is described. A raster-based classification, related to Vetter et al. (2011b), is presented in chapter 5. The results of both methods for water surface mapping, presented in these chapters, are important input files for hydraulic applications in general.

Chapter 5 is related to Vetter et al. (2011b), where a method is introduced to calculate river bed models using ALS elevation data and terrestrially measured river cross sections. To generate such a river bed model, the information of the existing water surface and terrestrially measured river cross sections are needed. The water surface extent is derived by using the point cloud based methods from chapter 3 or the raster based approach presented in chapter 4. By densification of the measured cross sections and a linear interpolation, the river bed model is generated and fi-

nally integrated into the DTM, resulting in a DTM of the watercourse (DTM-W). The advantage of this DTM-W is that the interpolation of the river bed is takes place only for the water surface area, whereas all non-water areas are used without any changes from the DTM. The results show the potential to estimate river bed changes during two major flood events. Furthermore, the DTM-W can be used as geometry input for hydrodynamic-numerical modeling.

In the field of hydraulics the use of the surface and vegetation roughness is an important component of the reproduction of realistic flood scenarios. The final methodological chapter 6 deals with the estimation of surface near vegetation roughness for hydrodynamic models. This chapter bases on Vetter et al. (2011a) and outlines a method where the surface-near vertical structure of the point cloud is analyzed. The main advantage of these methods is to generate a consistent data set of elevation and roughness parameters from the same data source and acquisition time. Both, elevation and roughness, are derived from the same ALS point cloud, which has never been done in hydrological research before. Therefore, all input data, which are extracted from remote sensing data (geometry and roughness), are derived from the same measurement.

A synthesis of the presented methods is given in chapter 7, where the advantages and disadvantages of

the methods are discussed. Finally, a summary of the major findings and an overview of future work is given.

As shown in Fig. 1.1 all methodological chapters are related to each other. The results of chapter 3 can be used as input for the calculation of the water surface area (chapter 4 and 5) using a buffer of the derived river network to pre-select the ALS data for water surface classification. The results of the water surface delineation are used in chapter 5. The last chapter 6 is important for hydrodynamic modeling, where the resulting DTM with the river bed (chapter 5) and the roughness from chapter 6 are combined.

1.3.3 Selected publications

It has to be clarified that Michael Vetter is the lead author of all four main contributions included in this thesis (chapter 3 - 6) and the co-author of the LiDAR theory chapter 2. The selected papers were written autonomously by the first author. The co-authors supported the research process, acted as excellent discussion partners and were involved in the proofreading process. The LiDAR theory part (Chapter 2) was also written by the thesis author and was published as a summary of the presented chapter in a book, where the thesis author was one of two co-authors. Four of the five contributions have already been published and one paper has been submitted.

Chapter 2, Wagner et al. (2011)

Wagner, W., **Vetter, M.** & Bartsch A. (2011): Novel Microwave- and Lidar Remote Sensing Techniques for Monitoring of In-Land Water Resources. Report for acatech - Deutsche Akademie der Technikwissenschaften; Report No. 7, 42 p.

Chapter 3, Vetter and Mandlbürger (2013)

Vetter, M. & Mandlbürger, G. (2013): Conditioning of high resolution airborne laser scanning data for river network delineation. Submitted to: Journal of photogrammetry, remote sensing and geoinformation processing, February 2013.

Chapter 4, Vetter et al. (2009b)

Vetter, M., Höfle, B. & Rutzinger, M. (2009): Water classification using 3D airborne laser scanning point clouds. Österreichische Zeitschrift für Vermessung & Geoinformation, 97(2), 227-238.

Chapter 5, Vetter et al. (2011b)

Vetter, M., Höfle, B., Rutzinger, M. & Mandlbürger, G. (2011): Estimating changes of riverine landscapes and riverbeds by using airborne LiDAR data and river cross-sections. *Zeitschrift für Geomorphologie/Annals of Geomorphology* 55(2), 51-65. doi:10.1127/0372-8854/2011/0055S2-0045.

Chapter 6, Vetter et al. (2011a)

Vetter, M., Höfle, B., Hollaus, M., Gschöpf, C., Mandlbürger, G., Pfeifer, N. & Wagner, W. (2011): Vertical vegetation structure analysis and hydraulic roughness determination using dense ALS point cloud data – a voxel based approach. *International Archives of Photogrammetry, Remote Sensing and Spatial Information Sciences*, XXXVIII - 5/W12, 265-270. doi:10.5194/isprsarchives-XXXVIII-5-W12-265-2011.

1.3.4 Additional publications

Many additional contributions have been published as first or co-author. Those are peer-reviewed journal papers or proceeding contributions, reviewed abstracts, book chapters or technical reports. The reviewed abstracts, most of them submitted to the European Geosciences Union (EGU), are not listed.

The additional contributions were published between 2007 and 2013. The previous ones (before 2009) were prepared during the master studies and can be seen as the stimulation for the chosen research topic. Most of the additional publications are related to the different thesis chapters and therefore, more or less relevant for the success of this thesis project.

Peer-reviewed articles:

1. Fritzmann et al. (2011): Fritzmann, P., Höfle, B., Sailer, R., Stötter, J. & **Vetter, M. (2011):** Multi-temporal surface classification of airborne LiDAR intensity data in high mountain environments - A case study from Hintereisferner, Austria. In: Pfeifer, N., Roncat, A., Stötter, J. & Becht, M.: *Laser Scanning Applications in Geomorphology*. *Zeitschrift für Geomorphologie/Annals of Geomorphology* 55(2), 105–126. DOI: 10.1127/0372-8854/2011/0055S2-0048.
2. Höfle et al. (2009): Höfle, B., **Vetter, M.**, Pfeifer, N., Mandlbürger, G. & Stötter, J. (2009): Water surface mapping from airborne laser scanning using signal amplitude and elevation data. *Earth Surface Processes and Landforms*, 34(12), 1635-1649. DOI:10.1002/esp.1853.
3. Pfurtscheller and Vetter (2013): Pfurtscheller, C. & **Vetter, M. (2013):** Assessing entrepreneurial and regional-economic flood impacts on a globalised production company base on LIDAR data and 2D flood modelling. Submitted to: *Journal of Flood Risk Management*, January 2013.

Peer-reviewed proceedings:

4. Eysn et al. (2010): Eysn, L., Hollaus, M., **Vetter, M.** & Pfeifer, N. (2010): Waldlückenerfassung aus ALS Daten mittels Alpha-Shapes. In: Kohlhofer, G. and Franzen, M. (eds): Dreiländertagung OVG, DGPF und SGPF, 30. Wissenschaftlich-Technische Jahrestagung der DGPF, Wien, 1.–3. Juli 2010, 552–560.
5. Mandlbürger et al. (2011b): Mandlbürger, G., **Vetter, M.**, Milenkovic, M. & Pfeifer, N. (2011): Derivation of a countrywide river network based on Airborne Laser Scanning DEMs - results of a pilot study . 19th International Congress on Modelling and Simulation, Perth, Australia, 12–16 December 2011, 2423-2429.
6. Rutzinger et al. (2010): Rutzinger, M., Rűf, B., Höfle, B. & **Vetter, M.** (2010): Change detection of building footprints from airborne laser scanning acquired in short time intervals. In: Wagner, W. and Székely, B. (eds): ISPRS Technical Commission VII Symposium, '100 Years ISPRS – Advancing Remote Sensing Science', Vienna, Austria, July 5–7, vol. XXXVIII, Part 7B, International Archives of the Photogrammetry, Remote Sensing and Spatial Information Sciences, 475–480.
7. Vetter et al. (2009c): **Vetter, M.**, Jochem, A., Franke, M., Schöberl, F. & Werthmann, M. (2009): Auswirkung der Geländemodellauflösung auf Hochwassermodellierungen. Angewandte Geoinformatik 2009, Beiträge zum 21. AGIT-Symposium Salzburg, Austria, Wichmann Verlag, Heidelberg, 378-386.
8. Vetter et al. (2008): **Vetter, M.**, Höfle, B., Mandlbürger, G. & Rutzinger, M. (2008): Ableitung von Flusssohlenmodellen aus Flussquerprofilen und Integration in Airborne Laserscanning Geländemodelle mit GRASS GIS. Angewandte Geoinformatik 2008, Beiträge zum 20. AGIT-Symposium Salzburg, Austria, Wichmann Verlag, Heidelberg, 382-391.
9. Wichmann et al. (2008): Wichmann, V., Rutzinger, M. & **Vetter, M.** (2008): Digital terrain model generation from airborne laser scanning point data and the effect of grid-cell size on the simulation results of a debris flow model. Böhner, J., Blaschke, T., Montanarella, L.: SAGA - Second Out. Hamburger Beiträge zur Physischen Geographie und Landschaftsökologie (19), Hamburg, Germany, S. 103-113.

Book chapters:

10. Rutzinger et al. (2011b): Rutzinger, M., Höfle, B., **Vetter, M.** & Pfeifer, N. (2011): Digital terrain models from airborne laser scanning for the automatic extraction of natural and anthropogenic linear structures. In: Geomorphological Mapping: a professional handbook of techniques and applications. In: Smith, M., Paron, P., Griffiths, J., S., pp. 475–488. Elsevier.

Technical reports:

11. Adams et al. (2007): Adams, M., Falkner, M., Franke, M., Jochem, A., Lochner, B., Link, S., **Vetter, M.** & Werthmann, M. (2007): Hochwasser Risiko Modellierung Innsbruck - Endbericht zum Projektmodul Geoökologie und Raumforschung 2006/2007. Interner Bericht, Institut für Geographie, Universität Innsbruck.
12. Pfurtscheller and Vetter (2012a): Pfurtscheller, C. & **Vetter, M. (2012)**: Betriebliche und ökonomische Schäden auf Basis einer Hochwassermodellierung. Internal report (Company 1), 18 p.
13. Pfurtscheller and Vetter (2012b): Pfurtscheller, C. & **Vetter, M. (2012)**: Betriebliche und ökonomische Schäden auf Basis einer Hochwassermodellierung. Internal report (Company 2), 18 p.

Master's thesis:

14. Vetter (2008): **Vetter, M. (2008)**: Punktwolkenbasierte Ableitung von Wasseroberflächen aus Airborne Laser Scanning Daten - Unter Verwendung von Radiometrie- und Geometrieattributen. Master's thesis, Institut für Geographie, Universität Innsbruck.

CHAPTER



LiDAR background and terminology

2.1 LiDAR technology

Nowadays, Laser Scanning, also referred to as LiDAR (Light Detection And Ranging) or LaDAR (Laser Detection and Ranging), is used as a fast and accurate technique to collect topographic Earth information (Baltsavias, 1999a; Wehr and Lohr, 1999). For capturing terrain data Airborne Laser Scanning (ALS) has become the state of the art data source. ALS is a time and cost effective method to acquire topographic data with a low amount of user interaction, a high ground sampling density (typically 1-50 points per m²) and a height accuracy of less than 15 cm. Many scientific studies show that the trend is to increase sampling rates, improve height accuracy, use different wavelength for specific applications and to establish Full-WaveForm (FWF) LiDAR systems (Bretar et al., 2009; Pfennigbauer et al., 2010; Wagner et al., 2004). ALS is mostly used for data acquisition of area-wide Earth surface information. ALS data are used in different scientific disciplines like archeology (Doneus et al., 2010), geology (Székely et al., 2009), geomorphology (Höfle and Rutzinger, 2011), hydrology (Marcus, 2010), urban change detection (Rutzinger et al., 2010), water surface mapping (Höfle et al., 2009), glaciology (Abermann et al., 2010) and many more. The main focus for non-remote sensing disciplines is on using Digital Elevation Models (DEMs) as basis for calculations. Mandlbürger et al. (2009) show the advantages of

using the ALS point cloud data for hydrodynamic-numerical flood simulations.

Besides the ALS data, TLS (Terrestrial Laser Scanning) is used for small areas like landslide volume calculation, snow height estimation, river monitoring and many others (Roncat et al., 2010; Grünewald et al., 2010; Heritage and Milan, 2009). Recent studies have investigated Mobile Laser Scanning (MLS) for corridor mapping, in which a TLS has been mounted on a car or boat to collect data of roads, the building facades or riverine landscapes (Rutzinger et al., 2011a; Alho et al., 2009; Hohenthal et al., 2011). The advantage of TLS is the high ground sampling density (several hundred points per m²). Limitations of TLS are the observing area, the data acquisition time and the range, which are small, time-consuming and short. Beside the data collection, the post-processing and registration of the point cloud is also time-consuming. TLS data can be used for monitoring, as independent source for validation of ALS data and as reference data sets for land cover mapping or roughness estimation of flood inundated areas (Straatsma et al., 2008). The sensor developing companies have changed their products in the last few years from huge and heavy scanners to small and light TLS systems. Furthermore, modern TLS systems record multiple echoes and use FWF technology (Cary, 2009).

The recent trend in the field of Space-

borne remote sensing related to LiDAR is towards the development of space-borne LiDAR scanners instead of LiDAR profilers, which are presented in Yu et al. (2010), by introducing the NASA project LiDAR Surface Topography (LIST).

For bathymetric studies a two wavelength laser system is used to measure the water surface and the river or sea bottom. One wavelength operates with 1064 nm in the near-infrared and reflects at the water surface, while the second wavelength is in the visible spectrum of electro magnetic wavelength from 520 nm to 532 nm (Irish and Lillycrop, 1999; Guenther et al., 2000). Restrict properties limit the measurements of rivers, lakes or sea beds. The main limitations of bathymetric LiDAR systems are that clear water conditions are required and a minimum water depth of about 1.5 m is necessary to distinguish the water surface from the riverbed targets depending on the used ALS system and pulse length (Guenther et al., 2000; Allouis et al., 2010). The maximum penetration depth of a bathymetric ALS System is typically 2 to 3 times the Secchi depth, which is the water depth where a black and white disk can barely be seen with the naked eye. The Secchi depth depends primarily on the turbidity of the water (Guenther et al., 2000). Ongoing developments are showing that companies are interested in building bathymetric LiDAR systems, which are able to collect data in shallow water areas by using

short pulse length (Mandlbürger et al., 2011a). The pulse length can only be decreased by using more energy for pulse generating, which leads to eye safety problems, or by a short observation distance.

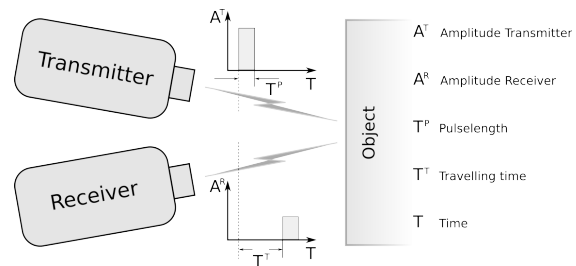


Figure 2.1: Principle of LiDAR distance measurement (cf. Thiel and Wehr (2004); Wagner et al. (2003)).

The main principle of data collection is identical for all LiDAR systems. A laser source is mounted in the system, which produces homogeneous light ranging from 905 nm to 1550 nm. The electromagnetic wave is transmitted by this laser source into the object direction. Most topographic LiDAR systems are pulsed. A continuous wave is transmitted for close range remote sensing (TLS only), which is not discussed here (more information in Baltsavias (1999a); Wehr and Lohr (1999)). The transmitted laser pulse reflects upon the objects surface and a part of the reflected energy can be recorded at the sensors receiver. The distance calculation is based on the travel time of the laser pulse between sensor and object (speed-of-light * travel time / 2; Fig. 2.1). Then, the precisely measured range is connected to the position and attitude of the remote sensing platform (GPS,

Global Positioning System; and IMU, Inertial Measurement Unit). The angle of the oscillating mirror, which is installed to generate the scanning pattern, has to be added in the process (Fig. 2.2) to calculate the x,y,z location of each measurement. Beside the x,y,z coordinates of each laser shot, the backscattered energy is recorded for each reflection or wave-form, in FWF systems the whole wave form is stored. The first generation of laser scanner collected the data as discrete echo recording system (max. 4). The new scanner generation (FWF systems) record the whole wave-form of the reflected pulse (Fig. 2.3).

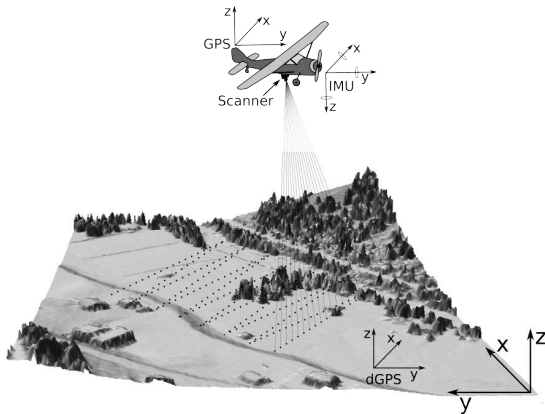


Figure 2.2: ALS-platform, scan pattern, GPS, INU (cf. Abo Akel et al. (2003) p. 3).

As seen in different scientific fields the use of FWF systems is increasing significantly because of better vertical resolution and the increase of information. As Pfennigbauer et al. (2010) presented, the trend for modern laser scanner systems is to produce short pulse length to increase the vertical resolution of FWF

scanners.

One of the main problems with LiDAR data is the lack of processing software, which is able to handle huge data sets at the same time. If the data are more accurate and dense, the processing demand is more important. Current investigations on software development for Orientation and Processing of Airborne Laser Scanning (OPALS) and for Digital Elevation Modeling and filtering (SCOP++) have been done by the Institute of Photogrammetry and Remote Sensing, Vienna University of Technology (IPF, Mandlbürger et al. (2010b); Pfeifer et al. (2001)). Other powerful tools are LAS-tools or Terasolid (Isenburg et al., 2006; Terrasolid, 2012). Beside the software, the storage and hardware components are very important for huge ALS and TLS data sets. The increase in sampling density also increases the storage space and processing demand. If the latest trend (the pulse length is being reduced while the digitizing interval is getting smaller) is achieved, the file size will increase again. Another important point is the use of data. Point cloud data are mostly used to generate Digital Elevation Models (DEMs) as input for several other applications like hydrodynamic-numerical modeling, change detection, etc. Applications operating on the original point cloud have become more popular (Höfle and Rutzinger, 2011). Beside the x,y,z information, also the radiometric information is of high importance and becomes a significant data source

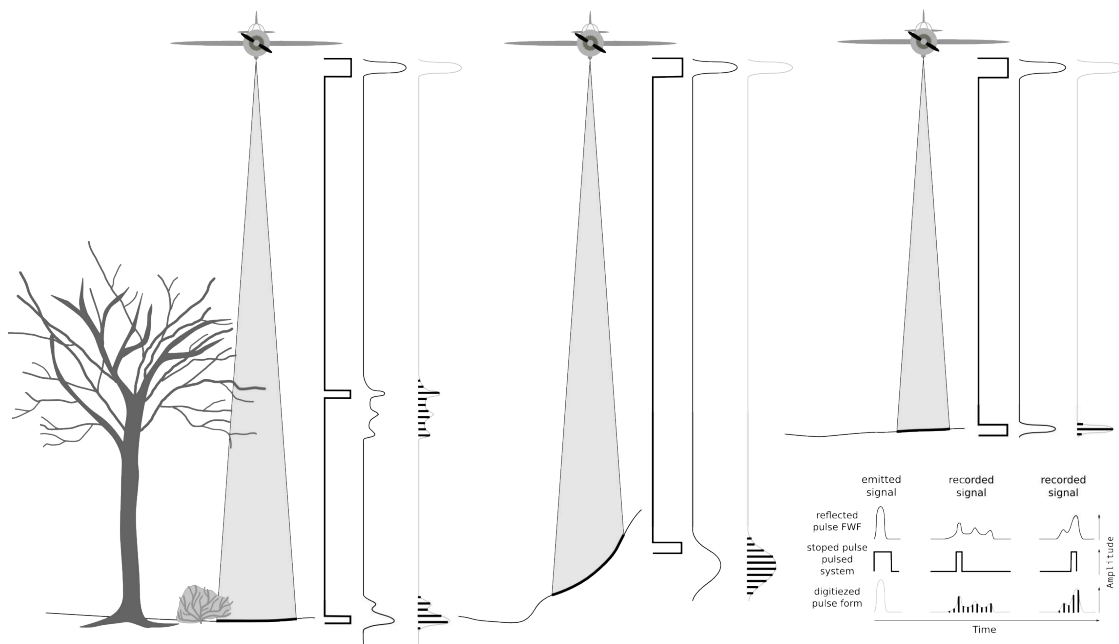


Figure 2.3: Discrete echo recording vs. full-waveform (cf. Hug et al. (2004) p. 25 and Wagner et al. (2004) p. 2).

for classification applications (Höfle, 2007).

As mentioned before, the main goals are to increase the accuracy and the ground sampling rate of the scanners, especially for FWF sensors. The latest trend in sensor development shows the change from sensors, which work with one pulse in air, to 'Multiple Pulses in Air' for Leica, 'multiple-time-around' for Riegl or 'multi-pulse technology' for Optech scanners, which operates with two pulses in air at the same time. The advantage of using this technology is to double the point density of the observed area. By using multiple-time-around, the aircraft can fly in a higher altitude than with conventional systems to collect the same ground sam-

pling density, while doubling the acquisition area and shortening the time demand. Another trend can be seen in reducing the transmitted pulse length while increasing the FWF digitizing interval, e.g. Riegl VQ820G (Bathymetric LiDAR with two wave length: 1 ns pulse length and 0.1 ns digitizing interval). The advantage of using short transmitted pulse length and increasing FWF digitizing interval is a better vertical resolution of the data. The results can improve shallow water bathymetry, vegetation classification and hydrodynamic models by a better representation of vertical structures of the ground near vegetation and the surface roughness.

2.2 ALS data and derivatives

The main ALS product is the point cloud, which is derived from the recorded data by applying different corrections, transformations and synchronizations of GPS and IMU to the raw data. The point cloud consists of x,y,z coordinates and different attributes like amplitude/intensity, No. of echoes, echo No. depending on whether a FWF or pulsed system is used or not.

The most common products beside the ALS point cloud are the derived Digital Elevation Models, which are generated by filtering the point cloud data. Those are the Digital Terrain Model (DTM), the Digital Surface Model (DSM), the normalized Digital Surface Model (nDSM) and the Digital Intensity Model (DIM), which are shown in Figure 2.3. The ALS point cloud contains all measurements of the ALS acquisition in x,y,z information, timestamp (GPS time of the collected laser shot) and the radiometric information (so-called intensity for discrete echo recording ALS or amplitude for FWF systems). Additional attributes per echo can be calculated in a post process after the flight campaign of FWF missions (echo width, number of echoes and echo number, (Wagner et al., 2006). With the point cloud the trajectory information is stored which contains the location of the flight trajectory, timestamp and the angles of attitude (IMU information, head-, pitch- and

roll-angle).

An important step to generate a DTM is to remove all off-terrain points from the point cloud (vegetation, buildings, power lines, ...). This process is called filtering and can be done in different ways. One solution is the robust interpolation approach (Kraus and Pfeifer, 1998), where all points are weighted by the vertical distance to the average surface. Points above the average surface get smaller weight. An improvement of this method by adding the FWF attribute of the Echo Width is presented by Mandlburger et al. (2007). A comparison of the most common filter approaches is presented in Sithole and Vosselman (2004). The DTM includes all points belonging to the Earth surface after filtering the point cloud (Fig. 2.4b). The quality of a derived DTM depends mainly on the ground sampling density and the used filtering algorithm (Sithole and Vosselman, 2004).

The DSM is a regular raster model computed by using the closest points to the scanner of each raster cell, as mentioned in Pfeifer and Mandlburger (2008) or Elmqvist et al. (2001) (Fig. 2.4). Sometimes a DSM is called Canopy Model and represents the upper most elevation information of each raster cell.

A normalized DSM (nDSM) can be calculated by subtracting the DTM from the DSM. The elevation data included in a nDSM are the heights of all off-

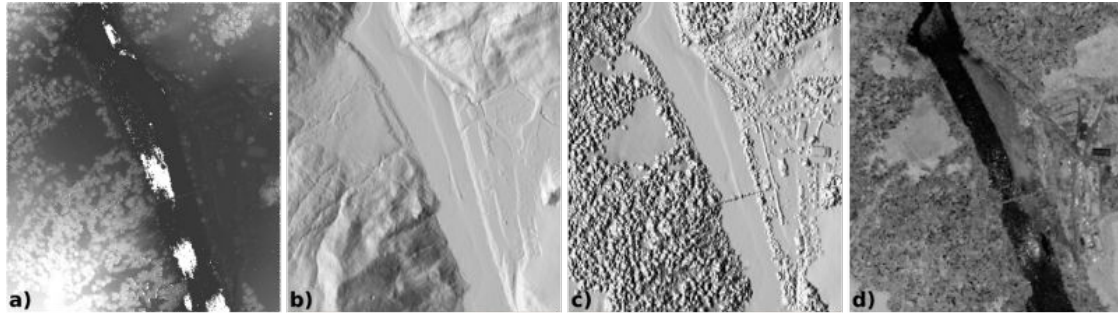


Figure 2.4: a) point cloud, b) shading of DTM, c) shading of DSM, d) DIM.

terrain objects (trees, buildings, cars, ...). The accuracy of a nDSM depends primarily on the used DTM and DSM.

A Digital Intensity Model (DIM) represents the radiometric information of the laser scanning data in a regular raster. DIMs are mostly used for classification applications of objects like forest or water areas (Höfle et al., 2007; Vetter et al., 2011b). In most cases the DIMs are calculated for the last or first echoes only. To receive adequate radiometric values (in a point cloud or a raster domain) an intensity correction has to be applied. A correction approach is presented by (Höfle and Pfeifer, 2007), where the range and the geometric influences are reduced. This approach is a strip-wise relative correction. Instead of a calibration the result of the correction is in digital numbers (DN) depending on the used scanner. The calibration results in radiometric information, which represent the reflectivity of the observed material (Wagner et al., 2008; Wagner, 2010). An on-line calibration of radiometric information is discussed in Pfen-

nigbauer and Ullrich (2010) for FWF systems.

For most scientific applications related to hydrology the derived terrain model is used as input. There are two main reasons for using the rasterized models instead of point cloud data. Firstly, the usability of rasterized data is much more easier than the use of the point cloud and the software tools for raster operations are widely spread and user friendly. Most of the point cloud tools need a profound knowledge of the point cloud structure and the physical properties of the used LiDAR system. Only a few commercial point cloud tools are available but most point cloud based studies are done by 'self-developed software' at the researcher's institutes. The used modeling software (e.g. hydrodynamic-numerical modeling software) uses mostly rasterized or meshed data sets as input. Some properties like vegetation structure or hydraulic friction coefficient are sometimes calculated in the point cloud domain and then transformed to a raster to use it with hydrodynamic-numerical

models.

As hydrodynamic-numerical modeling software is not able to handle huge sets of ALS data as input, the ALS data resolution has to be reduced without losing any hydrodynamic relevant terrain information as shown in Mandlburger et al. (2009). Without data reduction some numerical models (for small scale natural process modeling e.g. floods, debris flow) are not able to use the whole data resolution and complexity of ALS DTMs. The impact of more or less complex input data on numerical models are presented in Wichmann et al. (2008) by using different DTM cell resolutions for modeling debris flow. The extent of the modeled debris flow fits best to the terrestrial measured area by using a cell resolution of more than 5 m, which raises three questions. Are the input ALS data too dense and complex for the numerical model? Are the used numerical models optimized for less complex input data? Further, should future investigations concentrate on data reduction or on adapting natural process modeling algorithms for dense data set? The trends in sensor development and data collection techniques focus on the increase of sampling density and accuracy. Therefore, data complexity increases and the DTM cell resolution decreases, while numeric models are not being able to use these data. A challenge is to find a way to modify numerical models which use dense ALS data as input.

Another challenge is to find a possibility to use the existing numeric models, reduce ALS data complexity and minimize the calibrating effort of the model. Calibration is normally used to reach the assumed goal by changing some model parameters and values until the result seems realistic, which is state of the art. It is assumed that dense ALS data can improve model outputs and reduce calibration efforts.

2.3 Recent trends in LiDAR technology

The latest trend in LiDAR remote sensing can be seen on sensor development. The sensors weight and size have decreased successively within the last few years by increasing functionality and usability. This trend can be seen for both, ALS and TLS sensors.

Also in the sensor technology area a trend can be seen in shortening the pulse length while increasing the digitizing rate in the FWF sector. But also the use of FWF terrestrial scanner is a new trend which is becoming more and more important. The multi-pulse in air technology will become more popular in order to acquire data of large areas and with the space-borne LiDAR project LIST global data can be taken. In order to build a bathymetric shallow water scanner research is going on.

The use of radiometric information for classification and segmentation applications is often demonstrated in publications, because the radiometric calibration of data for accurate results is very important. Riegl plans to integrate an on-line radiometric calibration into the sensor (Pfennigbauer and Ullrich, 2010).

The potential of multi-temporal LiDAR data sets for change detection applications, large mass movement detection or flood damage estimation has been shown in several studies within the last years. Some communities, local authorities or scientists have started to collect data again (Vetter et al., 2009a), because many applications can only be done with multi-temporal data, e.g. to detect large and very slow mass movements. But to use multi-temporal data sets, a very accurate georeferencing including a strip adjustment is needed, which is not the case in most of the studies. So, user of ALS data as well as scientists should become aware of the importance of strip adjustment, radiometric calibration and filtering approaches. For those topics an intelligent software solution is necessary. With a software like

OPALS the handling of huge data sets is easy and the main topics of georeferencing, radiometric calibration and strip adjustment are implemented. Many scientific research groups or institutions are developing their own software, either as commercial software products or as open source tools in order to solve specific problems. If we focus on more interaction between scientists and their 'own-developed' software, a huge benefit in developing intelligent software solutions can be achieved. A fast progress in dealing with actual problems like organizing and storing point cloud or raster data can be assumed, if a global network of LiDAR software developer and users can be established. Another important issue is the use of standards in data collection, recording and storing. Such a standard is LAS 2, which should be the standard format. But as long as the scanning companies are not able to provide the data in such a standard, we can not expect that users use such a standard. Therefore, the focus should be on standard development and on building networks between different software developer teams.

CHAPTER

3

**Conditioning of high resolution airborne
laser scanning data for drainage network
delineation**

In this chapter a method is presented to adapt a 1m ALS (Airborne Laser Scanning) DTM (Digital Terrain Model) for drainage network delineation. 1m-DTMs are rarely used for mapping drainage networks because of the high relief energy, high amount of topographic features and the resulting negative influences, like wrong deflection of the drainage for the network delineation. This mainly applies to anthropogenic structures like roads and artificial embankments. We present a workflow to subtract the influence of roads in the DTM, replacing the actual road profile by an average hill slope of the neighboring terrain. This conditioned DTM is finally the basis for drainage network delineation using standard flow accumulation. The drainage networks are derived for four DTM variants (1m-DTM, 1m conditioned, 5m resampled and 5m conditioned DTM) and the results are compared to a reference data set. It is shown that the accuracy of the derived drainage network can be increased by 3-5% using the conditioned instead of the original 1m-DTM. The gain in accuracy amounts up to 12% if the conditioned 1m-DTM is used instead of the low pass filtered or conditioned 5m-DTM. Therefore, our conclusion is that high resolution and conditioned 1m-DTMs should be preferred instead of a coarse spatial resolution or original 1m-DTM to drainage network delineation, if anthropogenic structures, like roads, are removed strictly.

3.1 Introduction

Within the last two decades Airborne Laser Scanning (ALS) has become the prime acquisition technique for collecting topographic data in high spatial resolution (> 1 point/m²) and a good height accuracy of less than 15 cm (Wehr and Lohr, 1999; Baltsavias, 1999b), which is employed in many different fields (Höfle and Rutzinger, 2011; Mandlbürger et al., 2009; Sofia et al., 2011). While in many European countries the whole territory is already covered by ALS (NL, CH), other countries will be finishing data acquisition in the near future. Almost all European countries maintain a GIS based river network providing the main rivers, derived from low resolution Digital Terrain Models (DTMs) or topographic maps. The planimet-

ric accuracy and the completeness of the Austrian river network is currently poor, especially for small catchments. The European Water Framework Directive (WFD, EU, 2000) obligates the member countries to provide a detailed, up-to-date river network in high planimetric accuracy with additional attributes per river reach (e.g. length, bed slope, width stream ordering ...). Currently, there are activities being undertaken to standardize the data exchange on a transnational level. Respective guidelines for basic datasets have already been implemented (INSPIRE, EU, 2007).

The standard drainage delineation methods implemented in proper GIS-Software are based either on single-neighbor flow algorithms (D8, O'Callaghan and Mark, 1984) or multiple-neighbor flow algorithms like

multiple flow direction (FD8, Quinn et al., 1991). Both flow algorithms are used to compute drainage networks which indicate the potential watercourses. A comprehensive overview about flow algorithms and their differences are given by Gruber and Peckham (2009) and Wilson et al. (2008). Various implementations are available in standard GIS software providing specialized tools for individual environments. Besides flow accumulation, other methods exist to derive drainage networks and hydrological related features (Passalacqua et al., 2010, 2012).

The differences between drainage network delineation based on high spatial resolution and coarse DTMs are shown in Li and Wong (2010). The quality of a drainage network based on high spatial resolution data (e.g. 1m-DTM grid) is mainly influenced by man-made objects like streets, roads and banks, where the flow direction is deflected along the gradient of the road. Remaining bridges or missing objects like culverts or pipes acting as flow barriers, which are not represented in the DTM and yield unrealistic flow paths (Vianello et al., 2009).

3.2 Objectives

We present a study to map the potential river drainage network system by using high resolution ALS DTM in order to increase the level of detail, cor-

rectness and completeness of the final drainage system. Due to the fact that roads and streets produce massive errors for drainage network delineation (Vianello et al., 2009) it is our aim to show the positive impact of manipulating artificial structures in a high spatial resolution ALS DTM for the delineation quality. The goal of this chapter is the derivation of potential river drainage systems. Hereby, the term 'potential river' is taken to describe the watercourse following the terrain gradient under regular hydrological conditions. At locations where streets block the potential flow path, pipes and culverts are usually built to guarantee a continuous watercourse along ditches. Those pipes and culverts are dimensioned to cope with regular run-off volumes. As regular hydrological conditions are presumed in this chapter, no deflections alongside the streets are expected. As subsurface man-made structures under roads (e.g. pipes) are undetectable within ALS, the roads act as walls or barriers if they are not removed from the ALS DTM prior to the drainage delineation. As many countries already have a 1m-DTM available, the goal is to exploit the full potential of those data as source for drainage network delineation, which is not the case up to now (Mandlbürger et al., 2011b). Therefore, we present a method to condition a DTM by section-wise recalculating the near-natural slope before the road has been constructed and by replacing the actual road profile based on the average hill slope. This yields a conditioned 1m-

DTM without streets. The results are compared to a reference data set provided by the local mapping authority. We assume that the conditioning of the DTM leads to a better drainage network mapping accuracy when applying automatic delineation based on flow accumulation.

3.3 Test site and data

The chosen test site is a sub-catchment of the Bregenzer Ach (Vorarlberg, Austria) draining the Bregenzerwald. The Bregenzer Ach is an alpine river with an approximate length of 80 km, a total catchment area of 830 km², an average annual discharge of 46 m³/s and a maximum discharge of 1350 m³/s, which was measured in August 2005, as a 100 year flood event (Amt der Vorarlberger Landesregierung, 2005). The selected sub-catchment covers an area of 93 km² and is divided into an upper (Bolgenach) and a lower (Weißache) sub-catchment (cf. Figure 3.1, green and red). The terrain elevations range from 450 m at the confluence of the Weißach and the Bregenzer Ach to 1645 m at the Feuerstätterkopf. The dominant geological formation is Molasse with a dense drainage system (Egger et al., 1999).

For the test site Airborne Laser Scanning data are available from different epochs. For this study the Digital Terrain Model derived from the point

cloud, using the hierarchic robust filtering approach described by Kraus and Pfeifer (1998), of the November 2003 campaign, has been chosen. The average point density is 1.6 points/m² (last echoes). The data were collected with Optech's ALTM 2050 scanner in discrete echo recording with a maximum of four reflections per laser shot. The provided terrain model features a spatial resolution of 1m (regular grid). Based on the original 1m-DTM, an additional resampled 5m model was calculated.

Besides the topographic data, a street and a drainage network layer were provided by the local mapping authority (Landesamt für Vermessung und Geoinformation, LVG). The street layer contained several files each of them representing a different street/road type like high order streets, municipal roads, forest roads or hiking trails. The layers were produced by different departments within the authority of Vorarlberg on the basis of ortho images and shaded relief maps of the 1m-DTM. Before using the data in the actual processing, a consistency check was performed and the different layers were merged into a single data set. The street locations are checked by a visual inspection. The streets locations are in a range of maximum 5m compared to the shaded relief map of the 1m ALS DTM.

The drainage network data set was provided by the local hydrology and geoinformation department (Abteilung

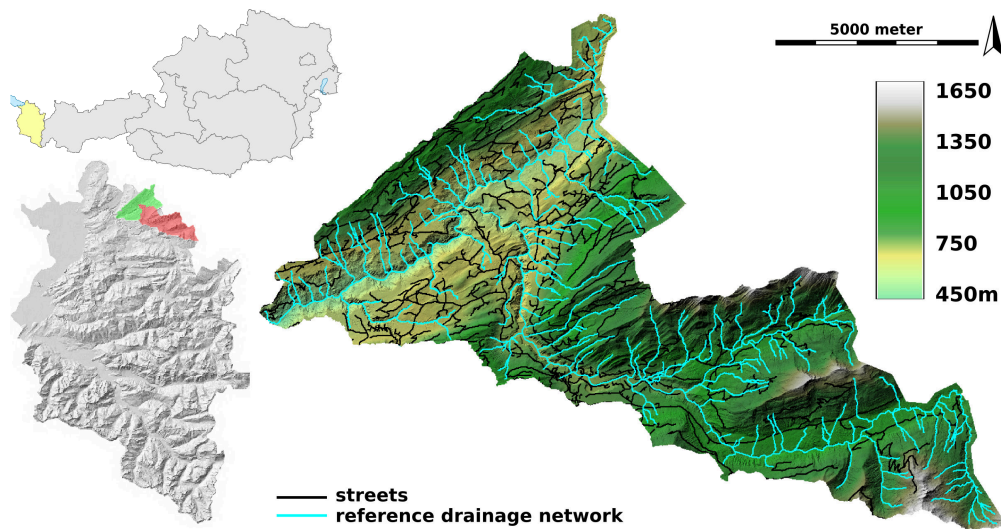


Figure 3.1: Test site (Bregenzerwald, Vorarlberg, Austria); shading superimposed with elevation coding, roads and existing river network. Map sources: Austria: Wikimedia.org as svg; Vorarlberg: <http://vogis.cnv.at/> (WMS); catchments, streets and official drainage network: Landesamt für Vermessung und Geoinformation (LVG, Amt der Vorarlberger Landesregierung).

Wasserwirtschaft; Landesamt für Vermessung und Geoinformation). This data set has been mapped in a semi-automatic way by deriving the main drainage network using standard flow accumulation methods based on the mentioned 1m ALS DTM from 2003. Based on the resulting vector data set, interactive editing has been applied using ortho images and 1m shaded relief maps to improve the correctness and completeness of the data set. This data set also includes all culverts, piped sections, bridges and fictive axes through lakes. The provided drainage network is constantly being improved and entirely supervised by hydrology experts and is the best available data set covering the entire area of one single fed-

eral state in whole Austria. The latest timestamp of the river network reference data is October 10, 2012. Those data are used for evaluating the presented methods. Although there is a time difference between the ALS DTM and the reference data set, this time gap is of minor importance, because no streets have been built and no major mass movements or other natural hazards have occurred. Only in one part a huge land slide is being currently active but in this area no streets are located.

3.4 Methods

The method relies on two data sets. The first data set is the ALS DTM with 1m spatial resolution, which is used as basic input for the conditioning workflow, presented later, and the drainage network delineation process. The second is a vector (polyline) layer representing the axes of the existing streets. Whenever possible street data from the local mapping authorities should be used as these datasets are generally well maintained in Europe concerning both, accuracy and up-to-dateness. If no such official data source is available, street layers can also be extracted from OpenStreetMap (OSM) or can be obtained from commercial navigation and routing system providers. If no centerlines of the streets are available, they can be derived by using a multi-scale segmentation approach (Baatz, 2003) or a raster based classification approach using elevation, slope, aspect and curvature (first and second order derivatives) as shown in Wood (1996), Brügelmann (2000) or Rutzinger et al. (2011b). The street areas can be used to get the centerlines. By using a point cloud based break-line detection approach as described in Briese (2004), the upper and lower edge can be used to calculate the centerline.

The developed workflow is shown in Figure 3.2, where the street layer is the main input (1) for DTM conditioning. First, the centerlines of the streets are buffered to define the extent for DTM

conditioning (2). Then, perpendicular lines (cross sections) with a fixed distance along the street axis and a predefined length are created (3). For each cross section the X,Y,Z coordinates of the start and end point are fetched from the ALS DTM and the intermediate point coordinates are calculated by linear interpolation, which results in an upper, middle and lower X,Y,Z coordinate triple (4). Further, all extracted points of a single street line are triangulated (5) and from the resulting TIN a regular grid of the buffer area (6) is derived representing the reconstructed near-natural slope. Finally, the buffer from step (2) is used to clip the ALS DTM (7) and, by a map algebra operation, the clipped ALS DTM and the reconstructed slope along the street are fused to the conditioned 1m-DTM (8), containing no streets.

In order to evaluate the influence of different spatial resolutions of the data, a resampled 5m-DTM is derived by applying an average filter (5x5m kernel). To simulate the influence of a coarser resolution on the final drainage network product, the 1m-DTM was down-sampled to 5m-DTM instead of using an other data set. The down-sampling was chosen to guarantee the comparability of the derived drainage systems using the same data source as for DTM conditioning. So, both models, the original and the conditioned 1m-DTM, are down-sampled. Therefore, four different DTM variations are used (origi-

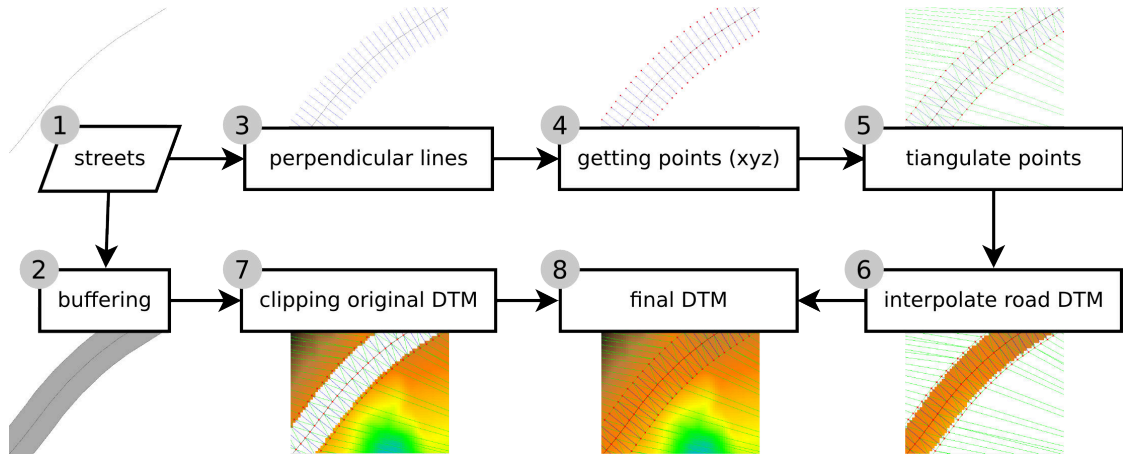


Figure 3.2: Workflow and processing chain for DTM conditioning (following the numbers).

nal 1m-DTM, conditioned 1m-DTM, re-sampled 5m-DTM and conditioned 5m-DTM).

For drainage network delineation, a standard flow accumulation method based on Multiple Flow Directions (MFD, FD8) is used to compute the drainage network, as implemented in GRASS-GIS (`r.stream.extract`, Jasiewicz and Metz, 2011; GRASS Development Team, 2013).

For the error assessment a line based approach as described in Rutzinger et al. (2012) is chosen. For each data set (i.e., reference and the derived drainage network) the lines are transformed to points with a fixed distance. The resulting point layers are analyzed by finding corresponding points of the reference layer in the derived drainage (correctness measure). Completeness is calculated from classification (drainage) to reference. Points

from both layers are accepted as corresponding, if they lay within the related search radius. Correctness and completeness are calculated for different search radii (1m, 5m, 10m and 15m). This provides a separation into true positives (TP, correctly identified in both), false positives (FP, reference corresponds to the derived layer) and false negatives (FN, derived layer corresponds to reference). Correctness (equ. 3.1), completeness (equ. 3.2) and quality (equ. 3.3) are calculated for each radius.

$$Correctness = \frac{TP}{TP + FP} \quad (3.1)$$

$$Completeness = \frac{TP}{TP + FN} \quad (3.2)$$

$$Quality = \frac{TP}{TP + FP + FN} \quad (3.3)$$

3.5 Results

In this section we present the results of data processing (DTM conditioning) as well as the comparison of the different drainage networks obtained by using the respective DTM variants: original and conditioned 1m-DTM and down-sampled 5m-DTM (with and without DTM conditioning). The comparison is carried out both, by visual inspection of the achieved drainage networks and by statistical analysis of the accuracy with respect to the reference data. The street layer is the main input for the workflow. The input street layer is a compilation of different layers with varying qualities and up-to-dateness, as mentioned in the method section

3.5.1 DTM conditioning

The used parameters for the DTM conditioning are a) the buffering distance, b) cross section distance along the street axis, and c) the length of the cross sections. The buffering distance a) is strongly related to the cross section length c). Because the length c) has to be larger than the buffering distance to guarantee that no data holes are produced during data fusing (e.g Figure 3.2, step 8). The cross section distance b) controls the granularity of the interpolated slopes and therefore should be kept small. If distance c) is too large, the linear interpolation (using a

delanay triangulation) has less interpolation points and results in a coarse representation of the near-natural slope. The used parameters are a): 7 m for buffering, results in a buffer width of 14 m, which is equal to a four lane road; b): 3 m distance along axis; c): 16 m in length for the cross sections. During the workflow (cf. Figure 3.2, step 4) the X,Y,Z coordinates of the start and end points of the cross sections are fetched from the DTM and the middle point coordinates are calculated by linear interpolation of the start and end point. All three coordinate points are used for the triangulation. If the ratio $c/3b$ is too large, the triangulation fails in curved road sections. Therefore, the ration should be lower than 2:1.

Figure 3.3 shows a color coded height difference image for a short street section. Three cross sectional plots based on the original and the conditioned 1m-DTM illustrate the straightening of the profile. Within the plots the original hill slope of the DTM is shown in blue and the conditioned profile in red. By using the three coordinate triples for the interpolation, the near-natural slope can be supposed as a reliable estimate for the near-natural slope before the road has been constructed. The interpolation is carried out for all streets and roads within the provided street layer, which results in a DTM where all roads are removed and replaced by the near-natural slope. This conditioned DTM is finally the basis for the fur-

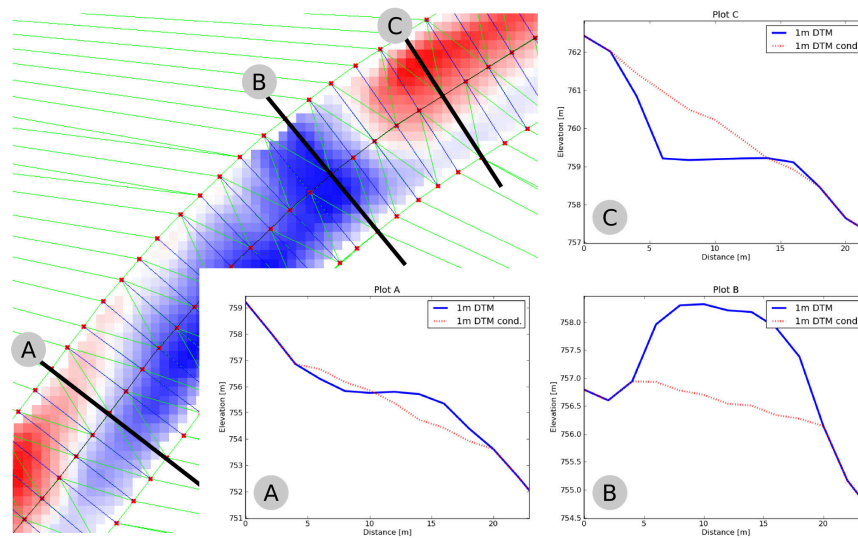


Figure 3.3: Difference between original and conditioned 1m-DTM with streets centerline (black), cross sections (blue), interpolation points (red) and triangulation (green); sections through original and conditioned DTM (DTM blue solid line, conditioned DTM red dashed line).

ther calculations of the drainage network. The conditioned 5m-DTM is calculated by resampling the conditioned 1m-DTM.

3.5.2 Drainage derivation

The Multiple Flow Direction was calculated based on the 1m and on the 5m resampled DTM with and without DTM conditioning. The parameters for drainage network delineation are I) minimum catchment area (2.5 ha) and II) minimum segment length (>100 m). Both are applied to the 1m and 5m-DTMs to produce comparable results. A discussion about different drainage delineation parameters is not given in this chapter.

The drainage networks based on the four different DTM variants are shown in Figure 3.4. It is clearly visible that the 1m-DTM results in many drainage segments alongside the streets (Figure 3.4a). A drainage segment is a part of the stream network which is between two nodes (nodes are intersection points, confluence points, source or end points). These problems are reduced but not completely removed by using a resampled 5m-DTM (Figure 3.4b). Using the proposed DTM conditioning along the streets, the artificial flow patterns are more effectively removed and the high level of detail is preserve at the same time (Figure 3.4c). The use of a conditioned 5m-DTM (Figure 3.4d) shows no deflection at all along the

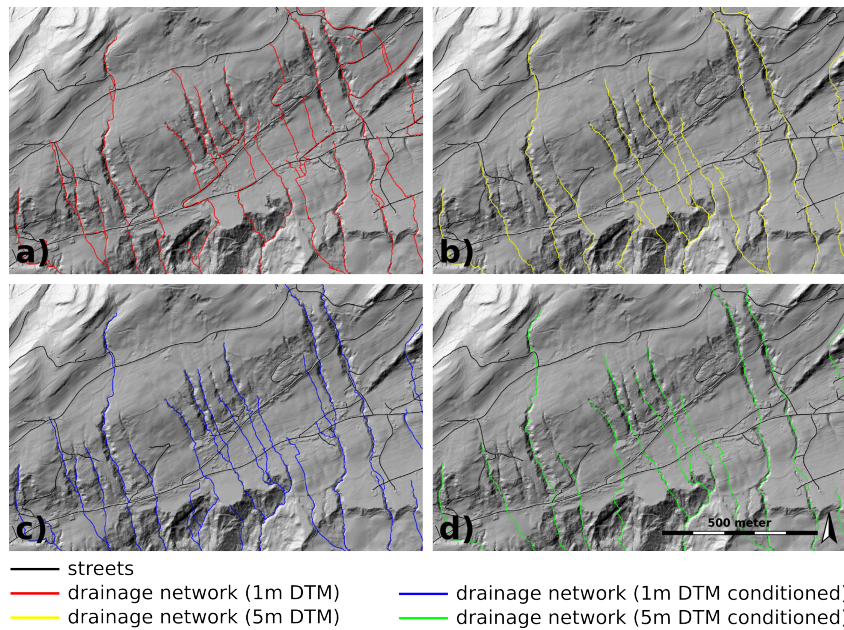


Figure 3.4: Drainage network based on original and conditioned DTMs (1m, 5m). a) 1m-DTM; b) resampled 5m-DTM; c) conditioned 1m-DTM; d) 5m conditioned DTM.

roads.

The differences between the results of the drainage network based on the original and conditioned DTMs are shown in Figure 3.4e (1m) and Figure 3.4f (5m). The deflection of delineated drainage segments is higher for the original 1m and the 5m resampled DTM as for both conditioned models. By resampling the DTM, small but sometimes relevant terrain features are removed. If an important terrain feature is removed, the direction of the drainage can be changed dramatically and can result in a wrong final network. This phenomenon can be seen in Figure 3.4b and Figure 3.5a alike. The level of detail of the derived drainage network

also decreases if a down-sampled 5m-DTM is used. On the one hand, the length in the direction to the stream source decreases and on the other hand, the spatial resolution and, therefore, the stream mapping accuracy also decreases.

3.5.3 Accuracy of the derived drainage network

A visual comparison of the derived drainage system of both conditioned DTMs (1m and 5m) and the provided official drainage system is presented in Figure 3.5a. The completeness of the derived drainage network based on the 1m conditioned DTM is satisfying. A

few locations at the stream head are missing, where the stream head is close to the catchment boundary. This results from the used catchment area threshold for the drainage network delineation. As can be seen in Figure 3.5a and 5b more stream candidates derived from the 1m conditioned DTM occur than in the official drainage network. The cumulative lengths of the reference data and the derived drainage networks are analyzed in Table 3.1. The reference subset (cf. Table 3.1) is a selection of the original reference data set, where all piped and fictive river segments are removed. Whereas, 7.5% of the reference data are segments which are fictive or piped sections (reference subset, Table 3.1). Those 7.5% are the difference between the reference and the reference subset (cf. Table 3.1). The derived network based on the conditioned and original 1m-DTM is more than two times the length of the reference (cf. Figure 3.5) and the drainage based on both 5m models are approx. 1.4 times longer than the reference, where a small part of the differences in length occur from the raster pattern (zig-zag), presented in the derived data. However, most of the differences occur from the high amount of drainage segments and the extended length. As can be seen in Fig. 5a, the test site contain piped sections alongside the road and consequently, the reference data set shows flow paths following the course of the road. In this specific case the piped section is a measure to prevent mass movements. As our approach can not

deal with such a piped section along the road. The evaluation was carried out without the respective piped sections in the reference data set (all in Table 3.2 & 3.3).

A 1m point spacing is used for the error assessment for all drainage networks and the reference data. The percentages of completeness, correctness and the quality are shown in Table 3.2. For all measures the reference data subset (cf. Figure 3.1) is used, which is the reference data set without non-overland drainage segments.

3.6 Discussion

The presented method of DTM conditioning, using existing street data to replace and remodel near-natural slopes along the roads, uses a global constant street buffer width. A global width was chosen as the GIS metadata of the reference do not contain any road classification information. It is assumed that a street width dependent buffering increases the quality of the conditioning process. As shown in Table 3.2, the completeness of the derived river network is much better than the correctness for all considered DTM variants using all derived stream segments. The completeness is almost the same for both 1m models, but up to 17% better between 1m and 5m-DTMs. Whereas, the correctness and the quality measure is

3 DTM conditioning

data	reference	reference subset	1m DTM	1m DTM cond.	5m DTM	5m DTM cond.
length [m]	246163	227688	518250	495106	353501	346980
percentage	100.0	92.5	210.5	201.1	143.6	141.0

Table 3.1: Cumulative length of networks, reference data, reference data without the fictive and piped sections (reference subset) and derived networks based on original DTM and conditioned DTM (1 & 5m).

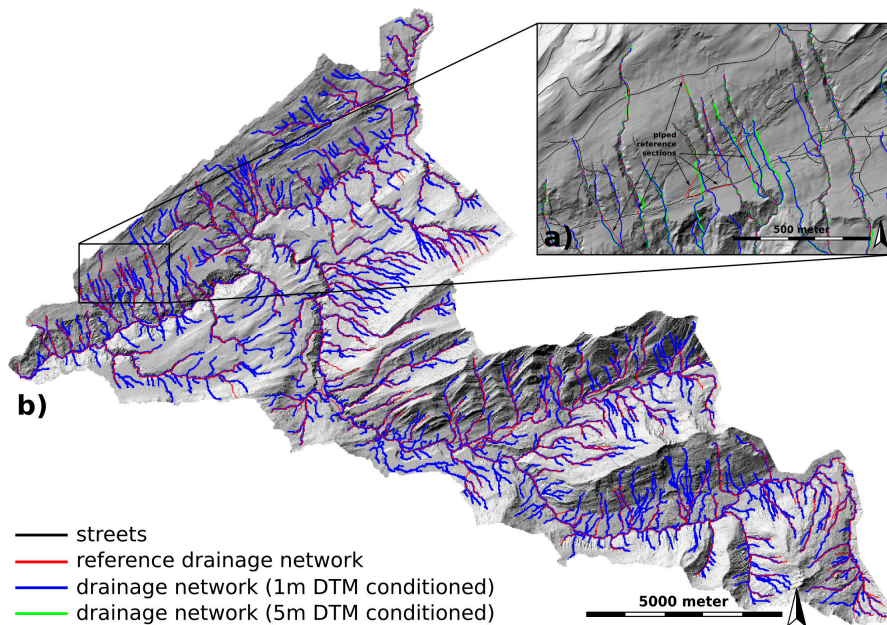


Figure 3.5: Results of drainage network delineation. a) drainage from conditioned 5m-DTM (green), conditioned 1m-DTM (dark blue) and the reference network (red), b) whole test site, 1m conditioned DTM and reference data.

all segments	1 radius			5 radius			10 radius			15 radius		
	comp.	corr.	quality	comp.	corr.	quality	comp.	corr.	quality	comp.	corr.	quality
DTM 1m	0.50	0.21	0.17	0.85	0.35	0.33	0.90	0.37	0.35	0.92	0.38	0.36
DTM 1m cond.	0.50	0.22	0.18	0.86	0.37	0.35	0.91	0.39	0.38	0.92	0.40	0.39
DTM 5m	0.33	0.20	0.14	0.78	0.47	0.42	0.83	0.50	0.46	0.85	0.51	0.47
DTM 5m cond.	0.33	0.20	0.14	0.79	0.48	0.43	0.84	0.51	0.47	0.86	0.53	0.48

Table 3.2: Error assessment (completeness, correctness and quality); complete drainage network compared with the reference subset (cf. Table 3.1, without piped segments).

much better for the 5m models. However, this is mainly due to the fact that more streams are detected using the 1m models. Therefore, additional error assessments are presented in Table 3.3. The presented method of DTM conditioning, using existing street data to replace and remodel near-natural slopes along the roads, uses a global constant street buffer width. A global width was chosen as the GIS metadata of the reference do not contain any road classification information. It is assumed that a street width dependent buffering increases the quality of the conditioning process. Additionally, the main rivers are excluded from the error assessment in the second part of Table 3.3 (Selection II) because the width of the Weißache and the Bolgenache is between 20 m and 50 m. For streams of that size, the planimetric accuracy of the river axis (centerline) based on flow accumulation is of low accuracy (derived line is meandering). For deriving the centerline of the main river in an accurate way more suitable approaches exist. Applicable methods are presented by Höfle et al. (2009) and Vetter et al. (2011b), where the backscattered intensity data from the ALS point cloud are included in the classification process.

The accuracy measures in Selection III of Table 3.3 are calculated for 96 reference data segments (same segments as shown in Figure 3.5a without piped and fictive sections). For those segments the derived drainage segments are se-

lected and cut to the same length as the reference, resulting in 153 drainage segments which spatially correlate to the reference segments. So, all fictive and underground sections as well as all additional segments, which are not included in the reference data set are cut out.

As shown in Table 3.2 and 3.3 the completeness measure is higher for the derived drainage network using the conditioned 1m-DTM than the drainage derived based on the original 1m or both 5m-DTMs. The correctness is the higher for the conditioned 1m-DTM compared to the other DTMs within the 1m search radius (Table 3.2). If the main river is included (Table 3.2) in the classification, the correctness of the streams based on the coarse resolution DTMs is higher. In Table 3.3 both, correctness and completeness are higher for the 1m conditioned DTM streams.

As mentioned in the method section the completeness is calculated from all reference candidates to the derived drainage and the correctness from the derived drainage to the reference data. The correctness is lower than the completeness, because only overland stream segments from the reference data are used. In contrast to that, the piped and fictive stream segments are existing in the derived network as a result of the DTM conditioning. Those segments can not be detected automatically. The correctness measures are in the same range or even higher for

3 DTM conditioning

	1 radius			5 radius			10 radius			15 radius		
Selection I	comp.	corr.	quality	comp.	corr.	quality	comp.	corr.	quality	comp.	corr.	quality
DTM 1m	0.49	0.36	0.26	0.83	0.61	0.54	0.88	0.65	0.60	0.90	0.66	0.62
DTM 1m cond.	0.49	0.38	0.27	0.85	0.65	0.58	0.90	0.68	0.63	0.91	0.70	0.65
DTM 5m	0.32	0.27	0.17	0.77	0.65	0.54	0.82	0.69	0.60	0.84	0.71	0.62
DTM 5m cond.	0.33	0.27	0.17	0.78	0.65	0.55	0.84	0.69	0.61	0.86	0.71	0.64
	1 radius			5 radius			10 radius			15 radius		
Selection II	comp.	corr.	quality	comp.	corr.	quality	comp.	corr.	quality	comp.	corr.	quality
DTM 1m	0.54	0.40	0.30	0.85	0.63	0.57	0.88	0.65	0.59	0.89	0.66	0.61
DTM 1m cond.	0.55	0.42	0.31	0.87	0.67	0.61	0.89	0.69	0.64	0.90	0.70	0.65
DTM 5m	0.34	0.29	0.19	0.77	0.66	0.55	0.80	0.68	0.58	0.81	0.69	0.60
DTM 5m cond.	0.35	0.29	0.19	0.79	0.65	0.56	0.82	0.68	0.59	0.84	0.69	0.61
	1 radius			5 radius			10 radius			15 radius		
Selection III	comp.	corr.	quality	comp.	corr.	quality	comp.	corr.	quality	comp.	corr.	quality
DTM 1m cond.	0.63	0.55	0.41	0.97	0.84	0.83	0.99	0.86	0.85	0.99	0.86	0.86

Table 3.3: Error assessment (completeness, correctness and quality); Selection I: all derived drainage segments spatially correlating with reference data segments are considered; Selection II: as in Selection I, but excluding main channels; Selection III: 153 selected drainage segments without piped and fictive river sections (selection area as in Figure 3.5a).

the coarse spatial resolution DTMs instead of the 1m-DTMs. This occurs mainly from the amount of derived segments (cf. Table 3.1) and within the subset I of Table 3.3 and 3.2, where the main river is included in the classification.

The accuracy of the derived drainage network is in average 3 to 5% more accurate for all three measures (completeness, correctness and quality), using the presented conditioned DTM, than the original 1m-DTM. We consider a 5% increase in quality as a relevant improvement. It is crucial to mention that not all man-made structures necessarily have high impact on the natural run-off. In other words, in most cases the run-off is dominated by the overall natural relief. Thus, the improvement potential in terms of 'gain of accuracy in

percent' is within narrow bounds, but nonetheless the remaining 5% improvement may locally make up a big difference. Comparing the conditioned DTM with the results of coarse spatial resolution DTM, the average is between 1 and 12% better using the conditioned DTM. The main differences between 1m and 5m results are in the completeness and only minor differences occur in the correctness. By using coarse resolution input data, the possibility of deflecting the derived drainage segment is much more evident. Some terrain features are resampled or erased, because of the resampling of a 1m-DTM to a 5m-DTM. Therefore, the flow accumulation follows a wrong slope (e.g. drain to a neighboring valley, cf. Figure 3.5a).

3.7 Conclusion

The main goal of this chapter is to find out, whether there is a benefit of using high resolution ALS elevation models for river network delineation? If so, what has to be considered to avoid maximum detail of drainage delineation accuracy and overcome the anthropogenic effects, which are existing in the elevation model? We conclude the use of high resolution ALS DTMs for river network delineation produces results in a high level of correctness and completeness, as anthropogenic effects, especially roads and streets, are removed strictly. Furthermore, high spatial resolution ALS DTMs for river drainage delineation applications have to be preferred instead to coarse resolution DTMs, because the resampling influences the flow accumulation especially at transition zones between torrent valleys. And finally, coarse spatial resolution shows to have a negative impact on the correctness and completeness of deriving river networks, based on flow accumulation methods, advocating for the use of high spatial resolution ALS DTMs, which are currently available on a country-wide level.

Quality and accuracy of derived drainage networks are strongly related to the input elevation data set and their spatial resolution. Not the whole potential of available high resolution DTMs from ALS have been used up to now, because of the influences of features

like streets for the delineation process. The main advantage of the DTM conditioning is that the deflections along the roads and streets, which are occurring during the flow accumulation process, are minimized. Therefore, the streets and roads are replaced by the near-natural slope. So, high resolution and conditioned DTMs are used for drainage network delineation resulting in a maximum available level of detail, correctness and completeness of the derived drainage network as the anthropogenic effects are removed strictly. The comparison of derived drainage networks based on four different DTMs show the potential of conditioned 1m-DTMs in the field of drainage network delineation.

An accurate, correct and complete drainage system is a mixture of an accurately derived drainage network, a complete data base of additional information like locations of bridges, pipes, culverts and the local knowledge of an expert, who is able to connect those information to one consistent data set. By using a conditioned 1m-DTM as input for flow accumulation, one part of getting an accurate drainage system can be optimized. By providing dense and accurate network, as presented, expert knowledge can be used for more sophisticated things than digitizing lines on ortho photos or shaded relief maps. But the proof of an expert is an essential part, because the flow accumulation methods are not able to distinguish between different features

influencing the drainage. Therefore, an automatically derived drainage network can not be derived 100% correctly in an anthropogenic affected environment.

By using conditioned 1m-DTM for drainage network delineation an increase in accuracy is shown. This finally results in the ability to use the whole potential of high resolution DTMs for drainage delineation processes. Besides this advantage there are also major disadvantages namely the computation time and area. The time of computation increases significantly if a 1m-DTM is used instead of a 5m or even coarse DTM, while the computation area decreases. The presented approach of DTM conditioning works locally. Therefore, the area of interest is not limited from this point of view. Limitation concerning the size of computation area is only caused by flow algorithm. The computation time of conditioning and drainage delineation is almost balanced. The presented method is created for drainage network delineation with the best available accuracy for small catchments with a minimum of ex-post editing of the results. By minimizing the delineation

errors, which mainly occur from the roads, the interactive editing part is minimized, while the accuracy and density of the derived drainage network is maximized.

3.8 Acknowledgments

The authors want to thank the 'Landesamt für Vermessung und Geoinformation' of Vorarlberg, Austria, namely to Peter Drexel for providing the elevation data as well as the reference data set of the drainage network. To the colleagues Bernhard Höfle from the University of Heidelberg and Martin Rutzinger from the University of Innsbruck for supporting the accuracy measure calculation. This study was co-funded by the Austrian Federal Ministry of Agriculture, Forestry, Environment and Water Management (Project: BIMLFUW-UW.3.2.5/0040-VII/2010). We would also like to acknowledge the financial support from the Austrian Science Funds (FWF) as part of the Vienna Doctoral Programme on Water Resource Systems (DK-plus W1219-N22).

CHAPTER

4

Water classification using 3D airborne laser scanning point clouds

Airborne laser scanning (ALS), also referred to as airborne LiDAR (Light Detection And Ranging), provides highly accurate measurements of the Earth surface. In the last twenty years, ALS has been established as a standard technique for delineating objects (e.g. buildings, trees, roads) and mapping changes. Studies on hydrology or geomorphology such as monitoring of braided river structures, calculation of erosion and accumulation potential in watercourses, or floodplain mapping require all the precise location of the water surface. This chapter shows a 3D point cloud based method, which allows an automatic water surface classification by using geometric and radiometric ALS information and the location of modeled lost reflections, which are called laser shot dropouts. The classification result can be used to map the watercourse, to improve DTM filtering routines or to replace water points with river bed heights for hydraulic modeling etc.

The method relies on a threshold based classification using geometry and radiometric information of the 3D point cloud. The method is divided into five major steps. First, we correct the amplitude values by reducing the atmospheric and geometric influences to the laser shots. A radiometric adjustment was applied to the amplitude values of the data sets, which allows multi-temporal analysis of the amplitude values. The second step is the interpolation of the coordinates of the laser shot dropouts, which are the most important input to delineate water surfaces. In step three and four the two attributes (standard deviation of height values and the amplitude density ratio value) are calculated at a fixed distance to each reflection and dropout. These are used in step five to distinguish water and dry land points. The exploration of the attributes for the classification and the evaluation of the classification results are done by comparing the results to a terrestrial orthophoto mosaic and dGPS measurements, which were taken simultaneously to the ALS campaign.

One of the major tasks is the use of modeled laser shot dropouts within a threshold based classification method to distinguish water and non-water echoes. The method is also suited to detect water under riverine vegetation, which is problematic by using data from sensors, that are not able to penetrate vegetation. The classification accuracy is about 95%. The achieved amplitude correction and the radiometric adjustment make the data sets comparable and allow to calculate changes in the channel flow paths within the different flights.

4.1 Introduction

The use of airborne laser scanning (ALS) has developed to the state-of-the-art technique for topographic data acquisition in the last twenty years. Most ALS sensors record the reflected laser

beam as X,Y,Z coordinates and the signal amplitude (also referred to as intensity) as a three-dimensional point cloud. Depending on the scanner type, single, multiple-echoes or even the full-waveform (Wagner et al., 2004; Briese et al., 2008) can be recorded. Most ALS

driven applications use Digital Surface Models (DSMs) or Digital Terrain Models (DTMs) in raster format computed from the 3D point cloud. To generate those models the point cloud is filtered and classified in e.g. ground, vegetation and building points (Sithole and Vosselman, 2004).

Most hydraulic applications use the modeled water surface, derived from a meshed or rasterized DTM, to calculate the volume of the water body, the flow velocity, the floodplain area or to compute flood simulations (Mandlbürger et al., 2009). The analysis of different ALS data sets makes the monitoring of changes in the watercourse and the flow path of rivers possible. The presented method demonstrates the ability to map water surfaces by using the 3D point cloud information. The calculation of radiometric adjusted amplitude values of multi-temporal ALS data makes the single data sets comparable to each other.

We demonstrate a new approach to distinguish water and non-water echoes from the 3D ALS point cloud by using geometry and signal amplitude values. We use this ALS data instead of optical images or radar data sets because the ALS data provide more information about the surface structure and has the positive effect that ground reflections beyond vegetation are recorded. It is possible to detect reflections (location and amplitude), which are lying on as well as under vegetation. The amplitude values under vegetation

are uninterpretable because of the unknown backscattering properties. Furthermore, the raster interpolation error is not present in point data sets. The advantage of the used data is that land, vegetation and water points can be distinguished. By using radiometric adjusted data sets just one set of classification parameters has to be found because the amplitudes of the different dates are comparable. The results of the presented classification can be used to improve DTM and DSM filtering. Furthermore, the combination of the topographic riverbed information computed from measured river cross sections and the derived water surface is essential to calculate a DTM of the watercourse (DTM-W). Such a DTM-W can be used as basis for hydraulic models (Brockmann and Mandlbürger, 2001; Mandlbürger et al., 2009).

The chapter is structured as follows. In section 4.2, the interaction of laser light in the near infrared wavelength with water and the related work on different water surface delineation methods are discussed. The test sites are presented in section 4.3 including the reference data production part. In section 4.4 the amplitude correction and the radiometric adjustment method, the laser shot dropout modeling routine, the data exploration and the classification method are explained. In section 4.5 the classification results are demonstrated. Finally, in sections 4.6 and 4.7 the results are discussed and a conclusion is

given.

4.2 Background

4.2.1 Interaction of near infrared laser light with water

Electromagnetic waves with 1064 nm wavelength, which are emitted by the Optech's ALTM 3100 (Optech, 2008), have special characteristics when they hit the water surface. Most of the emitted laser pulses are reflected specular on the water surface and a few are absorbed. The reflectance and absorption rate depend on the angle of incidence and the wavelength of the laser light (Wolfe and Zisis, 1989; Jensen, 2007). The incidence angle on water surfaces is almost the same as the scan angle of the laser range vector because of the low local slope of the water surface. If laser beams have an incidence angle larger than 9° , most of the light reflect specularly, but not in the direction of the ALS receiver, which is the reason for the high number of dropouts (Brzank et al., 2008; Höfle et al., 2009). In general, the water surface roughness is not homogeneous because of waves. So the specular reflected laser beam is fragmented into small single reflections. All of them are reflected in different directions because of different angles of incidence, which are a result of the locale slope and the roughness of the water surface within the laser footprint. The Bidirectional Reflectance Distribution Func-

tion (BRDF) of water is not Lambertian. Some of those reflections can reach the receiver. If there is not enough energy to detect an echo at the receiver, it won't be recorded (dropout). If there is enough energy at the receiver the echo will be detected at a very low amplitude. Incidence angles near 0° (nadir) most likely lead to specular reflections (i.e. if the water surface is smooth), which causes extremely high amplitude values (section 4.4.3.1) (Höfle et al., 2009).

4.2.2 Related work

Various remote sensing techniques are used to delineate water surfaces for floodplain mapping, natural hazard forecasting, water depth measurements, etc. The air- and spaceborne optical sensors provide the most common and popular data for classifying different land cover classes including water areas (Ustin, 2004; Jensen, 2007; Marcus and Fonstad, 2008). Many features can be derived for water by using the information of multi-spectral optical sensors (e.g. suspended load, proportion of organic material, water depth, etc.) (Jensen, 2007). Optical data are used for landcover classification and monitoring of large areas. The combination of optical data with near-infrared information is a standard method for water surface delineation.

Radar sensors are used for soil moisture mapping, floodplain mapping, water stage modeling etc. (e.g. Hall

(1996), Ustin (2004) and Crétaux and Birkett (2006)). The advantage of using spaceborn radar is the fast revisiting time of the sensor, the global coverage, the high accuracy and spatial resolution of the data especially of TerraSAR-X (SpotLight, 1 m) and the independence of weather situations (especially for tracking the water stage during and after flood events) (Schumann et al., 2007).

In the last few years, measurements with ALS have been established as an additional group of sensors for the data acquisition of the Earth surface. A large number of methods are available for measuring, monitoring and delineating features. ALS data are mostly used to generate Digital Surface Models (DSMs), Digital Terrain Models (DTMs) for the detection of buildings, trees, roads, etc. (Kraus and Pfeifer, 1998; Vosselman, 2003; Rutzinger, 2008) or to distinguish different surface classes (e.g. snow types) (Höfle et al., 2007). In bathymetry, ALS systems with two wavelengths are used to measure through the water body to derive the elevation model of underwater objects and the bottom of rivers, lakes, or the ocean (Irish and Lillycrop, 1999; Guenther et al., 2000).

In hydraulics, ALS data are used as raster or triangulated mesh models. Those are the basis for hydraulical models (Mandlbürger et al., 2009). By generating river bed models out of measured river cross sections (Brockmann

and Mandlbürger, 2001; Vetter et al., 2008) the ALS DTM can be modified and updated for hydraulical applications. Brügelmann and Bollweg (2004) and Mertes (2002) show different applications of ALS data for monitoring river environments using rasterized data.

Antonarakis et al. (2008) present an object-based classification method for delineating the water surface by using an elevation and an intensity model. They classify water by combining both rasters with near-infrared SPOT images, which have low intensities in the water areas. The delineation accuracy of raster based methods are always in the resolution of the used input models. To compute the location of the water surface only a few methods are established by using the 3D point cloud information (Brzank and Heipke, 2006; Höfle et al., 2009). Brockmann and Mandlbürger (2001) integrate the ALS points and an interpolated river bed model, which is generated from measured river cross sections, to derive the water-land boundary as well as the height of the water surface. Another approach is demonstrated by Brzank and Heipke (2006), who use a strip wise classification method by calculating a membership function for each point. As parameters they use the height information, slope, amplitude, missing points (not modeled, only the gap between two reflections) and the point density to classify water and land points in the Wadden Sea. Höfle (2007)

and Höfle et al. (2009) figured out that the use of corrected signal amplitudes, the standard deviation of height values and modeled dropouts can be used to run a seeded region growing segmentation to derive water surface information. Those methods operate on the 3D point cloud. The results are of high position accuracy and can be used as input for accurate hydraulic models.

4.3 Test sites and data

Three different river sections, which are located in Austria, covered by seven ALS data sets are used in the following study. We use different types of rivers and various ALS data sets (Tab. 4.1), with different water conditions, river geometries, morphological parameters, point densities, sensor parameters, vegetation covering, etc. in order to test the parameter settings and to demonstrate the robustness of the method.

4.3.1 Test sites

The test site at the Hintereisfernerbach is located in the upper Ötztal (Tyrol) at the glacier forefield of the glacier Hintereisferner ($46^{\circ}49'13.77''$ N; $10^{\circ}48'23.58''$ E). Five ALS flights are available at this test site, which were taken in the years 2003 to 2007 between

August and November (Geist and Stötter, 2007). One orthophoto is available from the flight of August 12, 2003 (H03).

This test site was chosen because of the available time series and the special river structure. The Hintereisfernerbach near the glacier is a braided river with a lot of sand and gravel bars in the channel, high suspended load and a turbulent, rough water surface, which makes the classification of water complex.

The test site at the Venter Ache is located in Zwieselstein (Ötztal, Tyrol; $46^{\circ}56'09.17''$ N; $11^{\circ}01'21.53''$ E). It is the reference area of the ALS campaign at the Hintereisferner of October 11, 2007 (H07). For this test site a terrestrial orthophoto mosaic was computed (sec. 4.3.2) which was used to check the relevant attributes for the classification method.

The Venter Ache near Zwieselstein is a torrent with many rocks in the channel. The water surface is characterized by a rough surface and fast flowing channel sections. At the edges of the channel many pools are located, surrounded by gravel and sand, with slow flowing and a smooth water surface.

	Date	p/m ²	Altit.[m]
H03	12.08.2003	2.0	1000
H04	05.10.2004	2.0	1000
H05	12.10.2005	2.0	1000
H06	08.10.2006	2.0	800
H07	11.10.2007	2.0	1000
Z07	11.10.2007	1.5	1000
D03	11.09.2003	1.6	728

	Scanner	frequ.[Hz]	v [m/s]
H03	ALTM 2050	30	75
H04	ALTM 2050	30	75
H05	ALTM 3100	40	75
H06	ALTM 3100	41	75
H07	ALTM 3100	41	70
Z07	ALTM 3100	41	70
D03	ALTM 2050	30	70

	Angle	PRF[kHz]	width[m]
H03	20°	50	155
H04	20°	50	155
H05	20°	70	400-600
H06	20°	70	300-600
H07	20°	70	300-600
Z07	20°	70	300-600
D03	30°	20	328-428

Table 4.1: Flight data: H = Hintereisferner (Hintereisfernerbach), Z = Zwieselstein (Venter Ache), D = Doren (Bregenzer Ache); 03 - 07 = year of flight (2003 - 2007); points/m² = mean point density; Altitude = flying altitude above ground; frequ. = scan frequency; v = speed of the aircraft; Angle = maximum scan angle; PRF = pulse repetition frequency; width = width of the swath

The Bregenzer Ache is the largest river in the Bregenzerwald (Vorarlberg; 47°28'26.93" N; 9°51'11.22" E). The site near Doren was chosen because of the confluence with the Weißache and the lake in the center of the test site.

The Bregenzer Ache is a strongly regulated river and therefore characterized by a smooth water surface. Huge sand and gravel bars inside the Weißache and the Bregenzer Ache are evident, which make the classification process more complex.

4.3.2 Reference data production

To analyze the ALS point attributes, it is necessary to know which material (including water) is hit by the laser beam. The use of orthophotos with higher resolution than the average point distance are a proper method to evaluate and analyze the ALS data. However, orthophotos from aerial images (taken parallel to the ALS campaign) are rarely available or the resolution of the images is too low. Thus, we use a terrestrial orthophoto mosaic with a cell size of 5 cm and a vertical position accuracy of 15 cm.

We took about 50 images of an approximate 70 m long section of the Venter Ache to generate the terrestrial orthophoto. The initial orientation, the bundle block adjustment, the semiautomatic terrain point extraction and the final orthophoto computation are done in ORPHEUS (Kager et al., 2002).

4.4 Water surface classification

The presented method uses the geometry and amplitude values of the 3D point cloud. The local roughness on water surfaces and bare Earth is very low. The smoothness depends on the water level and on the roughness of the riverbed. The amplitude values are mostly low on water because of the special reflectance and absorption properties (sec. 4.2.1). By analyzing smooth areas with very low amplitude values, water echoes can be classified (sec. 4.4.3).

The water surface classification method comprises five major steps (Fig. 4.1). Firstly, a correction and radiometric adjustment for amplitude values (i) and secondly, the locations of laser shot dropouts have to be computed (ii) (sec. 4.4.1 and 4.4.2). Next, the roughness parameter (standard deviation of height values) and the amplitude density ratio of each reflection (iii) and each dropout (iv) are computed at a fixed distance of 2 m (sec. 4.4.3). By analyzing a part of the laser shot attributes of the Venter Ache by using the terrestrial orthophoto mosaic it is possible to extract the proper information for the classification step (v), which has to be applied to distinguish water and non-water echoes (sec. 4.4.4). After the classification, the results are evaluated by using all laser shots, which are corresponding to the measured GPS line.

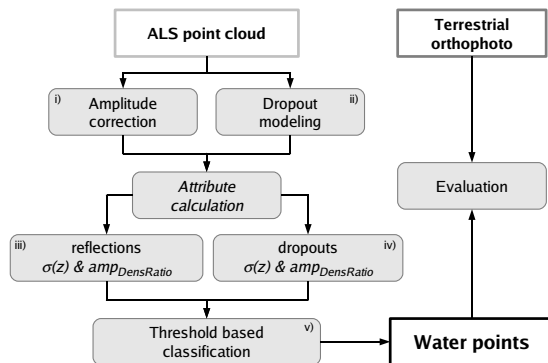


Figure 4.1: Work flow of the classification method; $\sigma(z)$ = standard deviation of height values; $amp_{DensRatio}$ = amplitude density ratio

4.4.1 Amplitude correction and radiometric adjustment

The amplitude correction of each laser shot is necessary to calculate amplitudes, which are almost free of atmospheric and geometric influences. The correction was applied by using the model-driven correction approach of Höfle and Pfeifer (2007). The used method is derived from the radar equation (Jelalian, 1992). The main goal of the amplitude correction is to calculate comparable amplitude values by (a) correcting the different ranges of all laser shots within the different flight strips, (b) accounting for atmospheric attenuation and (c) to normalize the reflection properties (Höfle and Pfeifer, 2007).

In this study, the amplitudes were corrected to a standard range of 1000 m. The influence of the atmosphere

was not corrected because of missing meteorological data. The directional scattering properties of the targets are considered by globally assuming Lambertian scatterers. Although water surfaces exhibit a strong contribution of specular reflection assuming this simple reflectance model was chosen as pragmatic solution for the a priori unclassified laser points. A data-driven solution, for example, is presented in Brzank et al. (2008) where an empirical model is estimated for the reflectance behavior of water. All data sets were corrected the same way (Höfle and Pfeifer, 2007).

The radiometric adjustment of amplitudes is necessary to make the amplitude values of each flight campaign comparable to each other, when using ALS data sets from different flight campaigns of one test site. For this study we did a radiometric adjustment for the flights at the Hintereisferner (H03-H07). For the two flights at the other test sites (Z07, D03) a radiometric adjustment of the amplitudes can not be realized because at least two different data sets must be available of one site.

The radiometric adjustment at the Hintereisfernerbach (H03-H07) was realized by analyzing the amplitude values of the different data sets. Thirty-five reference areas (4 m^2) with homogeneous amplitude values are chosen to calculate the radiometric adjustment factor between the data sets (Fig. 4.2). The

amplitudes of the points with a scan angle $< 10^\circ$ within each reference area are selected to calculate the mean amplitude value for each reference area. The angle criterion is used to guarantee that all reflections have almost the same scattering properties. By multiplying the corrected amplitude values with the radiometric adjustment factor, the data sets from all flight campaigns at the Hintereisferner (H03-H06) become comparable and correspond to the amplitude values of the reference data set (H07).

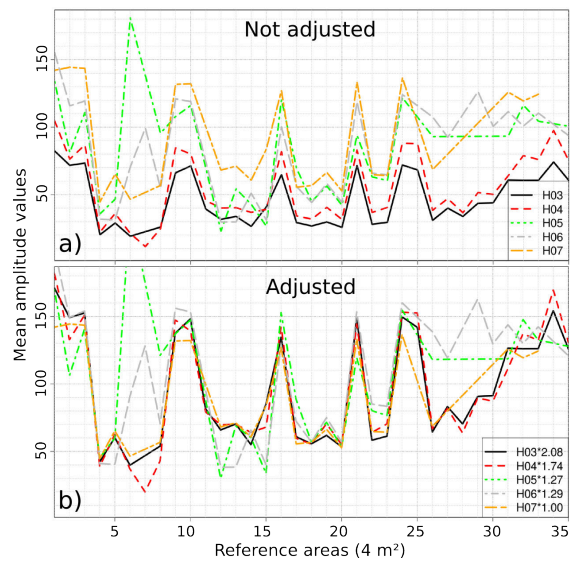


Figure 4.2: Radiometric adjustment: a) corrected amplitude values of all data sets (H03 to H07) at the Hintereisferner (mean values of all 35 reference areas, 4 m^2); b) radiometric adjusted amplitude values (adjusted to H07, red dashed line), the radiometric adjustment factors are shown in the legend

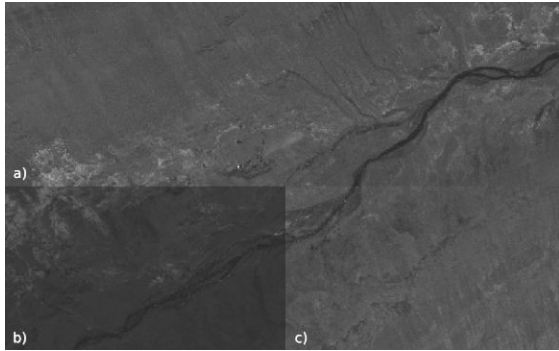


Figure 4.3: Corrected vs. radiometric adjusted amplitude values: a) corrected amplitudes (October 11, 2007, H07); b) corrected amplitudes (October 5, 2004, H04); c) corrected and radiometric adjusted (the radiometric adjustment factor is 1.74; October 5, 2004, H04); the graphic shows amplitude images (range from 0, black to 160, white)

The remaining strong deviations between the strips in figure 4.2 (reference areas 6 to 8 and 26 to 29 of H05 and H06) can be explained by changing surface conditions compared to the other ALS data (e.g. dry rock instead of wet rock). In figure 4.3, the reference data set of October 11, 2007 (H07) (Fig. 4.3a) and the data set of October 5, 2004 (H04), (Fig. 4.3b) with corrected amplitudes are shown. The results of the corrected and radiometric adjusted amplitudes of October 5, 2004 (H04) are displayed in figure 4.3c. The amplitude differences between figure 4.3a and 4.3b are the result of different sensors and campaign settings, which are not corrected by the amplitude correction approach (Höfle and Pfeifer, 2007). For the amplitude values of October 5, 2004 (H04), the radiometric adjustment factor is 1.74 (Fig.

4.3c).

4.4.2 Laser shot dropout modeling

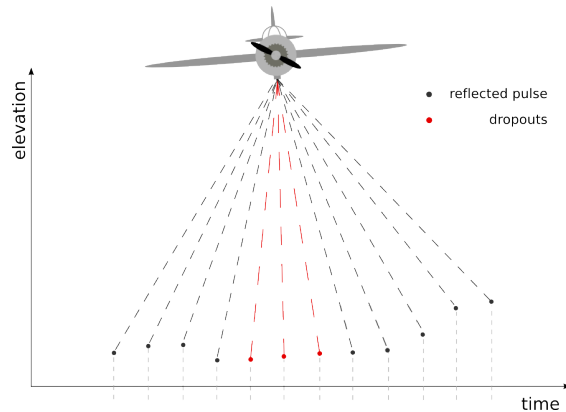


Figure 4.4: Dropout modeling schema (Höfle et al., 2009)

A laser shot dropout is a laser shot with no recorded echo. It can occur due to, (i) a specular reflection which is not in the direction of the ALS receiver, (ii) a strong absorption at the reflector or (iii) a lot of reflections on very small areas (foliage in the canopy) in a volume scatterer like a tree with a lot of inside scattering (Katzenbeisser and Kurz, 2004). By using information of the recorded timestamps of the laser shots, the PRF, the IMU and GPS data, the location of each dropout can be calculated (Fig. 4.4).

To model laser shot dropouts, the time gaps between neighboring points (P_1 to P_2), which are larger than Δt (equation 4.1) have to be found in the recorded timestamps (t_{P_1} and t_{P_2}). After finding the time gaps, the number of missing reflections n are calculated (equa-

tion 4.2). At each location where a reflection is missing the X, Y, Z coordinates are calculated (M_i) by using a linear interpolation (equation 4.3). The amplitude value is set to zero. Uncertainty in elevation leads to rather low vertical accuracy of the interpolated point. Therefore, the height value is not used for calculations but only for visualization.

$$\Delta t[s] = \frac{1}{PRF[Hz]} \quad (4.1)$$

$$n = \frac{t_{p_2} - t_{p_1}}{\Delta t} - 1 \quad (4.2)$$

$$n \in N, t_{p_2} > t_{p_1}$$

$$\vec{M}_i = \vec{P}_1 + \overrightarrow{P_1 P_2} * \frac{i}{n+1}, i = 1, \dots, n \quad (4.3)$$

4.4.3 Data exploration

To interpret the ALS data and its covered surface, the ALS point cloud is compared to the terrestrial orthophoto mosaic. Differential GPS (dGPS) measurements were acquired at the same time as the ALS campaign. These dGPS measurements are used for the terrestrial orthophoto production and for checking the position of the water-land boundary. The dGPS measured lines are also used for evaluation. The terrestrial orthophoto (Fig. 4.5) is only used for visual inspection.

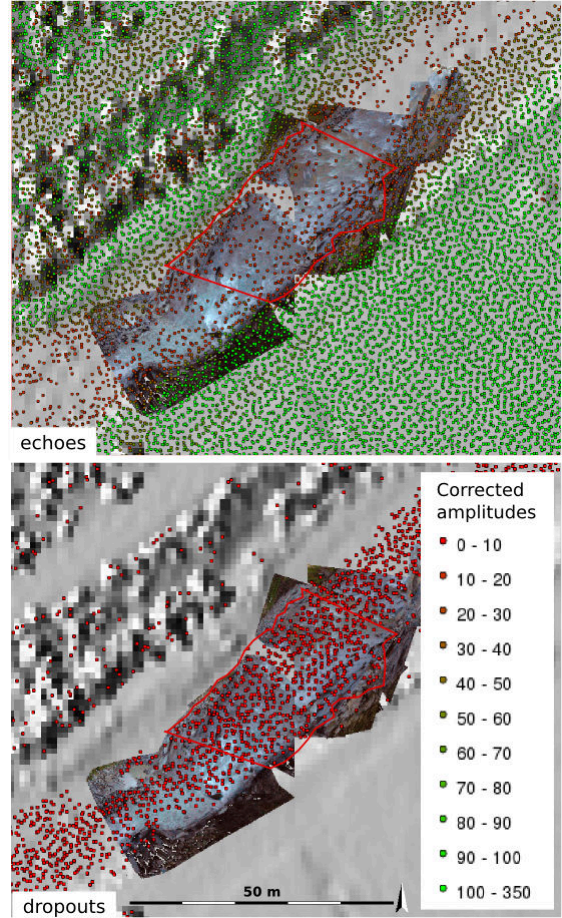


Figure 4.5: Terrestrial orthophoto superimposed by the dGPS measured water-land boundary (red line); upper image: corrected amplitudes of the last echoes (October 2007, Z07; color according to corrected amplitudes); lower image: modeled dropouts (colored by the amplitude value of zero)

For checking the amplitude values and the point density on water surfaces (sec. 4.4.3.1) an independent test site in Innsbruck, which is not listed in table 4.1, was used. This test site has the advantage that the whole range of scan angles is present within one connected

water area (river Inn). The test site at the Venter Ache (Z07) was used to analyze the geometric properties and the local roughness of the point cloud (sec. 4.4.3.2).

4.4.3.1 Amplitude values and dropouts

Figure 4.6 demonstrates the relation between the incidence angle and the signal amplitude on water. The selected points are from two ALS campaigns at the Inn in Innsbruck (Höfle et al., 2009). The red points are from a summer flight with a lot of suspended load and the blue ones are from fall with clear water conditions. This can also be seen in the different number and strength of the amplitudes in the plot (Schmugge et al., 2002). The summer flight with higher suspended load has a higher backscattering potential than the other, but not a Lambertian (Höfle et al., 2009). Those data were selected because the Inn is wide enough to guarantee that only water reflections are within the selection. The visual inspection of the amplitudes at the Venter Ache (Z07, Fig. 4.5) shows the same results as figure 4.6. Most of the water reflections have very low amplitudes.

A decrease of amplitude values is evident from nadir to the end of the scan line (incidence angle with 20°). The point density decreases and therefore the dropouts increase in the direction to the scan edges in a non linear regression (Brzank et al., 2008; Höfle et al.,

2009). Almost 85% of the points in figure 4.6 are lower than an amplitude of 50 and 95% of all reflections on water are within an incidence angle range between 0° to 10° . Therefore, water is characterized by low amplitude values, approximate 10 - 20 % of the whole range of the signal amplitudes (excluding outliers) and a high number of dropouts (Höfle et al., 2009). That can also be seen in figure 4.5. If no reference data set is available, 10 to 20% of the amplitude range of the whole data set can be used as estimate for the upper threshold in equation 4.5.

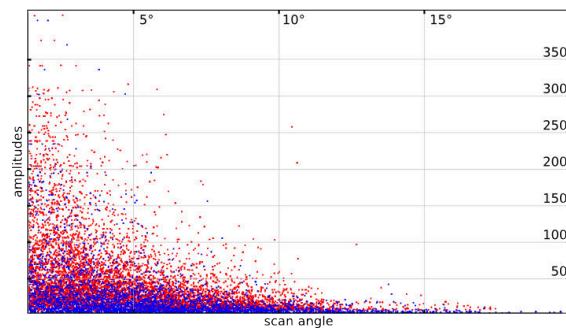


Figure 4.6: Relation between angle of incidence (=scan angle) and corrected amplitude values on water (water body at the Inn in Innsbruck in summer 2005, red; in fall 2005, blue) according to Höfle et al. (2009)

The amplitude density ratio (equation 4.5) is calculated by modifying the intensity density of Clode et al. (2005) (equation 4.4) by adding the dropout information. The amplitude density ratio $amp_{DensRatio}$ is the relation between the number of echoes with an amplitude value within a defined interval (0 to 50, derived from Fig.

4.6 and Fig. 4.5) $echoes_{AmpValue} < value_{max}$ AND $echoes_{AmpValue} > value_{min}$ plus the number of *dropouts* (with an amplitude of zero) divided by the number of $echoes + dropouts$ at a fixed distance of a point (2 m). If there are no dropouts within the search radius, the results of equation 4.4 and equation 4.5 are the same. The attribute $amp_{DensRatio}$ can be calculated for both, reflections and dropouts. The $amp_{DensRatio}$ is high if the points, which are surrounding the search point, have low amplitude values and/or most of them are dropouts. If only a few amplitude values are high and most of the points in the search radius are dropouts the $amp_{DensRatio}$ is also high. Both cases are evident on vegetation and on water (Fig. 4.8b). If no reflection is found within the search radius, the $amp_{DensRatio}$ is 100%. When all amplitude values are higher than $value_{max}$ and no dropout is found within the search radius, the value is 0%.

$$amp_{dens} = \frac{echoes_{AmpValue}}{echoes} * 100 \quad (4.4)$$

$$amp_{DensRatio} = \frac{dropouts + echoes_{AmpValue}}{dropouts + echoes} * 100 \quad (4.5)$$

The information of the $amp_{DensRatio}$ is used for calculating the point density and the relation of low amplitudes plus dropouts to all potential reflections at the same time. The $amp_{DensRatio}$ attribute can be used to distinguish

water and vegetation (with a lot of dropouts) from bare Earth characterized by a very few dropouts (Fig. 4.8b).

4.4.3.2 Geometry values

To remove the vegetation points, which have a high $amp_{DensRatio}$ because of the low reflection properties and a lot of dropouts, the standard deviation of height values $\sigma(z)$ is used.

The profile (Fig. 4.7) shows the elevation variation and the roughness of a river with a sand or gravel bar, river banks and vegetation. By visual inspection, the low roughness of the water surface can be seen.

By using a fixed distance search radius for each point (2 m) the standard deviation of height values $\sigma(z)$ is calculated for each reflection and each dropout.

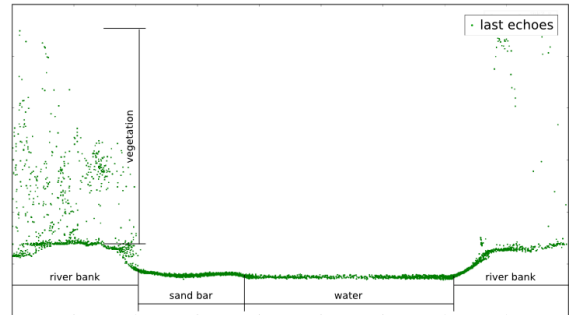
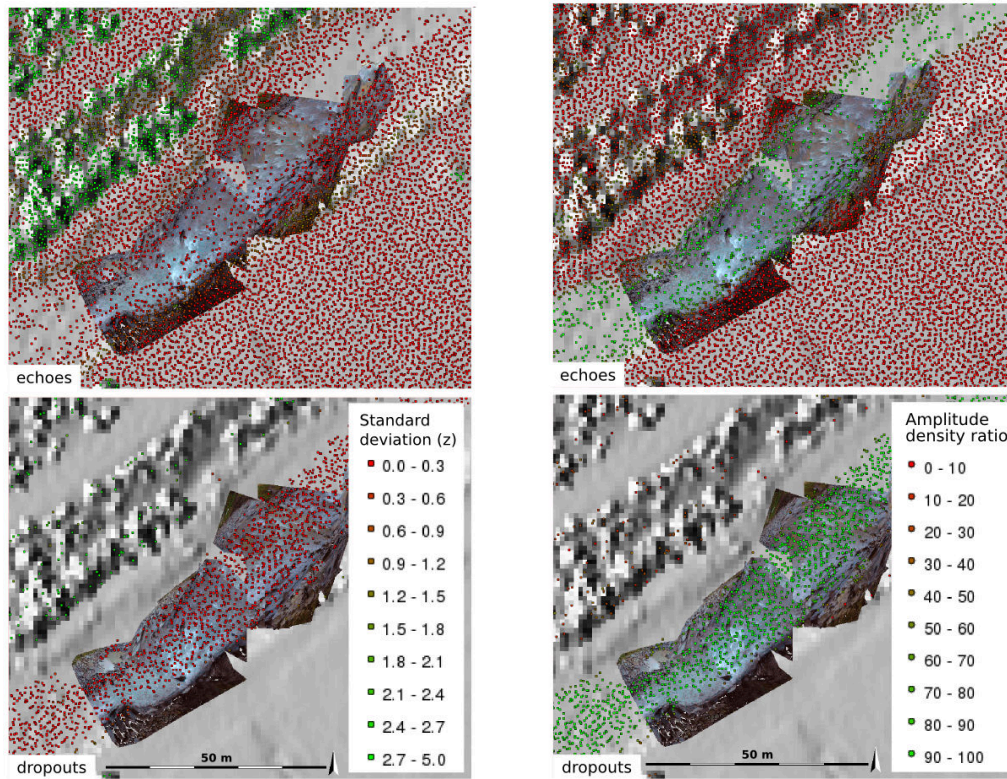


Figure 4.7: Profile through a watercourse, showing the elevation values of the ALS point cloud



(a) Standard deviation of height values $\sigma(z)$ at the Venter Ache: upper image: echoes; lower image: dropouts colored by $\sigma(z)$ in m

(b) Calculated amplitude density ratio at the Venter Ache: upper image: echoes; lower image: dropouts; colored by $amp_{DensRatio}$ in %

Figure 4.8: Standard deviation of height and amplitude density ratio at the Venter Ache superimposed by the terrestrial ortho image

The roughness parameters of water surfaces are very different from the surrounding areas of rivers, especially if riverine vegetation is present. In areas with vegetation the local roughness is higher than on bare Earth (e.g. fields) and much higher than on water (Fig. 4.8a). The information of the local roughness can be used for deleting all vegetation points in the classification process. Therefore, the threshold can be

figured out with < 0.3 m on rivers with smooth surface and < 0.5 m on rivers, which are rough and steep. The calculation of $\sigma(z)$ is done for both, reflections and dropouts. Sometimes there are no reflections within the search radius around a dropout (especially on water). In this case the $\sigma(z)$ is zero. Only the values of the reflections are used for calculating $\sigma(z)$. The very uncertain height values of dropouts are not used

for any calculations only for visualization.

4.4.4 Threshold based classification

The classification routine uses two different attributes to classify the points into water or non-water. The input attributes are the local roughness $\sigma(z)$ and the amplitude density ratio ($amp_{DensRatio}$, equation 4.5), which are described in section 4.4.3. The attribute $\sigma(z)$ is used for classifying horizontal areas (e.g. fields, roads, water) and the $amp_{DensRatio}$ is used to filter out the points with a high dropout rate (water and vegetation). By combining both, water can be localized.

The thresholds of the attributes are extracted by using a part of the echoes, which represent water in the terrestrial orthophoto mosaic at the Venter Ache. The thresholds of the classification are $\sigma(z) < 0.3$ m and $amp_{DensRatio} > 50\%$ for the class water. The value $\sigma(z)$ depends on the roughness of the water surface. If the surface is smooth the threshold can be set very low, in contrast to a torrent with a rough water surface. The $amp_{DensRatio}$ is set to 50%. If half of the reflections are on land (higher than the upper threshold) and half are on water (lower or dropouts) the 50% are fulfilled and the point can be a water point. First, the $\sigma(z)$ attributes (Fig. 4.9a) and then the $amp_{DensRatio}$ values are classified (Fig. 4.9b). If $\sigma(z)$ is lower and the attribute of $amp_{DensRatio}$

is higher than the specific threshold, the point belongs to water, otherwise to land.

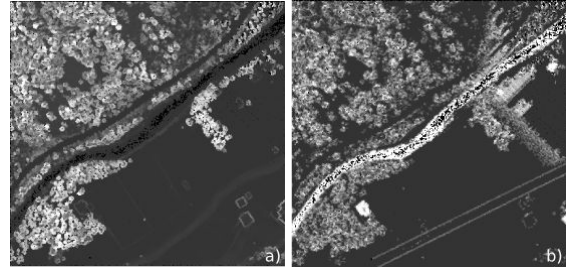


Figure 4.9: Pre-classification at the Venter Ache: a) $\sigma(z)$; b) $amp_{DensRatio}$; bright: high value; dark: low value

4.5 Results

The advantage of a 3D point cloud based classification is that the points are not manipulated in their 3D position. By using corrected and radiometrically adjusted amplitude values, the classification parameters have to be calculated only once and can be used for all data sets. The use of the modeled dropouts provides information on objects with no reflections, which is necessary for classifying water surfaces. The result of the Bregenz Ache (Fig. 4.10a) shows the advantage of using the modeled dropouts to classify water. The center of the test site contains a lake with no ALS returns. The lake can not be classified without the location information of dropouts. In this case, only the modeled dropouts are used to compute the water surface. Each reflection on the lake, which are only a few, are classified as water because of

a $\sigma(z)$ of zero and a $amp_{DensRatio}$ of 100%. The results of the classification at the Venter Ache are shown in figure 4.10b.

The results at the Hintereisfernerbach show the possibility to apply the method for multi-temporal analysis of the watercourse of a braided river (Fig. 4.11). In multi-temporal analysis the spatial change of the flow paths during the years (Fig. 4.11f) can be computed.

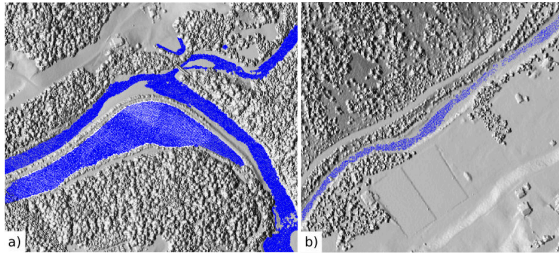


Figure 4.10: Classification results: a) Bregenzer Ache, D03; b) Venter Ache, Z07

The reference area Venter Ache is used to assess the accuracy of the method by comparing the result with the measured GPS lines. The classification accuracy of the presented method was evaluated by a manual selection of all water reflections at the reference area. All echoes, which are corresponding to the water surface of the measured waterland boundary are selected and compared with the number of classified water points. A comparison of the selected reflections with the calculated water points shows 95% of correct classified water points. Zero percent of the classified water points are outside the water

land boundary (GPS line), which shows that the classification underestimates the water surface area at the present thresholds. Visually the horizontal distance (i.e. underestimation) between GPS line and the outer classified water points lies between 0.5 m and 1 m, indicating that the horizontal accuracy is in the range of the given average point distance.

4.6 Discussion

With the presented dropout modeling method, only dropouts which have two neighbors along the scan line can be modeled. That means that dropouts which are located at the end of a scan line are not detected. In special cases, the end of the scan line is located in a water area and then the used modeling method will be stopped at the last reflection in the scan line.

In the future, the modeling of dropouts has to be improved by a pre-calculation of the scan line locations and an extrapolation method for dropouts to the swath edge. Another method for detecting dropouts is to use the information of the raw data from the providers. This is possible when providers can record and deliver the whole raw information of the scans, including the timestamps of the non-recorded reflections.

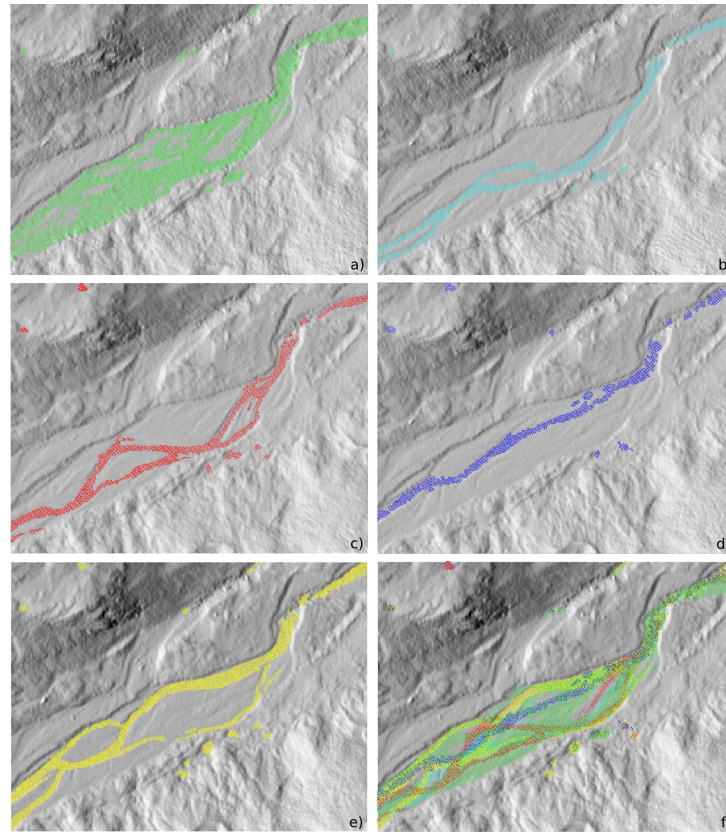


Figure 4.11: Classification results at the Hintereisfernerbach: a) August 12, 2003, H03; b) October 5, 2004, H04; c) October 12, 2005, H05; d) October 8, 2006, H06; e) October 11, 2007, H07; f) combination of all classification results

The availability of corrected and radiometric adjusted amplitude values is very important for deriving the water points of multi-temporal data sets because of the comparability of the different data sets.

To improve the comparability of multi-temporal data sets, exactly one flight pattern and one scanner type should be used for all flights in the same area. The radiometric adjustment method can be improved by using radiometric calibration targets (e.g. natural targets mea-

sured with a reflectometer). The same targets can be used at each campaign. The known reflectivity of that area can be used for radiometric calibration and adjustment after amplitude correction (Briese et al., 2008; Kaasalainen et al., 2008).

The computation time (including point selection, dropout modeling and classification) depends on the selected area and the point density. The use of a raster based flow accumulation for calculating the poten-

tial location of rivers and water areas can be implemented as a pre-selection routine to reduce the computation time.

4.7 Conclusion

The chapter presents a method to classify ALS reflections that belong to water by using the attributes of $amp_{DensRatio}$ and $\sigma(z)$. The attributes are calculated within the 3D ALS point cloud. The main novelty of this method is the use of modeled laser shot dropouts, which mainly occur on water and vegetation. The relation between low amplitudes and dropouts combined with the standard deviation of height values within a search radius of a point provides significant information to distinguish water and land. For the multi-temporal analysis of different ALS campaigns of the same area the amplitude correction and radiometric adjustment are required. The same classifica-

tion thresholds can be applied to data sets with corrected and radiometric adjusted amplitudes, improving the transferability and comparability to other data sets. A terrestrial orthophoto mosaic is used to check the thresholds for the calculated attributes by visual inspection. A classification accuracy of 95% correctly derived water reflections was reached.

4.8 Acknowledgments

Thanks to Camillo Ressler and Norbert Pfeifer for the calibrated camera, for providing the software and the lab and for supporting the generating process of the terrestrial orthophoto at the Institute of Photogrammetry & Remote Sensing, Vienna University of Technology. Thanks also to the local government of Vorarlberg (Vorarlberger Landesregierung, Landesvermessungsamt) for the ALS data set of the Bregenzer Ache.

**Estimating changes of riverine landscapes
and riverbeds by using airborne LiDAR
data and river cross-sections**

Today, Airborne Laser Scanning (ALS), also referred to as airborne LiDAR, derived Digital Terrain Models (DTMs) and Digital Surface Models (DSMs) are used in different scientific disciplines, such as hydrology, geomorphology, forestry, archaeology and others. In geomorphology, ALS data are used for studies on landslides, soil erosion, mass movements, glacial geomorphology, river geomorphology, and many others. In the field of river geomorphology, ALS data sets provide information on riverine vegetation, the water level and water-land-boundaries, the elevation of the riparian foreland and their roughness. Small-footprint ALS systems used for topographic data acquisition operate mainly in the near-infrared wavelength. Thus, topographic ALS is not able to penetrate water but to provide a highly detailed representation of the dry land. Therefore, a method to derive Digital Bathymetric Models (DBMs) by using river cross-sections acquired by terrestrial field surveys is presented in this chapter. The DBM, which is combined with the ALS-DTM to a DTM of the watercourse, is the basis for calculating changes of the riverbed and the riverine landscape between two ALS data epochs. The first step of the DBM delineation method is to separate water from land in the ALS data. A raster-based approach to derive the Water-Extent-Polygon (WEP) is presented which incorporates the signal strength of the ALS backscatter (referred to as intensity or amplitude), terrain slope and height differences between the DTM and DSM (i.e. the so-called normalized DSM, nDSM). In the second step, the river centerline is extracted by applying a shrinking algorithm to the WEP. Subsequently, a dense array of 2D-transects, perpendicular to the centerline, is defined. For these 2D-transects the heights are interpolated linearly from the measured river cross-sections. From the obtained 3D point cloud representing the riverbed a raster model can be calculated by applying a suitable interpolation technique. In the final step, the DTM and the DBM are combined to a DTM of the watercourse. For two available ALS-DTM data sets (years 2003 and 2006) the respective watercourse DTMs are calculated based on terrestrially measured river cross-section data sets. By computing difference-models changes in the water level between the two ALS-DTMs are calculated. To estimate the accumulation and erosion potential of the riverbed between the two periods, the difference-model of watercourse DTMs is used. The results show the potential of using ALS in combination with river cross-section data as input for DBM modeling, watercourse DTM generation, riverine landscape and riverbed change detection. The main objectives of the chapter are on presenting an accurate WEP delineation approach and a workflow to model a watercourse DTM.

5.1 Introduction

During the last decades a series of major floods occurred throughout Europe. Several of them generated severe damages, especially the August 2005 event

(on August 22/23, 2005), which was at least a 100 year event. The damages on human property and infrastructure rose up to 178,200,000 € for the Federal State of Vorarlberg, Austria (Amt der Vorarlberger Landesregierung, 2005). Apart

from economic damages on human property also non-monetary measurable changes occurred at the riverine landscape and the riverbed topography. A novel method to estimate and quantify these riverbed changes after flood events is presented in this chapter. The main objective of the chapter is to introduce a set of methods to generate Digital Bathymetric Models (DBMs) by combining Airborne Laser Scanning (ALS) elevation, radiometric data, and river cross-sections of field surveys to estimate changes of the riverine landscape and the riverbed. Therefore, a Water-Extent-Polygon (WEP) delineation approach, operating on rasterized ALS input data, and the method to derive a DBM from measured river cross-sections are presented. It is also aimed at investigating the potential of multi-temporal ALS data sets featuring additional radiometric information together with accurate and dense river cross-sections with respect to change detection.

In geomorphology, the use of topographic data collected with ALS or TLS (Terrestrial Laser Scanning) systems, are manifold. An extensive overview of ALS-related applications in geomorphology is given by Höfle and Rutzinger (2011). In hydrology, ALS is mostly used to generate Digital Terrain Models (DTMs) for hydrodynamic simulations of flood inundated areas and for roughness parametrization (Mandlbürger et al., 2009; Straatsma and Baptist, 2008). Several stud-

ies present approaches for the generation of Digital Bathymetric Models (DBMs) used in hydrodynamic applications. Most of them use a water-course DTM, which is the combination of the DBM and the ALS-DTM (Brockmann and Mandlbürger, 2001), for applications in 1D or 2D hydrodynamic models (Carter and Shankar, 1997; Merwade et al., 2008; Legleiter and Kyriakidis, 2008).

Regarding river geomorphology, the main interest for creating a DBM is to estimate the volume and the changes of the riverbed and the riverine landscape (Lane et al., 2006). To measure the riverbed, topographic laser scanning systems, ALS and TLS, cannot be used as most topographic LiDAR systems use laser sources operating in the near-infrared light spectrum with wavelengths varying from 905 nm to 1550 nm, which are not able to penetrate water bodies (Höfle et al. (2009)). A bathymetric LiDAR system has to be used to measure the depth of water bodies. Those systems provide two different wavelengths, one in the green spectrum (from 520 nm to 532 nm), penetrating water, and a second in the near-infrared with e.g. 1064 nm reflecting at the water surface (Irish and Lillycrop, 1999; Guenther et al., 2000). The main limitations of bathymetric LiDAR systems are that clear water conditions are required and a minimum water depth of about 1.5 m is necessary to distinguish the water surface from the riverbed targets depending on the used

ALS system and pulse length (Guenther et al., 2000; Allouis et al., 2010). The maximum penetration depth of a bathymetric ALS System is typically 2 to 3 times the Secchi depth, which is the water depth where a black and white disk can barely be seen with the naked eye. The Secchi depth depends primarily on the turbidity of the water (Guenther et al., 2000). A broad overview of different active and passive remote sensing techniques for monitoring water bodies is given by Mertes (2002) and Marcus and Fonstad (2008) (e.g. water quality, temperature and depth). Legleiter et al. (2004) show the ability to calculate water depth using the color information of the green and red band of passive optical remote sensing data. With echo sounding systems bathymetric data can be acquired (Dinehart, 2002; Schmitt et al., 2008), but echo sounding cannot be used in shallow water due to a minimum depth restriction of approx. 1 m (Beyer et al., 2003). This restricts echo sounding to rivers exceeding this minimum depth, the requirement of using a boat or access from the river bank for acquiring the measurements.

Methods to derive water surface areas from ALS data using the intensity information were published by Brzank and Heipke (2006); Höfle et al. (2009) and Vetter et al. (2009b). Brzank and Heipke (2006) present a strip-wise classification method using a membership function to distinguish water and non-water points. They use elevation, slope,

intensity and the point density to classify the ALS point cloud into water and land points. Höfle et al. (2009) and Vetter et al. (2009b) use modeled laser shot dropouts, geometry and radiometric information of the raw ALS point cloud to classify and map water surface locations. Dropouts are non-recorded laser shots, which mainly occur on water because of specular reflections not directed towards the receiver or high absorption. By detecting gaps in the timestamps of the ALS point cloud the x,y,z coordinates of dropouts can be calculated.

Different approaches to model a DBM and integrate it into a DTM are already published. Most of them are related to applications in hydrology or hydraulics. However, the ability to calculate changes of the riverbed between multi-temporal data sets is not investigated yet. Brockmann and Mandlbürger (2001) are using a water-land-boundary derived from ALS data. This water-land-boundary is a contour line based approach and the result is comparable to the presented WEP method described in Sec. 5.3.1. The measured cross-sections are transformed into an axis-oriented system, where a dense set of profiles perpendicular to the river axis is calculated using bi-linear interpolation method. After back transformation, a DBM is derived from those data and the results are used as input for hydrodynamic flood modeling. Flanagan et al. (2007) use a cubic-spline-interpolation to cal-

culate a DBM by generating a fixed number of interpolation nodes along the measured cross-sections. Then, a dense mesh of intermediate nodes is computed between the cross-sections, which are used to generate the DBM. Various studies present the advantage of different spatial interpolation methods for improving the accuracy of the interpolated riverbed models. Legleiter and Kyriakidis (2008) use a Kriging method to calculate DBMs. Heitzinger and Kager (1998) introduce a triangulation with integrated breaklines. Merwade (2009) compares several interpolation methods on a large data set. He uses inverse distance weighted (IDW), regularized splines, splines with tension, TOPOGRID, natural neighbors, and ordinary Kriging based on isotropic and anisotropic variograms. The outcome of this study is that the accuracy of the interpolation primarily depends on the quality and the density of the cross-sections and secondly on the used interpolation method.

The chapter is structured as follows: In section 5.2, the used data sets, the test site and the used model acronyms are described and defined. A description of the developed method and the different processing steps are presented in section 5.3. The results are presented in section 5.4. The chapter ends with a discussion, a conclusion and an outlook in section 5.5 and 5.6.

5.2 Test site and data

The test site is located in the western part of the Bregenzer Wald (Federal State of Vorarlberg, Austria). The river Bregenzer Ache crosses the test site from southeast to northwest (Fig. 5.1). The catchment area of the Bregenzer Ache at the nearest gauging station (Kennelbach) is 826.3 km². Within the test site, the Bregenzer Ache is an almost non-regulated river. Two weirs are situated within the test site and one is located upstream, regulating the discharge and ensuring the availability of enough water for the lake, which is connected to a hydroelectric power plant (Fig. 5.1). The study was carried out for a 3.5 km long section of the Bregenzer Ache directly after the confluence of the Weissache and the Bregenzer Ache. The mean annual discharge at the gauging station in Kennelbach is 46 m³/s and the water level height averages out at 1.53 m. The mean low annual discharge is 5 m³/s, the average annual maximum discharge (HQ1) adds up to 480 m³/s and the 100 year event discharge (HQ100) is 1450 m³/s. The annual sediment transportation rate is approx. 5,000 m³/year (Rudhardt+Gasser and Hunziker, Zarn und Partner, 2004; Amt der Vorarlberger Landesregierung, 2005) and the average bed slope is 4.45 ‰.

For the test site, two ALS flight campaigns were carried out in the years 2003 and 2006. The first was collected with an Optech ALTM 2050

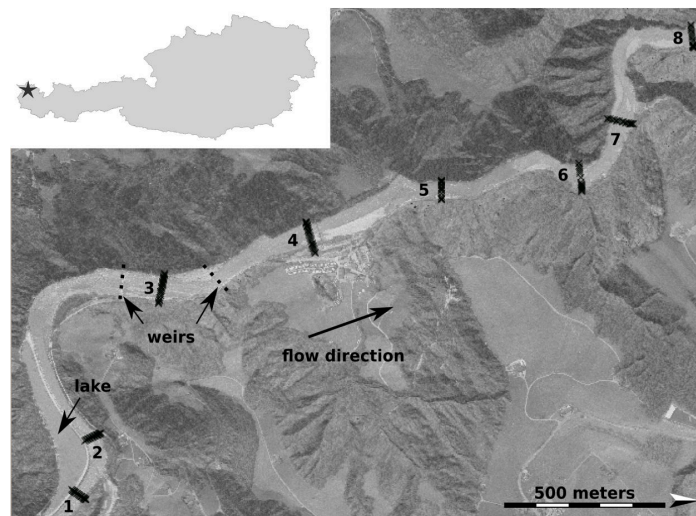


Figure 5.1: Test site and cross-section locations: shading of the DTM_{2003} , superimposed with an aerial image from 2001; black dots; river cross-sections with IDs; black dots: weir locations.

on September 11, 2003. The average point density is 1.6 points/m^2 for the last echoes. After the flood event in August 2005, the river corridor was scanned again on June 11, 2006, with an Optech ALTM 3100 and the same average point density of 1.6 points/m^2 .

The terrestrially measured river cross-sections are provided as ASCII-files (with year, ID, point No., X, Y and Z). In total, nine different river cross-sections data sets are available, measured with GPS in one or two year intervals. Eight cross-sections of the years 2004 and 2005 are used for this study. Therefore, the data sets (ALS-DTM and cross-sections) for the different epoch are DTM_{2003} with the cross-sections from 2004 and DTM_{2006} with

the cross-sections of 2005. The distance between the cross-sections range from 150 m to 820 m along the flow path.

In the following paragraph, the used terms and acronyms of the different models are introduced and described. The original ALS point cloud includes all echoes of the ALS measuring campaign with the coordinate triple X,Y,Z and the intensity values for each reflection (Fig. 5.2a). From the three dimensional ALS point cloud, digital elevation models (2.5D) in regular raster structure are derived. These are the Digital Terrain Model (DTM), representing the elevations of the bare Earth (Fig. 5.2b) and the Digital Surface Model (DSM), which comprise the nearest objects to the sensor (Fig. 5.2c)

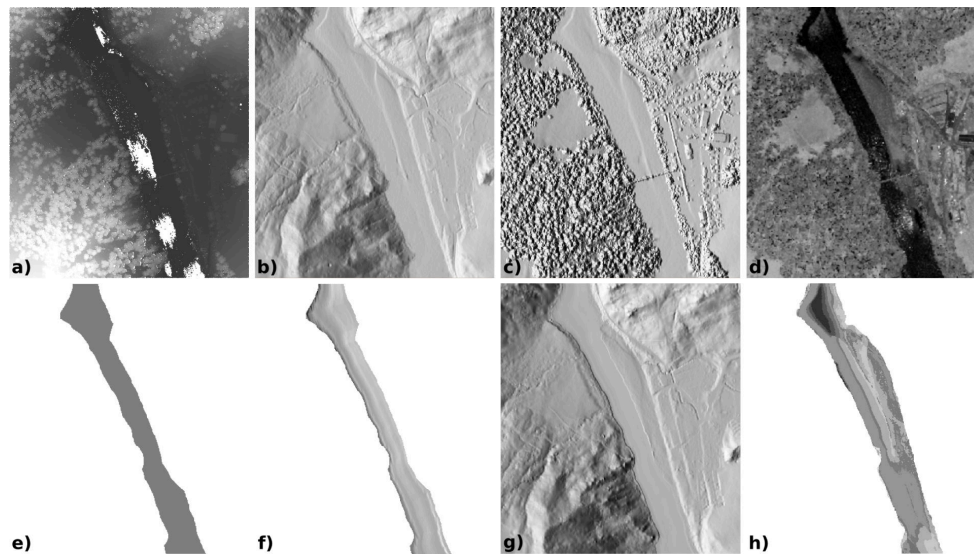


Figure 5.2: Used digital models: a) ALS point cloud (Z-coded); b) DTM (shading); c) DSM (shading); d) DIM (0 to 255); e) WEP₂₀₀₆; f) DBM₂₀₀₆ (shading); g) water-course DTM₂₀₀₆ (DTM-W₂₀₀₆) (shading); difference-model of watercourse DTMs (DTM-W₂₀₀₆ - DTM-W₂₀₀₃, 0.5 m classes).

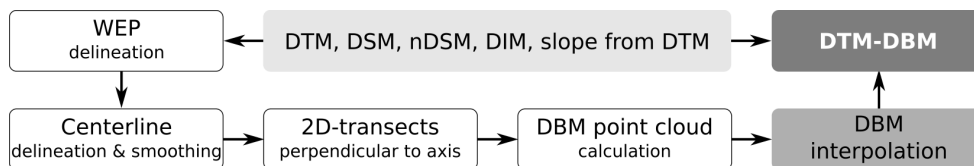


Figure 5.3: Workflow of the DBM derivation method.

(Elmqvist et al., 2001; Pfeifer and Mandlbürger, 2008). The difference model DSM-DTM represents the object heights above ground and is often referred to as normalized DSM (nDSM). An intensity model (Digital Intensity Model, DIM) can be derived from radiometric information either from the first or the last echoes of the ALS point cloud (Fig. 5.2d; Collin et al. 2010). For this study, only the last echo DIM is

used. The 2D Water-Extent-Polygon (WEP) represents the current extent of the water body of the ALS acquisition time (Fig. 5.2e). The Digital Bathymetric Model (DBM) is a 2.5D elevation model of the riverbed within the WEP (Fig. 5.2f). The DTM of the watercourse represents a 2.5D model of the flow-effective area (Brockmann and Mandlbürger, 2001) of the DTM and the DBM [DTM-W = DBM if(DBM

< DTM) else DTM] (Fig. 5.2g). The difference-model between epoch 2006 and 2003 is shown in Figure 5.2h represents the elevation changes within the extent of the combined WEP of both years. The raster models, which are derived by the presented method (see Sec. 5.3) are shown in Fig. 5.2e to 5.2h.

5.3 Methods

The presented workflow consists of five sequential processing steps (Fig. 5.3). The first step is to detect water and non-water areas, resulting in a WEP (Sec. 5.3.1). The WEP, representing the extent of the water surface, is of high importance because only the parts within the WEP are used for the DBM calculation, whereas the surrounding dry areas are taken from the ALS-DTM. Based on the derived WEP, the centerline can be extracted by shrinking the WEP area to a single line (Sec. 5.3.1). In the next step, a dense set of 2D-transects is generated perpendicular to the centerline. Moreover, the measured river cross-sections are integrated and 2D-longitudinal-profiles almost parallel to the centerline are produced (Sec. 5.3.2). By mapping heights to the 2D-longitudinal-profiles a 3D-riverbed point cloud is derived (Sec. 5.3.2). This riverbed point cloud is interpolated to a DBM. The DBM is then implemented into the DTM as last step resulting in a watercourse DTM

(Sec. 5.3.3). All steps of the workflow are implemented in Python programming language (Python Software Foundation, 2012). The scripts run within the framework of the open source Geographic Information System GRASS (Geographic Resources Analysis Support System; GRASS Development Team (2013)).

5.3.1 Water surface delineation

The first step of the riverbed derivation is to calculate a WEP in order to exclude water areas from the ALS data and define the DBM interpolation extent. The WEP is used on the one hand for the derivation of the centerline and on the other hand as a clipping polygon for the perpendicular 2D-transects. The rasterized intensity model (DIM) and the DTM are used as input for a threshold-based classification into water and non-water areas. The classification is done by using raster algebra. The classification thresholds on intensity, nDSM heights and surface slope (from DTM) are defined empirically. As the DIMs are provided as non-calibrated raster models, in gray scale ranging from 0 (low) to 255 (high), different thresholds are used for each data set. This means the intensity values of the data sets are not directly comparable to each other depending on the ALS acquisition parameters altitude and scan frequency. For further details refer to Höfle and Pfeifer (2007). As presented in Höfle et al. (2009) and Vetter et al.

(2009b), water areas can be characterized by low and very high intensity values. The high intensity values mainly occur when scanning in nadir direction (vertically beneath the sensor) where the laser signal reflects mostly specularly toward the receiver. Therefore, a lower and an upper intensity threshold are used for the classification. After the threshold-based classification, small areas occurring from misclassifications are erased using an area threshold of 50 m^2 . Then, the outlines are smoothed using an alpha shape approach (Edelsbrunner and Mücke, 1994) erasing small gaps and distortions of the WEP outline.

5.3.2 Centerline computation

An essential step for the DBM calculation is the derivation of the river centerline. The centerline is derived by applying a shrinking algorithm (also referred to as skeletonization or thinning) to the WEP. The used shrinking algorithm is a raster-based iterative algorithm, which works from the outer most part of an area to the center. In each iteration the outer most pixel row is erased at the edge of the raster until only a row of single pixels remains (Zhou et al. 1995). This raster is vectorized resulting in a centerline. Small branches, which are artifacts of the shrinking process, are removed by applying a length criterion. Finally, the resulting vector representation of the centerline is

smoothed by a moving average approach.

5.3.3 Three-dimensional riverbed point cloud generation

To generate the DBM, the terrestrially measured cross-sections have to be transformed from discrete point measurement into continuous area-wide information. Therefore, a dense set of 2D-transects perpendicular to the centerline has to be generated (Fig. 5.4a). The 2D-transects are lined up in a regular spacing orthogonal to the centerline (10 m in this study) in order to construct the topography of the river between the cross-sections. Those 2D-transects are cut at the edges of the WEP, as the DBM is restricted to the area of the WEP (Fig. 5.4a). The final pre-processing step is to apply appropriate heights to the 2D-transects. Therefore, the 2D-transects and the river cross-sections are divided into a fixed number of segments. The lengths of those segments are in percent relative to the length of the corresponding cross-section or 2D-transect. Segment labels are assigned to each segment point of all cross-sections and 2D-transects. By connecting corresponding segment labels, 2D-longitudinal-profiles are calculated (Fig. 5.4b), which are almost parallel to the flow direction. Then, the elevation information of the cross-sections can be interpolated linearly from one to the next cross-section at each intersection location of the longitudinal-profiles

with the transect resulting in a 3D-riverbed point cloud. The 3D-riverbed point cloud is used to generate the DBM (Fig. 5.4c).

5.3.4 DBM generation

After all previous steps, the 3D-riverbed point cloud is interpolated into a regular raster of the DBM by using any suitable interpolation technique. In this study, a natural neighbor interpolation method is used (Fan et al., 2005). By combining the DBM with the DTM, a watercourse DTM (containing bathymetric information) can be produced. Those areas of the DBM representing lower elevations than the DTM are used from the DBM to calculate a DTM of the watercourse. All other areas are used from the DTM. Therefore, the watercourse DTM represent only the lowest elevation of both models (DBM and DTM).

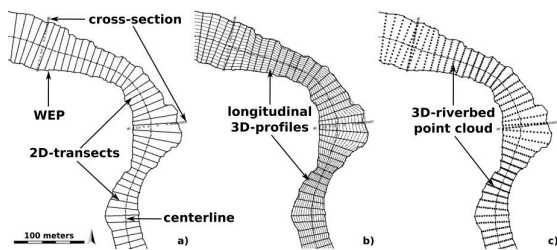


Figure 5.4: Steps of the 3D-riverbed point cloud calculation: a) WEP with cross-sections, smoothed centerline and 2D-transects (perpendicular to the centerline); b) Fig. a) plus the 3D-longitudinal-profiles; c) 3D-riverbed point cloud.

5.4 Results

At the beginning, the WEP delineation method results are analyzed. Then the DBM derivation and the watercourse DTM production are shown in different plots. Finally, the area-wide estimation of the riverine landscape and riverbed change detection are demonstrated.

Two independent sets of thresholds are empirically derived for the WEP classification of WEP₂₀₀₃ (Fig. 5.5a) and WEP₂₀₀₆ (Fig. 5.5b). The classification thresholds for WEP₂₀₀₃ are [nDSM<1.5 m AND slope<3° AND (DIM<25 OR DIM>70)] and for WEP₂₀₀₆ [nDSM<1.5 m AND slope<3° AND (DIM<65 OR DIM>110)]. The values of the DIM are in digital numbers ranging from 0 to 255. After smoothing the WEPs using the alpha shape approach (with alpha values of 5m for both WEPs), a visual inspection using the DIM as reference is recommended. A manual manipulation of the WEPs was done at maximum 8 locations per WEP (Fig. 5.5, white stars). This step is necessary because the alpha shape approach smooths only small irregularities of the boundary. The DBM delineation is isotropic and cannot handle back water areas. Therefore, back water areas are erased from the WEP (Fig. 5.5c and 5d). The final WEP₂₀₀₃ and WEP₂₀₀₆ presenting the different water extents of the two ALS acquisition times after smoothing and cleaning of the back water areas are shown

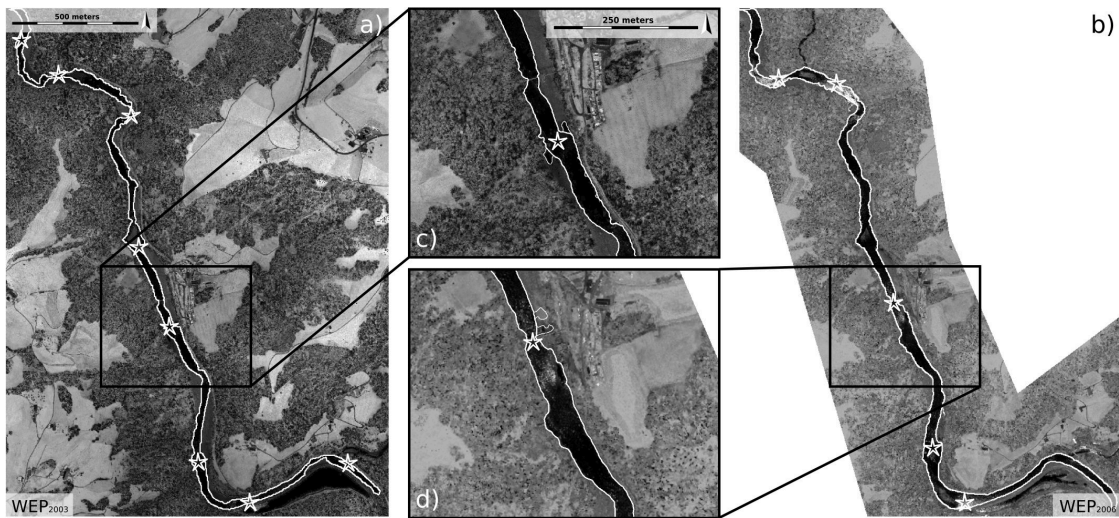


Figure 5.5: DIMs and WEPs: a) DIM of the last echoes and WEP₂₀₀₃; b) DIM of the last echoes and WEP₂₀₀₆; c) Zoom of a); d) Zoom of b); Thick white line is final WEP after cleaning and manual correction; Thin white line in c) and d) WEP before cleaning and correction; White stars: Locations of manual correction.

in Figure 5.5.

To estimate changes along the measured cross-sections, plots through the DTMs, the related DBMs and the cross-sections are presented in Figure 5.6a and 5.6b. For an area-wide estimation of the changes, difference-models are calculated for the DTMs, the DTM minus DBM and the watercourse DTMs, which are shown in Figure 5.7. A huge change of the water stage between the two DTMs can be seen in Figure 5.6, where the water level is 0.5 m to 1.0 m higher in DTM₂₀₀₆ than in DTM₂₀₀₃ (also shown in Fig. 5.7a). In the plots, a horizontal expansion of the water body (2006) can be seen due to the change in the water level. The horizontal expansion between the river

width of WEP₂₀₀₃ and WEP₂₀₀₆ in Figure 5.6a is 5 m, which is 120% related to the width of WEP₂₀₀₃. The area difference of the WEPs for the whole test site is 10.22 ha (WEP₂₀₀₃) to 13.71 ha (WEP₂₀₀₆), which is 34% more in 2006 than in 2003 (see Fig. 5.5a and 5.5b). As mentioned in Sec. 5.3 the WEP represents the extent for the DBM calculation.

The blue and red rings in Fig. 5.6 are the points of intersection between the measured river cross-section and the DTM. They represent the location of the WEP based on the DTM and the cross-section of each year. The result shows the accuracy of the WEP delineation method. The accuracy of the WEP at the location of the measured cross-sections (cross-

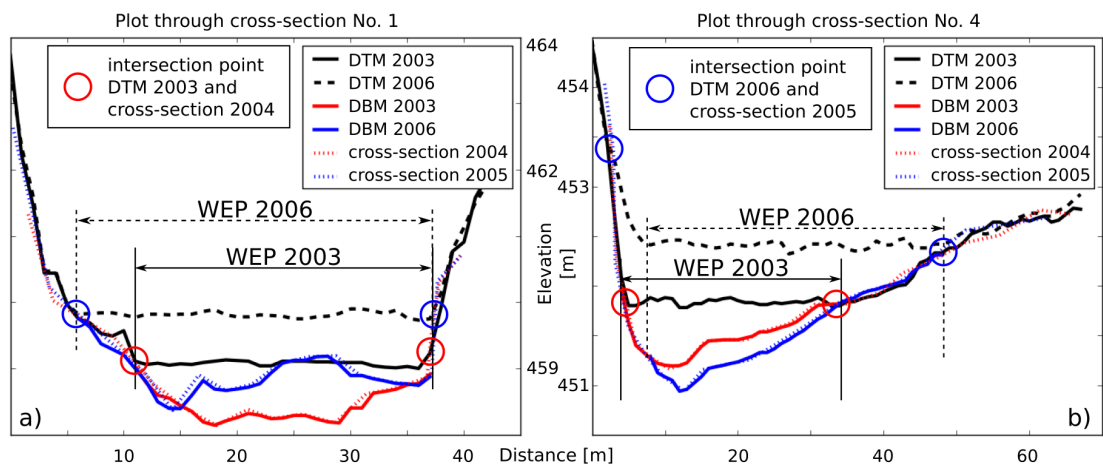


Figure 5.6: Plots through cross-section No. 1 and No. 4 (see locations in Fig. 5.1) with DTM, DBM and cross-section of both years: a) Profile No. 1 (Fig. 5.1); b) Profile No. 4 (Fig. 5.1).

section No. 1 and No. 4; see Fig. 5.1) is in the range of plus/minus the used raster resolution (1 m). A larger difference can only be observed at the intersection between DTM₂₀₀₆ and cross-section 2005 at the left river bank in Figure 5.6b (is not comparable with the location of the WEP and the DTM) due to a DTM interpolation or a cross-section measuring problem. The intersection between the derived WEP and the DTM shows the correct location of the water surface based on the geometrical and hydrological properties of the DTM.

In Figure 5.6a, an accumulation area in the middle of the riverbed can be seen between the measured cross-sections and the two calculated DBMs. For the whole river width, erosion is dominant in Figure 5.6b. The deposit and ero-

sion areas can be clearly seen in Figure 5.7. The distance between the calculated DBMs and the measured cross-sections (Fig. 5.6) are in the range of ± 5 cm, originating from the aggregation of the measured cross-section points to a raster DBM and the linear interpolation of the cross-section data to the riverbed point cloud (cf. Sec. 5.3.3). Due to the lack of reference data between the measured cross-sections the accuracy of the DBM can only be estimated at the cross-section locations. A 'leave-one-out cross-validation' using the cross-section data can not be applied, because of the large distance between the cross-sections.

To demonstrate the area-wide changes, difference-models are shown in Figure 5.7. To calculate the changes between the two DTMs, a DTM-

difference-model was calculated (Fig. 5.7a). The changes between the DTMs along the river corridor occur from the different water stages. The differences of the riverine landscape are dominated by elevation changes due to erosion or accumulation. In the forested areas, the changes (Fig. 5.7a) mainly occur from uncertainties in DTM generation and differences in ALS data collection season and settings. The water level of 2003 is on average -0.75 m lower than in 2006 (cf. Fig. 5.6, 5.7a, 5.7e and 5.7f). In Figure 5.7b, the difference between the DBM_{2003} minus DTM_{2003} and in Figure 5.7c for DBM_{2006} minus DTM_{2006} is shown, which present the depth of the water body of the different years.

At the outlet of the test site between cross-section no. 7 and 8 (cf. Fig. 5.1 and 5.7), the differences are positive (Fig. 5.7b and 5.7c), which is the result of the watercourse DTM fusion process occurring from two natural steps in the riverbed where only upstream of the steps a measured cross-section is located. As mentioned in Sec. 5.3.3, the elevation data are interpolated linearly from one measured cross-section to the next. If no measured cross-section is available before and behind the elevation step in the riverbed, the interpolated DBM is above the water level resulting in a wrong DBM (Fig. 5.7e).

Figure 5.7d shows the difference model of the watercourse DTM_{2006} minus watercourse DTM_{2003} , which includes the

amount of change. The reddish color represents deposit areas from 2003 to 2006 and the bluish erosion. The erosion and accumulation rates range mainly from 1.25 m to -1.25 m. Only at the measured cross-sections the erosion and accumulation rates can be estimated properly. Between the cross-sections the result is a rough approximation. The changes in between the measured river cross-sections are shown in the plots through no. I and no. II in Figure 5.7e and 5.7f (plot locations in Fig. 5.7). An evaluation for the accuracy of the changes is only possible at the cross-sections (Fig. 5.6) due to the lack of independent reference data from the cross-section measuring epochs.

5.5 Discussion

In August 2005, a major flood event occurred in the westernmost part of Austria with a discharge of more than $1350 \text{ m}^3/\text{s}$ at the Bregenzer Ache. The gauging station in Kennelbach failed at $1350 \text{ m}^3/\text{s}$ and an even higher discharge can be assumed. A general trend in changes of the riverbed can be seen in the main channel after the flood event of 2005. By using the presented methods, it is possible to locate and quantify these changes. A comparison of the WEP and the related DIM shows that it is possible to derive a Water-Extent-Polygon with an accuracy in the range of the DTM resolution (Fig. 5.5 and 6). By

using a point-cloud-based WEP delineation approach, it is possible to derive the WEP even more accurately (Höfle et al. (2009)). But since – as *fstudy* – the point cloud is not always available, a raster-based approach was chosen. In general, to derive water surface areas using ALS data, it is essential to include ALS backscatter data (i.e. signal intensity data).

The locations of the measured cross-sections have a critical influence on the results of the final DBM. Mainly, the distance between the cross-sections in flow direction should be short enough to guarantee that all major river structures are included (e.g. stationary sand or gravel bars, point bars, cutbanks and weirs), which is not the case in this data set. The average cross-section distance in the used data set is 450 m, since those data are not produced for creating DBMs. They are only used for cross-section-based monitoring purposes. Hence, it is impossible to gather the strong change of hydraulic steps caused by weirs within the river. The quality of the DBM depends mainly on the density of measured cross-sections (i.e. spatial resolution along and across the river axis) and on the shape and flow path of the river. If the cross-sections data contain all significant elevation changes (point bars, cutbanks and weirs), the quality of the derivation will be increased. Hence, the number of cross-sections should depend mainly on the quantity of weirs and the number of curves. Therefore, in front and behind

of each weir as well as at each curve a cross-section should be measured. A relation between the number of cross-sections and the sinuosity index (ratio between river length and valley length) is assumed. The higher the sinuosity index of a river, the denser the cross-sections should be measured. If a dense set of river cross-sections is available a 'leave-one-out cross-validation' can be applied to calculate the accuracy of the derived DBMs and the change detection result (erosion/accumulation). This can not be done if the distance between the cross-sections is too large as in the presented study.

5.6 Conclusions and Outlook

The chapter introduces a novel approach to derive the Water-Extent-Polygon (WEP) using raster data comprising radiometry (intensity) and geometry (DTM). The innovation of the chapter is the utilization of intensity data for deriving the WEP, which results in a WEP with an accuracy of less than one meter. This accuracy is usually sufficient for hydraulic studies. We showed the estimation of changes along river corridors by using the WEP as input data for digital bathymetric model (DBM) derivation. The DBM delineation extent is restricted by the derived WEP allowing the estimation of changes of the riverbed. The presented method produces proper results for DBM derivation and change detec-

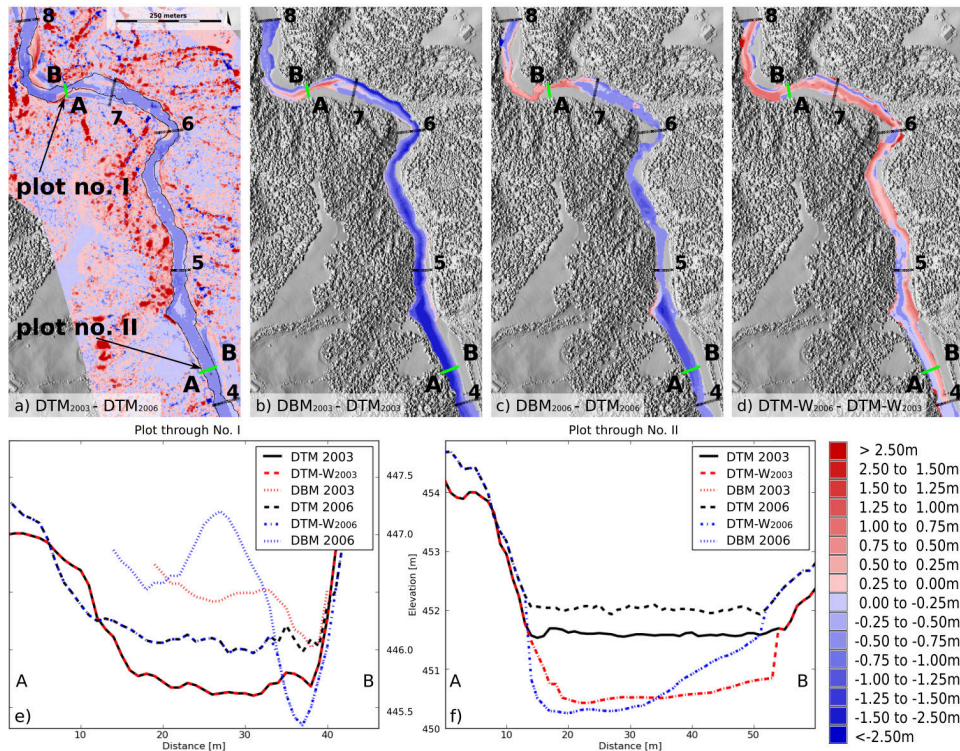


Figure 5.7: Difference-models and plots through the river: a) $DTM_{2003} - DTM_{2006}$; b) $DBM_{2003} - DTM_{2003}$; c) $DBM_{2006} - DTM_{2006}$; d) Difference model of the watercourse DTMs (cut at the combination of WEP_{2003} and WEP_{2006}) $DTM-W_{2006} - DTM-W_{2003}$; e) Plot through river at location No. I; f) Plot through river at location No. II; cross-section No.: 4 to 8 (i.e. Fig. 5.1); No. I and II: Plot locations from A to B; Black line in a): WEP_{2006} .

tion with a minimum of manual interaction for the user. The main problems occur due to the large distance between the river cross-section data set and the non-corrected intensity raster data sets.

Nowadays, with methods like echo sounding, it is possible to collect bathymetric data in short distances and periods with high accuracy. But still, it

is not possible to collect these data in shallow water. The focus of future investigations should concentrate on the development of sensors and techniques, which are able to collect data in shallow water with high density and accuracy. However, with a dense set of river cross-sections or echo sounding data the quality of the bathymetric model can also be increased significantly.

The information of the water depth during the measuring process of the cross-sections at one location, mainly in the middle of each measured cross-section, could be helpful to get an independent source of the water level. Then, the water depth information could be used to verify the WEP delineation procedure. Assuming an almost horizontal water surface (perpendicular to the flow direction), the water depth information could be used to derive a 3D-centerline and 3D-orthogonal-profiles, which can be intersected with a given DTM to derive the WEP.

Multi-temporal data sets are essential for change detection. Therefore, a dense measuring network of topographic and bathymetric data is a requirement. The importance and benefit of a simultaneous data collection of ALS and bathymetric field information needs to be emphasized. Beside the data collection (time series and location), further investigations should concentrate on the development of adequate methods to calculate the total volume changes of the riverbed. The lack of ground truth on the transported material is a fundamental drawback. Therefore, only a relative estimation of areas of accumulation and erosion could be performed.

For land cover classification studies, the derived WEP can be used for water surface classification, which is an accurate and fast solution instead of field surveying or digitizing from aerial imagery. By combining the water ar-

reas with additional roughness information of the riverine landscape derived from the ALS point cloud, new input data sets for numerical hydraulic models can be provided. A combination of derived roughness coefficients from ALS data, WEP and watercourse DTM can provide input data for numeric hydraulic models from one specific time, which is not the case yet.

It is demonstrated that the radiometric information of the ALS data can be used to delineate Water-Extent-Polygons. The radiometric ALS data exhibit a high potential for calculating features, which are not distinguishable on the basis of elevation data only. Therefore, the use of radiometric data, DIM or point cloud intensity values, should be increased for classification and change detection applications. An additional point density raster including laser shot dropouts (as used by Höfle et al. (2009) and Vetter et al. (2009b)) can be useful to improve the presented raster-based WEP approach by using the numbers of laser shot dropouts per raster cell. In general, the use of laser shot dropouts can be used to improve several raster or point-cloud-based classification approaches. Another point is the lack of intensity correction approaches for raster intensity data, which is of high importance to use the intensity values. If the point cloud, including coordinates, timestamps and flight trajectory information are not available, the data cannot be corrected, which result

in intensity values affected by scan angle and range. For an accurate use of intensity values, a correction is essential. By using multi-temporal data sets, a radiometric adjustment or calibration of the intensity data have to be applied to produce intensity values of each period, which are comparable.

5.7 Acknowledgements

We thank the Federal State of Vorarlberg (Vorarlberger Landesregierung, Landesvermessungsamt Feldkirch, Austria) for the geospatial data of the Bregenzer Ache, which are the ALS elevation and intensity raster data. And we cordially thank the Vorarlberger Illwerke AG (Bregenz, Austria) for providing the river cross-sections data sets.

Vertical vegetation structure analysis and hydraulic roughness determination using dense ALS point cloud data – a voxel based approach

In this chapter the complexity of the vertical vegetation structure, based on dense airborne laser scanning (ALS) point cloud data (25 echoes/m²), is analyzed to calculate vegetation roughness for hydraulic applications. Using the original 3D ALS point cloud, three levels of abstractions are derived (cells, voxels and connections) to analyze ALS data based on a 1x1 m² raster over the whole data set. A voxel structure is used to count the echoes in predefined detrended height levels within each cell. In general, it is assumed that the number of voxels containing echoes is an indicator for elevated objects and consequently for increased roughness. Neighboring voxels containing at least one data point are merged together to connections. An additional height threshold is applied to connect vertical neighboring voxels with a certain distance in between. Thus, the connections indicate continuous vegetation structures. The height of the surface near or lowest connection is an indicator for hydrodynamic roughness coefficients. For cells, voxels and connections the laser echoes are counted within the structure and various statistical measures are calculated. Based on these derived statistical parameters a rule-based classification is developed by applying a decision tree to assess vegetation types. Roughness coefficient values such as Manning's n are estimated, which are used as input for 2D hydrodynamic-numerical modeling. The estimated Manning's n values from the ALS point cloud are compared with a traditional Manning's map. Finally, the effect of these two different Manning's n maps as input on the 2D hydraulics are quantified by calculating a height difference model of the inundated depth maps. The results show the large potential of using the entire vertical vegetation structure for hydraulic roughness estimation.

6.1 Introduction

Airborne Laser Scanning (ALS), often referred to as LiDAR, is used as a fast and accurate technique to collect topographic information. ALS has become a state-of-the-art data source for capturing terrain data. ALS is a time and cost-effective method to acquire large area topographic data with low amount of user interaction, high ground sampling density and height accuracy of less than 15 cm. It is used for area-wide 3D data acquisition to support a range of scientific disciplines like (geo)archeology, geology, geomorphology, hydrology and many more (Höfle and Rutzinger, 2011).

Hydrology and water management benefit mostly from technological advances in airborne, mobile and terrestrial laser scanning. It is a permanent process that sensor weight and size continue to decrease whereas the functionality (full-waveform, multiple pulses in air, multiple wavelengths, on-line radiometric calibration, higher sampling density, increasing vertical resolution etc.) and the usability are improving (Pfennigbauer and Ullrich, 2010). Because laser pulses can penetrate the vegetation canopy only through gaps of the foliage, a very dense ALS data set is needed to determine vertical vegetation structure parameters. Dense laser scanning point cloud data provide precise

geometry and high vertical resolution allowing an improved 3D surface classification for hydraulic roughness map calculation.

The roughness of the terrain and the type of vegetation (trees, shrubs or grass) have a strong influence on the floodplain and channel flow regime. Thus, hydraulic models need to parameterize the effect of roughness through the use of hydraulic friction coefficients such as Manning's n or Chézy's C , which describe the resistance of the channel and floodplain to the flow of water (Acrement and Schneider, 1984; Straatsma and Baptist, 2008). The state-of-the-art in hydraulic roughness parametrization is to use land cover maps derived from aerial images and/or field trips to estimate representative roughness values that show the most realistic flood inundation patterns. As highlighted in literature this method is not optimal because of the deficits in the model scheme and computation method. The model input may be compensated by using roughness values that are physically not representative (Straatsma and Baptist, 2008).

The main objective of this study is to improve the determination of the near surface vegetation structure affecting the flow regime and being essential for hydraulic simulation, and to calculate hydraulic roughness maps for 2D hydrodynamic-numerical simulations. With a minimum of user interaction and a standardized method,

the delineation of Manning's n values from ALS point cloud data lead to a time consistent geospatial input data set. As a major benefit, the digital terrain model (DTM) and the roughness are derived from the same ALS point cloud and, thus, have no temporal difference. This improves the modeling results and may replace the preparation of roughness maps by digitizing aerial images and performing field surveys.

6.2 Background

6.2.1 Vegetation structure and surface roughness

Remote sensing has been applied for Earth observation since the 1950s. The introduction of multi-echo LiDAR technology at the end of the 1990s, made simultaneous measurements of the canopies, inside the vegetation and the Earth surface under the vegetation possible. A huge community related to forestry using LiDAR data has been established in the last two decades. The main objectives are in the fields of mapping forested areas, detection of vegetation in urban areas, biomass calculation, species differentiation and many others (Hyypä et al., 2004; Naesset et al., 2004; Rutzinger et al., 2008; Höfle and Hollaus, 2010; Jochem et al., 2010). In forestry applications the use of the point cloud and the nDSM (normalized Digital Surface Model) is dominant. Since a

few years an increasing number of studies make use of radiometric information together with the 3D point cloud from discrete echo recording or full-waveform (FWF) signal analysis or rasterized data with additional attributes for segmentation or classification approaches (Koch, 2010). The use of FWF technology increases the ability to map vegetation in a more dense horizontal and vertical structure than with discrete echo recording systems (Doneus et al., 2010).

Fisher et al. (2009) use a voxel based approach to estimate the vegetation types in a semiarid region by deriving point density in different height levels. Hollaus et al. (2011), Hollaus and Höfle (2010) and Aubrecht et al. (2010) present new methods for estimating vertical vegetation structure parameters of forested and urban areas using detrended terrain points (ALS) for plane fitting to describe the vertical distribution of ALS points per raster cell. By calculating the vertical vegetation structure it is possible to estimate the volume of vegetation in different layers above the terrain (Hollaus et al., 2011). The studies of Hollaus et al. (2011), Aubrecht et al. (2010) and Hollaus and Höfle (2010) show the ability of accurate close-surface vegetation structure data extraction.

An accurate DTM and roughness data are of high importance to simulate water flow characteristics. Due to recent developments in sensor technology, current ALS systems pro-

vide more information such as vertical resolution, point density, which can be used to generate more accurate DTMs (Pfennigbauer and Ullrich, 2010).

By using radiometric attributes of either discrete echo recording or FWF-systems vegetation mapping can be improved (Höfle et al., 2009; Vetter et al., 2011b). An additional attribute derived from the FWF signal is the 'echo width', which is a measure of the height variation of a single echo within the laser footprint (Hollaus et al., 2011).

6.2.2 LiDAR used in hydraulics and hydrology

An extensive overview about active and passive remote sensing techniques in river environments is given by Marcus (2010), in which the main focus is on the water course. From a LiDAR perspective three main topics are relevant for hydraulic studies: (i) the extent of the water surface, (ii) the digital elevation or terrain data of the river bed and the inundation area and (iii) the riparian vegetation, artificial objects (e.g. buildings) within the inundation area and roughness parameter delineation.

Höfle et al. (2009) and Vetter et al. (2009b) present methods to extract the water surface extent from the ALS point cloud using radiometric and geometric information to map the wa-

ter course. Heritage and Milan (2009) demonstrate a method using terrestrial laser scanner (TLS) data to calculate the river bed roughness. Vetter et al. (2011b) present a study about river bed model implementation into the DTM by using terrestrially measured cross-section data to calculate the volume differences along the river bed caused by erosion and accumulation processes between two flood events.

Several studies are presented about DTM generation in general (Kraus and Pfeifer, 1998; Doneus et al., 2010). Related to hydraulic simulations the main focus is on reducing the complexity of the DTM with minimum loss of information as presented in Mandlbürger et al. (2009).

The used roughness term in hydraulic studies relates mainly to Manning's or other empirical equations, in which the roughness value is used to describe the loss of energy of the fluids occur from grain size (in the channel) and/or form parameters such as vegetation type (Naudascher, 1992). However, the term roughness is used differently in various scientific disciplines and spatial scales of interest. Roughness in hydraulics has a different meaning than roughness in remote sensing (Acrement and Schneider, 1984; Naudascher, 1992). The challenge is to define roughness in the sense of the related discipline and to describe the way of the derived parameters and establish standards. Beside the cross-discipline definition problem,

even within the remote sensing community there are different meanings of the term 'roughness'. While in microwave remote sensing a surface may appear smooth, the very same surface is rough for LiDAR, because of the different scales (i.e. wavelengths). Thus, it is also a scaling problem, which increases by getting a better spatial and vertical resolution. Therefore, roughness should be related to the scale or spatial resolution of the data and the application or discipline (Hollaus et al., 2011).

Related to hydraulic roughness, vegetation and type of land cover have a significant influence on the output of hydrodynamic-numerical modeling. Many studies use ALS data for land cover mapping and vegetation classification for hydrodynamic-numerical models (Straatsma and Baptist, 2008; Alexander et al., 2010; Hollaus et al., 2011). Forested and flood inundated areas are covered by trees, shrubs and grass, which influence the flow characteristics of water, represented by a distinct Manning value for each land cover class. By using ALS data the hydraulic friction coefficients for each vegetation cover type can be derived and used as input for 2D hydrodynamic-numerical models. Straatsma and Baptist (2008) present a workflow to calculate hydrodynamic relevant vegetation parameters for 2D hydrodynamic-numerical models from ALS data.

The state-of-the-art input data for flood

modeling are: (i) the geometry provided as DTM of the watercourse (LiDAR, photogrammetry or terrestrial survey), (ii) roughness information, based on land cover maps which are produced from aerial images or field trips, and (iii) the boundary conditions (water levels and/or discharge data).

Casas et al. (2010) present a workflow to estimate hydraulic roughness values using the ΔZ value calculated from subtracting the DTM elevation from each laser echo within the related DTM cell. Finally, they use the DTM detrended laser echo height to estimate the off-terrain vegetation.

Regarding roughness scaling issues, another problem is the sub-footprint roughness. If the footprint of a laser shot is 10 to 50 cm in diameter, the recorded elevation of the echo will be a mixture of the slope and the footprint internal surface roughness. If the sub-footprint vertical height distribution is large enough, multiple distinct echoes can be recorded, which will be enabled by a better vertical resolution via an increased digitizing rate of 10^{10} Hz (0.1 ns) (Pfennigbauer and Ullrich, 2010). Components of the surface roughness which are lower than the vertical resolution of the used scanning system are contained in the recorded echo, which is also influenced by the terrain slope (Hollaus et al., 2011).

6.3 Method

The method focuses on hydraulic roughness estimation, where particularly roughness of the near surface layer is investigated. This approach demonstrates the possibility to map hydrodynamic-numerical roughness parameters such as Manning's n by using the ALS point cloud data. The main concept is to derive connected vertical vegetation structures and to use them as input for a rule-based classification to derive vegetation types, from which the Manning's n can be derived.

6.3.1 General concept

The main idea for delineating homogeneous roughness areas of surface-near vegetation is based on the spatial discretization of the laser echoes and an aggregation of the points into (a) cell-, (b) voxel- and (c) connection-level, which are the different spatial aggregation units (cf. Figure 6.1). We use this approach to calculate different levels of abstraction within a predefined search extent (1 x 1 m) to generate connected vertical vegetation structures.

Before sorting the echoes into the different aggregation levels the height of each echo is normalized to the Z^0 level, which is the height of the DTM at the XY-position of the laser point. All additional calculations are

using this normalized height (nZ) values.

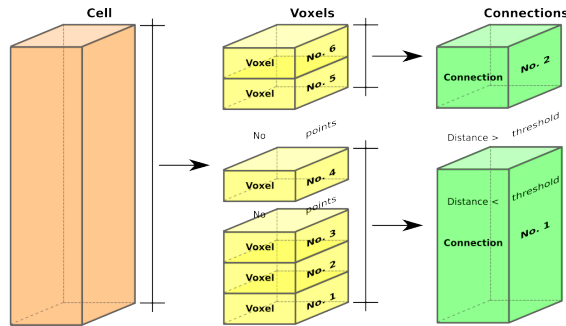


Figure 6.1: Basic concept: spatial discretization of the ALS point cloud into cell-level (a, left), voxel-level (b, middle) and connection-level (c, right)

In a first step, all laser echoes are sorted into cells of 1×1 m size. In a second step, voxels are generated by slicing the cell into vertical height levels of equal height (0.5 m). Based on the nZ value each ALS echo is sorted into the related voxel. In a last step, vertically neighboring voxels are combined to larger units of arbitrary vertical extent (connections) where gaps between the voxels smaller than a predefined threshold (1.1 m) are ignored. Standard descriptive statistics (min, max, mean, median, std, ...) are derived for the cells, voxels and connections (18 parameters per level).

The statistical parameters of the cell-, voxel- and connection-levels serve as basis for a rule-based classification to derive vegetation types, which are finally transferred to Manning values. It is assumed that the descriptive statistical values of the

connections-level are significant parameters to derive hydraulic resistance values.

Bare ground areas will contain only a single compact voxel/connection per cell whereas vegetated areas are characterized by a larger vertical range of normalized height values within a cell. In the latter case, a certain number of occupied voxels per cell will be available. Depending on the vegetation structure, these voxels will be grouped together to one or more connections. The connections are a measure describing the compactness of the vegetation, which can be used for roughness classification.

In Figure 6.1 and 6.2, the cell-, voxel- and connection-level abstraction concept is demonstrated. First, the echoes per cell are collected, then the voxels are created and finally the vertical connections are derived. In the right part of Figure 6.2 a schematic ALS point cloud is shown covering different vegetation types. The furthestmost left part of Figure 6.2 represents all three levels at once for the cell with the blue echoes of the right generalized point cloud. The results are evaluated by visual comparison of the classification maps in Figure 6.3 as well as by comparing the hydrodynamic-numerical modeling results (depth and extent, Figure 6.4).

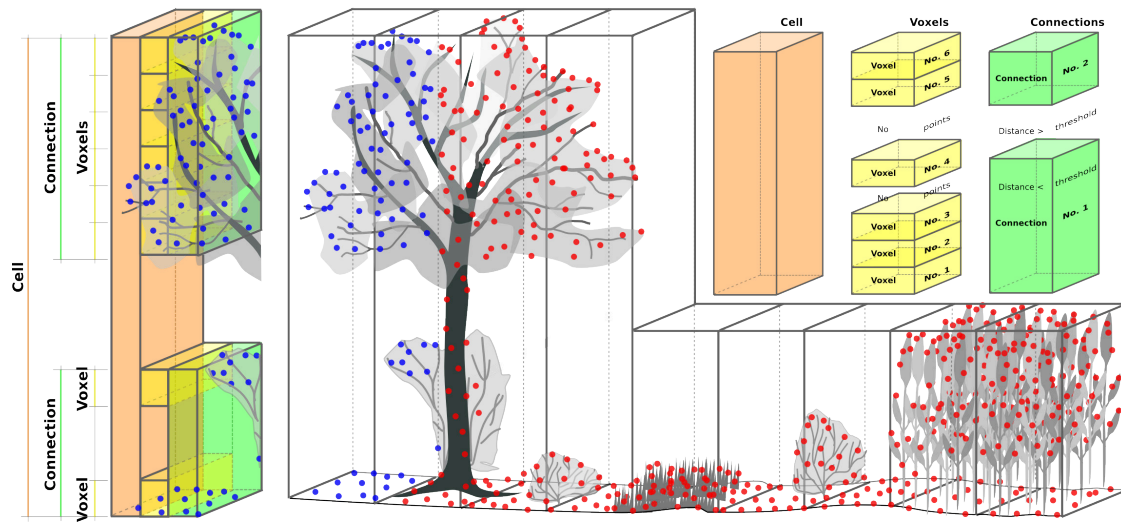


Figure 6.2: Schema of the cell-, voxel- and connection-level related to a generalized ALS point cloud for different vegetation structures

6.3.2 Cell-level

The cell-level is calculated in a X/Y domain of 1×1 m for the whole region, which is also the classification extent. Within each cell, the contained laser echoes are sorted by the nZ value. The cell-level is the input for generating the voxels and can be used to classify forested areas using the maximum height.

6.3.3 Voxel-level

The Voxels represents a cube or a cuboid with either a regular or an irregular size. In this chapter the term voxel is used to describe a 3D bounding box. All echoes of the cell-level are sorted into the related voxels using the nZ heights. The voxels are defined by the cell extent (X, Y) and the height

of 0.5 m. Voxels without any echo are erased and no longer used. The voxels are used to generate the connected vertical structures by merging vertically neighboring voxels into single structures.

6.3.4 Connection-level

Connections describe vertically connected vegetation structures which are apparent in the ALS point cloud. In other words, the connections represent vegetation units or single plants. Connections are derived by merging vertical neighboring voxels which are closer than a certain distance (1.1 m). This distance criterion is used to merge non illuminated areas which are assumed to be of the same vegetation structure as shown in the left part of Figure 6.2.

6.3.5 Hydraulic roughness classification

For hydraulic roughness classification as input data for a 2D hydraulic simulation based on the ALS point cloud the statistical parameters of the cells, voxels and connections are used. Different roughness products can be generated by using a rule-based classification. Therefore, the surface-near vegetation roughness is important and used in the classification of the lowest connection. For other roughness products like canopy roughness the upper connections are of interest.

The rule-based classification thresholds for the statistical parameters are derived by a decision tree (available in the RapidMiner software using default settings), which is based on a reference map with vegetation types and related hydraulic resistance values (Figure 6.3 a). A sample of 5,000 ALS echoes with the additional cells, voxels and connections parameters for 6 vegetation types was used to create the decision tree.

Finally, the derived rule-base (decision tree) is applied to the ALS data using the statistical values shown in Table 6.1. After classifying the 1x1 m cells in to vegetation types and transferring to Manning's n values a modus filter with 8 neighbors is used to smooth the result and to reduce the spatial heterogeneity of the resulting classification raster.

With the presented method it is not possible to derive the related river bed roughness parameters. Therefore, the roughness values are manually classified for areas that are covered by water. The water surface extents are delineated based on a DTM and an ALS intensity image by a raster-based classification of low ALS intensity values and a maximum DTM slope of less than 2° as described in Vetter et al. (2011b).

6.4 Results and discussion

The results of the classification are shown in Figure 6.3b. A visual evaluation of the results has been carried out between the classified ALS and the traditionally derived Manning's n values in Figure 6.3a. As shown in Figure 6.3 the dominant spatial patterns of the Manning's values are comparable. But the ALS derived values represent the whole area in more detail than the traditionally derived map. Major differences are predominantly characterized by the neighboring Manning classes in the ALS derived data. Between class 0.045 and 0.050 or 0.100 and 0.125 large differences are evident, which we assume that they occur from wrong classification rules due to the low overall accuracy of 65% for those four classes. For all other classes the overall accuracy is better than 90%.

6 Hydraulic roughness estimation

Manning's n	Rule-base	Vegetation type
0.045	max. height(lowest connection) < 0.15	streets, short grassland
0.050	max. height(lowest connection) > 0.15 AND < 0.25	grassland, agriculture
0.070	max. height(lowest connection) > 0.25 AND < 2.00	shrubs
0.090	max. height(lowest connection) > 2.00 AND < 5.00	reed
0.100	number of connections > 1 AND max. height(cell) < 10.00	small trees
0.125	number of connections > 1 AND max. height(cell) > 10.00	forest

Table 6.1: Rule-base for hydraulic roughness classification

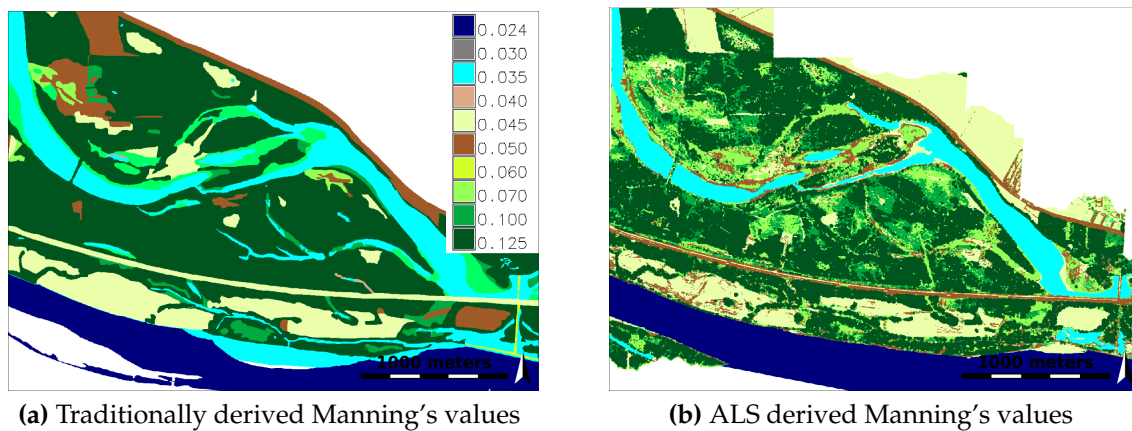


Figure 6.3: Traditionally derived Manning's values vs. the ALS derived values [$s/m^{1/3}$]

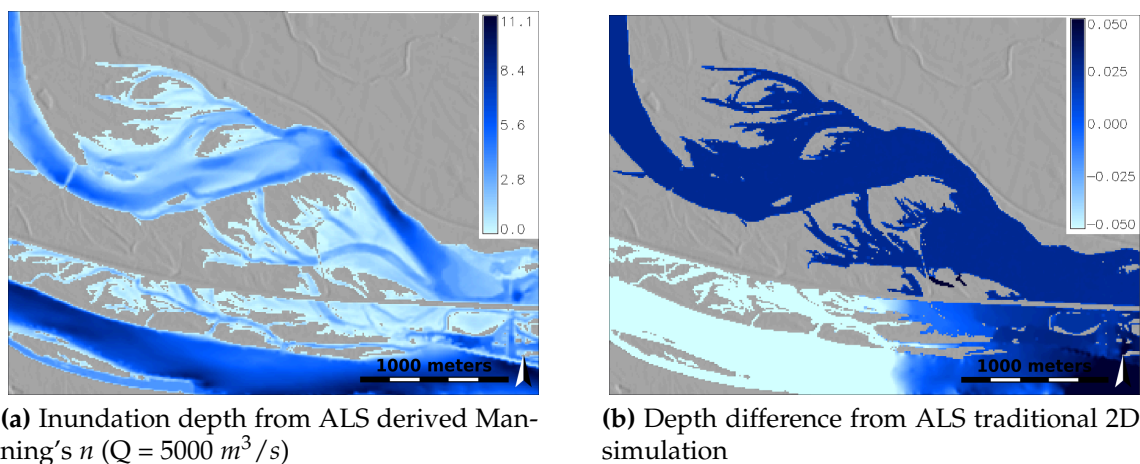


Figure 6.4: Depth of inundated area and difference model from 2D simulation based on the same boundary conditions for ALS and traditional derived Manning's n [m]

Furthermore, the hydrodynamic-numerical modeling results (depth and area of inundation) are compared by using both roughness maps as input. A calibrated model was used to perform two simulations with the same boundary conditions and the same DTM input data with both roughness maps (original and ALS derived). Differences of the two simulation results are in the range of 2 to 3 cm in water depth and a difference in inundation area extent of less than 2800 m^2 (< 1% of total inundated area, Figure 6.4).

The roughness classification rules are based on a decision tree using a subsample of the ALS data with calculated voxel and connection statistical values (ALS derived) created from the original Manning's n map. These results in already calibrated Manning's n values for the classification of the connections where the derived roughness map can be used as input for the 2D simulation without any further calibration. If no calibrated reference data are available, the calibration effort is the same as with traditional data. But the advantage of using ALS data for roughness estimation is the standardization and transferability of the classification and therefore the reduction of manual classification errors. The second benefit is that the calculation is performed fully automatically without any user interaction. The main potential of the proposed method is to reach one consistent input data set for the geome-

try and roughness data (elevation and Manning's n) both derived from ALS data originating from one date of acquisition. Which is not the case if different land use and land cover data are used to produce Manning's n maps from different sources as it is state-of-the-art up to now.

6.5 Conclusions and future work

The presented method has shown the potential to use ALS data as foundation for hydraulic surface roughness estimation using vertical vegetation structure information. The proposed approach derives hydraulic roughness parameters representing the near surface vegetation roughness. As the results have shown, the degree of detail clearly increases by the use of the proposed method, as well as having only little effects on the 2D hydraulic simulation results (water depth and inundated extent). Therefore, we assume that this method is applicable to produce hydraulic roughness maps, which base on geometry data. The low differences between the two hydrodynamic-numerical model results lead us to the conclusion that the spatial distribution of the Manning's values in our study is a feature with low impact on the hydraulic modeling results. However, Manning's n is an empirical value, the transfer of the ALS based method to other regions can be prob-

lematic. We assume that a more physically founded parameter such as the Darcy-Weissbach value f performs better. Therefore, some further tests should be done with the presented method to identify the roughness value that can be described best by ALS geometry data. A further approach is to use the FWF echo width and backscatter information to improve classification results especially for smooth areas such as roads and short grassland.

The presented approach does not include the slope effect for the normalized height value calculation, which results in overestimation of the height value. This results in misclassification in areas with steep slopes which were not evident in the used test site. By applying a slope adaptive nZ value the classification is made free of slope effects and should finally result in better classification accuracy.

One important feature of the approach is the point density which has yet to be investigated. The proposed method uses statistical values per cell, voxel and connection and we assume the point density is an important affecting pa-

rameter. It should be possible to derive an inundation depth dependent hydraulic friction coefficient by using the connection-level values in different heights.

For hydrodynamic-numerical models further follow up investigation should focus on using dense vertical vegetation data sets as input. It is not clear if the hydrodynamic-numerical models are able to use dense input data sets (e.g. DTMs and vegetation of 1×1 m). There is a need to verify whether the use of friction factors in the models are adequate, or the models have to be adopted for dense ALS derived vegetation parameters.

6.6 Acknowledgements

We would like acknowledge financial support from the Austrian Science Funds FWF as part of the Doctoral Programme on Water Resource Systems (DK-plus W1219-N22). This work is partly funded by the Federal Ministry of Economics and Technology (BMW_i), Germany, in the framework of the project "HyLand" (FKZ 50EE1014).

CHAPTER



Synthesis and conclusions

This thesis shows the capacity of using high resolution ALS data within hydrological and hydraulic studies. Methods are presented where ALS data are modified and specific features are derived from the gridded and point cloud data for hydro-related applications. As shown in the different chapters, a huge potential to improve the accuracy of the modeling results is evident if the gridded ALS data are adapted or features are directly derived from the ALS point cloud. The whole potential of ALS data can be used and can increase the accuracy of results applying the presented methods, instead of using standard ALS data and derivatives.

7.1 Synthesis and major findings

While ALS data or the gridded derivatives are used in different scientific fields and application domains (e.g. drainage delineation, hydrodynamic-numerical modeling) as standard input data, the whole potential and advantages of such spatially dense data sets have not been exploited entirely yet. In this thesis it is presented that conditioned DTMs, used with a specific application, increase the quality of results. Relevant features can be derived directly from ALS by using the complete information provided by the point cloud. Within the hydro-related scientific field it is not commonly used to improve ALS data as discussed in this thesis.

Therefore, by using ALS data the spatial resolution and the accuracy of such hydro-related applications can be improved significantly if the data are pre-processed and relevant information is extracted for a specific application instead of using standard data sets. The methods presented in this thesis and the workflow in chapter 1 are devel-

oped in order to prove the assumption that ALS data as basis for hydro-related applications affect the modeling results positively. If the data are consequently manipulated for such an application the results can be assumed to be more accurate than without manipulation. In the hydro-related field like hydrodynamic-numerical modeling or drainage network delineation many different methods are available to improve the model results by using different algorithms or models but only a few change the input data (e.g. Mason et al., 2011; Mandlbürger et al., 2009).

7.1.1 Drainage network delineation

It is shown that by using flow accumulation methods anthropogenic structures, mainly roads, produce unrealistic potential drainage networks. By replacing the original slope alongside roads with an interpolated near-natural slope, a conditioned DTM can be calculated, and therefore the resulting drainage network is no longer influenced by anthropogenic structures. As subsurface man-made structures (e.g. pipes) are

undetectable within ALS, the roads act as walls or barriers if they are not removed from the ALS DTM prior to the drainage delineation. Using the conditioned DTM for network delineation, the results are more accurate than the results based on an original DTM or even the coarse 5m-DTM compared to a reference data set. The reference data is created manually from shaded relief maps and ortho images by the mapping authority. Due to the concept of removing the roads priorly to the drainage delineation process, the high spatial resolution and the full capacity of the topographic data from ALS can be used instead of using smoothed DTMs.

As shown in different studies (e.g. Vianello et al., 2009; Mandlbürger et al., 2011b), the influences of roads included in the DTM on the drainage delineation process using a 1m-DTM are enormous. In the presented method the DTM is conditioned, which is a relatively simple procedure compared to changing the drainage delineation method. In many studies the GIS implemented standard flow algorithms (D8, FD8 or MFD) are used on coarse resolution data (Li and Wong, 2010), and others are creating alternative methods for drainage delineation (Passalacqua et al., 2010; Cazorzi et al., 2013; Gruber and Peckham, 2009). Using the presented approach, the standard GIS flow algorithms can be used by increasing the accuracy of the derived drainage network.

The result of chapter 3 is a drainage network, which represents the potential locations where water might be running, derived on input data with the best available spatial resolution. Related to the workflow in chapter 1 this drainage network can also be used as input for further calculations. So, the drainage network can be used to decrease computation time for the water surface delineation process, using the buffered drainage network as a pre-selection for the calculation area. Besides the water surface delineation the selected data within the drainage buffer of a riparian environment can be used for filtering tasks. It is assumed that specific filtering and DTM generating procedures within riparian zones or along the watercourse have to be used in order to compute more suitable DTMs of river corridors (Mandlbürger et al., 2011b). The intensity values (water surface information) and the vertical vegetation structure can be used to improve riparian filtering tasks.

Another advantage of using the conditioned DTM is the detection of piped river sections. It is assumed that the comparison between the drainage network, based on the conditioned 1m-DTM, and the network from a regular 1m-DTM, results in locations where the probability of piped river sections is very high. To find those piped river sections automatically, the relation between all three, the two different drainage networks (derived from

the conditioned and original DTM) and the street layer, have to be analyzed. Another main advantage is that an established standard flow algorithm can be used for drainage delineation, because the main error source, which are roads, are smoothed away from the DTM, while the rest of the DTM comprise the whole spatial capacity of the ALS data.

7.1.2 Water surface mapping

Nowadays, the radiometric values of ALS data are underrepresented in classification tasks because of the radiometric information complexity and the lack of fully automatic adjustment, correction and calibration tasks. Instead of uncorrected intensity data, the use of corrected intensity data leads to a more robust classification result (Höfle et al., 2009, 2007). An adjustment of the corrected data of multi-temporal data is used to classify data of different periods with the same classification rules. To classify a water surface area from ALS point clouds is an important application for many hydro-related research questions, such as land use mapping or hydraulic modeling.

In order to make the radiometric information of multi-temporal ALS data sets comparable, an absolute calibration has to be applied as described in Wagner (2010). Reference data and measurements from a reflectometer are needed for the calibration (Briese et al., 2008;

Lehner and Briese, 2010). If no reflectometer measurements are available, a calibration without assumptions can not be applied. To analyze radiometric data in a proper way, the minimum requirement is a correction of the radiometric information (Höfle and Pfeifer, 2007). This approach is a stripe-wise relative correction. If a multi-temporal data set has to be used, an adjustment is needed as described in this thesis. The radiometric adjustment is important to produce data with the same range of values (Vetter et al., 2009b). A similar adjustment method is presented by Fritzmann et al. (2011) to map land cover classes. As shown in various literature the radiometric information is increasingly used for classification tasks. Kaasalainen et al. (2010) use the radiometric information to measure soil moisture directly from ALS data. Alexander et al. (2010) use the backscattered information for land cover classification. The correction, calibration and the adjustment of intensity data play an important role in classification of ALS data (Höfle et al., 2012). It has to be considered during the planning of data acquisition that the data which are needed for calibration are collected simultaneously with the ALS campaign Wagner (2010).

Only pioneer studies had applied intensity information when the presented method was created. Up to now it has become more common to use the radiometric data for classification tasks (e.g. Höfle et al., 2012; Kaasalainen et al.,

2010; Korpela et al., 2010; Alexander et al., 2010). The quality of the backscattered information increases, the data are ready to be used and the methods for correction and calibration are available. Efforts to calibrate radiometric data directly during data acquisition have already been done (Pfennigbauer and Ullrich, 2010). The capability of increasing classification accuracy using radiometric information combined with full-waveform attributes is stated in many studies (e.g. Bretar et al., 2009; Alexander et al., 2010; Höfle and Hollaus, 2010; Hollaus et al., 2011; Schmidt et al., 2011). If a radiometric calibration can not be applied, a very simple adjustment method should be used to classify multi-temporal data as presented in this thesis.

7.1.3 River bed modeling

Although bathymetric laser scanning systems use two wavelengths to map shallow water bodies (Guenther et al., 2000), many countries are covered by conventional near infrared laser data, which are not able to penetrate water. Therefore, terrestrially measured river cross sections are used to generate river bed information (Merwade, 2009). While the terrain surface surrounding the water body is collected in high spatial resolution, the aim is to integrate only the interpolated river bed into the DTM and not to change the terrain information from interpolation (Vetter et al., 2011b).

This is presented in the water surface mapping and river bed interpolation part.

Recent trends in LiDAR system development show the ability of shallow water mapping, as presented in Mandlbürger et al. (2011a). Therefore, it will become easier to combine bathymetric and land surface data without any interpolation steps. If bathymetric data are measured without LiDAR, as in most cases, the river bed has to be reconstructed from terrestrially measured cross sections. The approach of using the derived water surface first and then interpolate the river bed for the water surface area is used similarly in a few studies with comparable results (e.g. Mandlbürger, 2006). Besides all assumptions, which have to be made during river bed interpolation using cross section data, the final DTM with the integrated watercourse elevation influences the modeling results of hydrodynamic processes positively (Mandlbürger et al., 2009; Mason et al., 2011).

By integrating the river bed model into the DTM and using intelligent ALS data reduction methods for mesh generation, the set up time and the storage size of the mesh decreases, while the expected quality of the mesh is similar to meshes without data reduction (Mandlbürger et al., 2009).

7.1.4 Hydraulic roughness estimation

The friction coefficient like the Manning's n value is one important input parameter for hydrodynamic-numerical models. In this thesis the aim is to find a method, where the ALS point cloud data can be used to generate a land cover classification automatically. The main findings show that the geometry data can be used to connect the vertical vegetation structures and can then be classified as different land cover classes. These land cover classes can also be derived by using a normalized DSM (nDSM), the point cloud, full-waveform ALS data or the combination of image information and ALS data as presented in many studies (Rutzinger et al., 2008; Mallet et al., 2008; Casas et al., 2010; Höfle and Hollaus, 2010; Nordkvist et al., 2012). The crucial class of bushes under trees can not be derived by using the mentioned methods. The vertical point distribution of the ALS point cloud and the derived vertical connectivity parameter are used to detect underlying vegetation in a reproducible and objective way. This can not be done with traditional methods and data, like image classification or raster-based classification approaches.

Within an ongoing research project (collaboration with the University of Heidelberg) the influences of differently derived land cover classes for hydrodynamic-numerical modeling are being tested. The used land cover mod-

els are 1) land cover map from authority, 2) land cover from OpenStreetMap (OSM, OpenStreetMap (2013)), 3) land cover from CORINE data (ministry of environment), 4) land cover derived from ortho images, 5) land cover derived from nDSM and intensity image and 6) land cover derived with the presented voxel approach (chapter 6). The preliminary results of a hydrodynamic-numerical model based on land cover classes derived from nDSM & intensity, the OSM and the voxel approach show almost identical flood inundated areas and flow velocities, compared to a real flooding event. The hydraulic model calibration was done with the voxel data. It can be assumed that a combination of the nDSM & intensity, the voxel approach and OSM data will yield the most realistic results. Therefore, the land cover classes have to be derived from the nDSM & intensity image for non-vegetated areas, the buildings have to be extracted from OSM and the voxel approach has to be used in the vegetation. Finally, the Manning's n values and the land cover classes are linked within the hydrodynamic-numerical model.

7.1.5 Ongoing work

The importance of the methods presented in this thesis, regarding to the workflow described in the 'Introduction' chapter, has been summarized and applied in (Pfurtscheller and Vetter, 2013). The main steps of the

workflow were used to set up a flood model.

The main outcome of Pfurtscheller and Vetter (2013), where the thesis author was the second author, being responsible for the ALS and hydrodynamic-numerical modeling part, can be identified as the conclusion of this thesis regarding the remote sensing and the feature extraction part for hydrodynamic-numerical models. The main goal in Pfurtscheller and Vetter (2013) was to calculate the entrepreneurial and regional-economic impacts on globalised production companies caused by flood events. This was done by using ALS data and a 2D hydrodynamic-numerical model.

In order to underline the consistency and applicability of the developed thesis methods, the procedure within Pfurtscheller and Vetter (2013) needs to be described shortly. First of all, the water surface area was derived by using the point cloud based classification approach (chapter 4). The conditioning of the DTM and deriving the drainage network (chapter 3) was not carried out because the methods were developed after this study had been realized. Then, the river bed model was calculated (chapter 5). Because of the huge distance of the terrestrially measured cross sections (up to 200m), the river bed model was not used. Instead of using the DTM with the included river bed model, the hydrograph was reduced by the amount of water, which

was measured in the streams during the ALS flight campaign ($29 \text{ m}^3/\text{s}$). Finally, the vertical vegetation structure was calculated and land cover classes were derived. The streets were derived by using the intensity image in combination with the nDSM and the buildings were taken from OpenStreetMap. Then, the Manning's n values were added to the related land cover classes. The Manning's n value for the channel was added to the derived water surface. A hydraulic mesh was generated with a slightly modified method compared to the method presented by Mandlbürger et al. (2009). Based on this mesh a 2D hydrodynamic-numerical model was prepared as described in Vetsch et al. (2011). A flood scenario was created based on the hydrograph of the regional flood event in 2005. The discharge of a flood with a one-hundred-year return period (HQ100) is at $1450 \text{ m}^3/\text{s}$. An approx. 3% increase of discharge was added to the final hydrograph of the HQ100, simulating the impact of climate change in this region (cf. Blöschl et al., 2011), resulting in discharge peak of $1490 \text{ m}^3/\text{s}$. A worst case scenario was calculated with a log jam at the bridge close to the production site of the companies. The hydrodynamic-numerical model was calibrated with the data from the flood event in 2005. The resulting flood inundated areas (depth and velocity maps) were used to compute the vulnerability of two selected companies and finally to calculate the entrepreneurial and regional-economic impacts.

Within Pfurtscheller and Vetter (2013) all presented methods, described in this thesis are combined in order to run a hydrodynamic-numerical model. The main advantages are primarily the use of the water surface and the land cover classification approach. If no river bed model is available or only in poor quality, the original DTM can be used if the hydrograph is reduced by the discharge value during the ALS campaign without any loss of quality of the final modeling results. The channel Manning's n value can be added directly to the water surface while the land cover classes besides the water surface are taken from the ALS data. The combination of land cover classification methods for friction parameter description based on intensity, nDSM and point cloud data are efficient and reproducible. The challenge to find underlying vegetation is avoided by using the vertical vegetation structure analysis, while the streets are classified by using the intensity and nDSM information. The classification task is assumed as being the most effective part of the presented workflow, while the elevation and land cover data used for hydrodynamic-numerical modeling are from one single measurement. The time consistency of the data is given and the one data set can be analyzed with a high degree of automatization to reduce hydrodynamic-numerical model setup time.

7.2 Conclusion

Finally, it need to be pointed out that the presented methods in this thesis have been developed to improve the quality and accuracy of the results of hydro-related studies. These methods show possible solutions to solve challenging questions related to hydrology or hydraulics. However, several solutions have been developed by other scientists solving similar problems (e.g. Mandlburger, 2006; Straatsma and Baptist, 2008; Straatsma et al., 2008; Höfle et al., 2009; Casas et al., 2010; Sofia et al., 2011; Rutzinger et al., 2011b; Cazorzi et al., 2013). To sum up, the main focus of this thesis was to present methods where the full spatial and radiometric potential of ALS data can be used in order to achieve an increase in accuracy of such hydro-related applications. The presented methods demonstrate the ability to change the input data in order to get the expected increase of the results by protecting the high spatial resolution of the data. It is shown that instead of using low resolution data specific manipulations of the 1m-DTM or the extraction of selected features are useful in order to solve hydro-related topics.

7.3 Future work

The main suggestions for future research has already been given in the different thesis chapters. More general future research goals are listed be-

low. It is assumed that this list of ideas for future work might improve the discussed methods to a further extent. The following points are important to take another step further to solve more ALS and hydro-related challenges.

- *Full-waveform laser scanning:* To improve the delineation results, discussed in the different chapters, the impact of full-waveform information needs to be figured out. The influence of point density has to be in center of further research as well. It can be assumed that the use of FWF data and a higher point density will increase the resulting feature accuracy, especially the drainage network delineation and the hydraulic friction estimation.
- *Laser shot dropouts:* The use of laser shot dropouts is essential for water surface classification and delineation, but also for vegetation mapping. The computation of dropouts is up to now outside of the ALS acquisition process. The recording of the lost laser shots during data collection can be realized easily, which could increase the potential of data classification in different fields. As long as the information of the laser shot dropouts are not used, the necessity to record the data is not of further interest for laser scanning companies.
- *Hydro-related applications:* Most of hydro-related applications use coarse resolution input data (e.g. low pass filtered ALS DTMs). The existing methods and applications should be adopted to high resolution ALS data. The amount and accuracy of the ALS data as well as the computation speed and storage capacity are increasing constantly, but only minor or slow developments are registered in the hydro-related application field. The use of 1m spatial resolution data as basis for hydro-related applications is not prevalent. The ALS data themselves have to be modified for each project separately instead of changing the hydro-related application's methods only once.

7.4 Final paragraph

In this thesis it has been shown that the use of conditioned data and different feature extraction methods for specific hydro-related applications re-

sult in more accurate and reproducible outcomes. It has also been demonstrated that ALS is more than a state-of-the-art technique for topographic data collection if the whole capacity of the data is used like the intensity infor-

mation and the 3D information of the point cloud. Nevertheless, the knowledge about the functionality of the used model and the applied algorithm is essential to generate an appropriate input data set from ALS data. It has been clarified that there is no standard ALS terrain or surface model available, which

can fit to various applications. So, the input data have to be manipulated and specific features have to be derived separately with customized methods for different applications in order to solve diverse research questions successfully.

'Measure what is measurable, and make measurable what is not so.'
Galileo Galilei (1564-1642)

Bibliography

- Abermann, J., Fischer, A., Lambrecht, A., and Geist, T. (2010). On the potential of very high-resolution repeat DEMs in glacial and periglacial environments. The Cryosphere, 4:53–65.
- Abo Akel, N., Zilberstein, O., and Doytsher, Y. (2003). Automatic DTM Extraction from Dense Raw LIDAR Data in Urban Areas. In Proceedings of FIG Working Week 2003, pages 1–10, Paris.
- Acrement, G. and Schneider, V. (1984). Guide for selecting Manning's roughness coefficients for natural channels and floodplains. Report FHWA-TS-84-204, U.S. Department of Transportation, Federal Highways Administration.
- Adams, M., Falkner, M., Franke, M., Jochem, A., Lochner, B., Link, S., Vetter, M., and Werthmann, M. (2007). Hochwasser Risiko Modellierung Innsbruck – Endbericht zum Projektmodul Geoökologie und Raumforschung 2006/2007. Technical report, Institut für Geographie, Universität Innsbruck.
- Alexander, C., Tansey, K., Kaduk, J., Holland, D., and Tate, N. (2010). Backscatter coefficient as an attribute for the classification of full-waveform airborne laser scanning data in urban areas. ISPRS Journal of Photogrammetry and Remote Sensing, 65(5):423–432.
- Alho, P., Kukko, A., Hyyppä, H., Kaartinen, H., Hyyppä, J., and Jaakkola, A. (2009). Application of boat-based laser scanning for river survey. Earth Surface Processes and Landforms, 34(13):1831–1838.
- Allouis, T., Bailly, J.-S., Pastol, Y., and Le Roux, C. (2010). Comparison of LiDAR waveform processing methods for very shallow water bathymetry using Raman, near-infrared and green signals. Earth Surface Processes and Landforms, 35(6):640–650. Published Online. DOI: 10.1002/esp.1959.
- Amt der Vorarlberger Landesregierung (2005). Das Starkregen- und Hochwasserereignis des August 2005 in Vorarlberg. Technical report, Amt der Vorarlberger Landesregierung.

Bibliography

- Antonarakis, A., Richards, K., and Brasington, J. (2008). Object-based land cover classification using airborne LiDAR. Remote Sensing of Environment, 112(6):2988–2998.
- Aubrecht, C., Höfle, B., Hollaus, M., Köstl, M., Steinnocher, K., and Wagner, W. (2010). Vertical roughness mapping - ALS based classification of the vertical vegetation structure in forested areas. In The International Archives of the Photogrammetry, Remote Sensing and Spatial Information Sciences, volume XXXVIII-7B, pages 35–40, Vienna, Austria.
- Baatz, M. (2003). eCognition - user guide 3. Definiens Imaging GmbH.
- Baltsavias, E. P. (1999a). Airborne laser scanning: basic relations and formulas. ISPRS Journal of Photogrammetry & Remote Sensing, 54(2-3):199–214.
- Baltsavias, E. P. (1999b). Airborne laser scanning existing systems and firms and other resources. ISPRS Journal of Photogrammetry & Remote Sensing, 54(2-3):164–198.
- Beyer, A., Schenke, H. W., Klenke, M., and Niederjasper, F. (2003). High resolution bathymetry of the eastern slope of the Porcupine Seabight. Marine Geology, 198(1-2):27–54. Geosphere-Biosphere Coupling: Cold Seep Related Carbonate and Mound Formation and Ecology.
- Blöschl, G., Viglione, A., Merz, R., Parajka, R., Salinas, J., and Schöner, W. (2011). Auswirkungen des Klimawandels auf Hochwasser und Niederwasser. Österreichische Wasser- und Abfallwirtschaft, 63:21–30.
- Bretar, F., Chauve, A., Bailly, J., Mallet, C., and Jacome, A. (2009). Terrain surfaces and 3-d landcover classification from small footprint full-waveform lidar data: application to badlands. Hydrology and Earth System Sciences, 13(8):1531–1544.
- Briese, C. (2004). Three-dimensional Modelling of Breaklines from Airborne Laser Scanner Data. In Altan, O., editor, International Archives of Photogrammetry, Remote Sensing and Spatial Information Sciences, volume XXXV-B3, pages 1097–1102, Istanbul.
- Briese, C., Höfle, B., Lehner, H., Wagner, W., Prenningbauer, M., and Ullrich, A. (2008). Calibration of Full-Waveform Airborne Laser Scanning Data for Object Classification. In Proceedings of SPIE - The International Society for Optical Engineering, volume 6950, page 8. SPIE. DOI: 10.1117/12.781086.

- Brockmann, H. and Mandlbürger, G. (2001). Modelling a watercourse DTM based on airborne laser-scanner data - using the example of the river Oder along the German/Polish border. In OEEPE Workshop on Airborne Laserscanning and Interferometric SAR for Detailed Digital Terrain Models, Stockholm.
- Brügelmann, R. (2000). Automatic breakline detection from airborne laser range data. In International Archives of Photogrammetry, Remote Sensing and Spatial Information Sciences, volume XXXIII-B3, pages 109–116.
- Brügelmann, R. and Bollweg, A. (2004). Laser altimetry for river management. In International Archives of Photogrammetry, Remote Sensing and Spatial Information Sciences, volume XXXV-B2, pages 234–239, Istanbul.
- Brzank, A. and Heipke, C. (2006). Classification of Lidar Data into water and land points in coastal areas. In International Archives of Photogrammetry, Remote Sensing and Spatial Information Sciences, volume XXXVI-B3, pages 197–202, Bonn.
- Brzank, A., Heipke, C., Goepfert, J., and Soergel, U. (2008). Aspects of generating precise digital terrain models in the Wadden Sea from lidar - water classification and structure line extraction. ISPRS Journal of Photogrammetry and Remote Sensing, 63(5):510–528.
- Carter, G. and Shankar, U. (1997). Creating rectangular bathymetry grids for environmental numerical modelling of gravel-bed rivers. Applied Mathematical Modelling, 21(11):699–708.
- Cary, T. (2009). Lidar Market: Status and Growth Trends. In International LiDAR Mapping Forum 2009, page 10.
- Casas, A., Lane, S., Yu, D., and Benito, G. (2010). A method for parameterising roughness and topographic sub-grid scale effects in hydraulic modelling from LiDAR data. Hydrology and Earth System Sciences, 14(8):1567–1579.
- Cazorzi, F., Dalla Fontana, G., De Luca, A., Sofia, G., and Tarolli, P. (2013). Drainage network detection and assessment of network storage capacity in agrarian landscape. Hydrological Processes, 27(4):541–553.
- Clode, S., Rottensteiner, F., and Kootsookos, P. (2005). Improving City Model Determination by Using Road Detection from LIDAR Data. In International Archives of the Photogrammetry, Remote Sensing and Spatial Information Sciences, volume XXXVI-3/W24, pages 159–164, Vienna, Austria.

Bibliography

- Cobby, D. M., Mason, D. C., Horritt, M. S., and Bates, P. D. (2003). Two-dimensional hydraulic flood modelling using a finite-element mesh decomposed according to vegetation and topographic features derived from airborne scanning laser altimetry. Hydrological Processes, 17(10):1979–2000.
- Crétau, J. and Birkett, C. (2006). Lake studies from satellite radar altimetry. Comptes Rendus Geosciences, 338(14-15):1098–1112.
- Dinehart, R. L. (2002). Bedform movement recorded by sequential single-beam surveys in tidal rivers. Journal of Hydrology, 258(1-4):25–39.
- Doneus, M., Briese, C., and Studnicka, N. (2010). Analysis of Full-Waveform ALS Data by Simultaneously Acquired TLS Data: Towards an Advanced DTM Generation in Wooded Areas. In Wagner, W. and Székely, B., editors, The International Archives of the Photogrammetry, Remote Sensing and Spatial Information Sciences, volume XXXVIII-7B of ISPRS Technical Commission VII Symposium, '100 Years ISPRS - Advancing Remote Sensing Science', pages 193–198, Vienna, Austria.
- Edelsbrunner, H. and Mücke, E. (1994). Tree-dimensional alpha shapes. ACM Transactions, 13(1):43–72.
- EEA (2010). Mapping the impacts of natural hazards and technological accidents in Europe – An overview of the last decade. Technical report 13/2010, European Environment Agency.
- Egger, H., Krenmayer, H., G.W., M., Marura, A., Nowotny, A., Pascher, G., Pestal, G., Pistotnik, J., Rockenschaub, M., and Schabel, W. (1999). Geologische Übersichtskarte der Republik Österreich 1:1500 000. Technical report, Geologische Bundesamt, Wien, www.geologie.ac.at/pdf/Uebersichtskarten/GeolKarteAUT-15.pdf.
- Elmqvist, M., Jungert, E., Lantz, F., Persson, A., and Söderman, U. (2001). Terrain Modelling and Analysis using Laser Scanner Data. In International Archives of Photogrammetry, Remote Sensing and Spatial Information Sciences, volume XXXIV-3/W4, pages 219–226, Annapolis, MD, USA.
- Erpicum, S., Dewals, B., Archambeau, P., Detrembleur, S., and Piroton, M. (2010). Detailed inundation modelling using high resolution DEMs. Engineering Applications of Computational Fluid Mechanics, 2(4):196–208.
- EU (2000). Water Framework Directive, 2000/60/EC. Official Journal of the European Union (OJL), 327:173.

- EU (2007). Infrastructure for Spatial Information in the European Community (INSPIRE), directive 2007/2/EC. Official Journal of the European Union (OJL), 50:114.
- Eysn, L., Hollaus, M., Vetter, M., and Pfeifer, N. (2010). Waldlückenerfassung aus ALS Daten mittels α -Shapes. In Kohlhofer, G. and Franzen, M., editors, Dreiländertagung OVG, DGPF und SGPF, 30. Wissenschaftlich-Technische Jahrestagung der DGPF, Wien, 1.–3. Juli 2010, pages 552–560.
- Fan, Q., Efrat, A., Koltun, V., Krishnan, S., and Venkatasubramanian, S. (2005). Hardware-assisted Natural Neighbor Interpolation. In Proc. 7th Workshop on Algorithm Engineering and Experiments (ALENEX).
- Fisher, J., Erasmus, B., Witkowski, E., van Aardt, J., Asner, G., Kennedy-Bowdoin, T., Knapp, D., Emerson, R., Jacobson, J., Mathieu, R., and Wessels, K. J. (2009). Three-dimensional Woody Vegetation Structure across Different Land-use Types and -land-use Intensities in a Semi-arid Savanna. In IGARSS (2)'09, pages 198–201.
- Flanagin, M., Grenotton, A., Ratcliff, J., Shaw, K. B., Sample, J., and Abdelguerfi, M. (2007). Hydraulic Splines: A Hybrid Approach to Modeling River Channel Geometries. Computing in Science & Engineering, 9(5):4–15.
- Fritzmann, P., Höfle, B., Sailer, R., Stötter, J., and Vetter, M. (2011). Multi-temporal surface classification of airborne LiDAR intensity data in high mountain environments – A case study from Hintereisferner, Austria. Zeitschrift für Geomorphologie/Annals of Geomorphology, 55(2):105–126.
- Geist, T. and Stötter, J. (2007). Documentation of glacier surface elevation change with multi-temporal airborne laser scanner data - case study: Hintereisferner and Kesselwandferner, Tyrol, Austria. Zeitschrift für Gletscherkunde und Glazialgeologie, 41:77–106.
- GRASS Development Team (2013). Geographic Resources Analysis Support System (GRASS GIS) Software. Open Source Geospatial Foundation. <http://grass.osgeo.org> (13-04-2013).
- Gruber, S. and Peckham, S. (2009). Chapter 7 Land-Surface Parameters and Objects in Hydrology. In Hengl, T. and Reuter, H., editors, Geomorphometry Concepts, Software, Applications, volume 33 of Developments in Soil Science, pages 171–194. Elsevier.

Bibliography

- Grünewald, T., Schirmer, M., Mott, R., and Lehning, M. (2010). Spatial and temporal variability of snow depth and ablation rates in a small mountain catchment. The Cryosphere, 4:215–225.
- Guenther, G. C., Brooks, M. W., and LaRocque, P. E. (2000). New Capabilities of the SHOALS Airborne Lidar Bathymeter. Remote Sensing of Environment, 73(2):247–255.
- Hall, D. K. (1996). Remote sensing applications to hydrology: imaging radar. Hydrological Sciences Journal, 41(4):609–624.
- Heitzinger, D. and Kager, H. (1998). High quality DTMs from contourlines by knowledge-based classification of problem regions. In Proceedings of the International Symposium on 'GIS - Between Visions and Applications', volume 32 of ISPRS Comm. 4, pages 230–237, Stuttgart.
- Heritage, G. L. and Milan, D. (2009). Terrestrial laser scanning of grain roughness in a gravel-bed river. Geomorphology, 113(1-2):4–11.
- Höfle, B. (2007). Detecting and Utilizing the Information Potential of Airborne Laser Scanning Point Cloud and Intensity Data by Developing a Management and Analysis System. PhD thesis, Institut für Geographie, Universität Innsbruck.
- Höfle, B., Geist, T., Rutzinger, M., and Pfeifer, N. (2007). Glacier surface segmentation using airborne laser scanning point cloud and intensity data. In International Archives of Photogrammetry, Remote Sensing and Spatial Information Sciences, volume XXXVI-3/W52, page on CD, Espoo, Finland.
- Höfle, B. and Hollaus, M. (2010). Urban vegetation detection using high density full-waveform airborne LiDAR data - Combination of object-based image and point cloud analysis. In The International Archives of the Photogrammetry, Remote Sensing and Spatial Information Sciences, volume XXXVIII-7B, pages 281–286, Vienna, Austria.
- Höfle, B., Hollaus, M., and Hagenauer, J. (2012). Urban vegetation detection using radiometrically calibrated small-footprint full-waveform airborne LiDAR data. ISPRS Journal of Photogrammetry and Remote Sensing, 67(0):134–147.
- Höfle, B. and Pfeifer, N. (2007). Correction of laser scanning intensity data, data and model-driven approaches. ISPRS Journal of Photogrammetry and Remote Sensing, 62(6):415–433.

- Höfle, B. and Rutzinger, M. (2011). Topographic airborne LiDAR in geomorphology: A technological perspective. Zeitschrift für Geomorphologie, Annals of Geomorphology, 55(2):1–29.
- Höfle, B., Vetter, M., Pfeifer, N., Mandlbürger, G., and Stötter, J. (2009). Water surface mapping from airborne laser scanning using signal amplitude and elevation data. Earth Surface Processes and Landforms, 34(12):1635–1649.
- Hohenthal, J., Alho, P., Hyyppä, J., and Hyyppä, H. (2011). Laser scanning applications in fluvial studies. Progress in Physical Geography, 35(6):782–809.
- Hollaus, M., Aubrecht, C., Höfle, B., Steinnocher, K., and Wagner, W. (2011). Roughness Mapping on Various Vertical Scales Based on Full-Waveform Airborne Laser Scanning Data. Remote Sensing, 3(3):503–523.
- Hollaus, M. and Höfle, B. (2010). Terrain roughness parameters from full-waveform airborne LIDAR data. In The International Archives of the Photogrammetry, Remote Sensing and Spatial Information Sciences, volume XXXVIII-7B, pages 287–292, Vienna, Austria.
- Hollaus, M., Wagner, W., and Kraus, K. (2005). Airborne laser scanning and usefulness for hydrological models. Advances in Geosciences, 5:57–63.
- Hubbart, J. A. (2008). Encyclopedia of Earth, chapter History of hydrology. Environmental Information Coalition, National Council for Science and the Environment.
- Hug, C., Ullrich, A., and Grimm, A. (2004). Litemapper-5600 a waveform-digitizing lidar terrain and vegetation mapping system. In International Archives of Photogrammetry, Remote Sensing and Spatial Information Sciences, volume XXXVI-8/W2, pages 24–29, Freiburg, Germany.
- Hyyppä, J., Hyyppä, H., Litkey, P., Yu, X., Haggrén, H., Rönnholm, P., Pyysalo, U., Pitkänen, J., and Maltamo, M. (2004). Algorithms and Methods of Airborne Laser Scanning for Forest Measurements. In International Archives of Photogrammetry, Remote Sensing and Spatial Information Sciences, volume XXXVI-8/W2, pages 82–89.
- Irish, J. L. and Lillycrop, W. J. (1999). Scanning laser mapping of the coastal zone: the SHOALS system. ISPRS Journal of Photogrammetry and Remote Sensing, 54(2-3):123–129.

- Isenburg, M., Liu, Y., Shewchuk, J., Snoeyink, J., and Thirion, T. (2006). Generating Raster DEM from Mass Points via TIN Streaming. In GIScience'06 Conference Proceedings, pages 186–198.
- Jasiewicz, J. and Metz, M. (2011). A new GRASS GIS toolkit for Hortonian analysis of drainage networks. Computers and Geosciences, 37(8):1162–1173.
- Jelalian, A. V. (1992). Laser Radar Systems. Artech House Publishers.
- Jensen, J. R. (2007). Remote sensing of the environment: an earth resource perspective. Prentice Hall Series in Geographic Information Sciences, 2 edition.
- Jochem, A., Hollaus, M., Rutzinger, M., Höfle, B., Schadauer, K., and Maier, B. (2010). Estimation of aboveground biomass using airborne LiDAR data. In Proceedings of Silvilaser 2010, the 10th International Conference on LiDAR Applications for Assessing Forest Ecosystems, Freiburg, Germany. digital media.
- Kaasalainen, S., Kukko, A., Lindroos, T., Litkey, P., Kaartinen, H., Hyyppä, J., and Ahokas, E. (2008). Brightness measurements and calibration with airborne and terrestrial laser scanners. IEEE Transactions on Geoscience and Remote Sensing, 46(2):528–533.
- Kaasalainen, S., Niittymäki, H., Krooks, A., Koch, K., Kaartinen, H., Vain, A., and H., H. (2010). Effect of Target Moisture on Laser Scanner Intensity. IEEE Transactions on Geoscience and Remote Sensing, 48(4):2128–2136.
- Kager, H., Rottensteiner, F., Kerschner, M., and Stadler, P. (2002). ORPHEUS 3.2.1 User Manual. Technical report, Institute of Photogrammetry and Remote Sensing, Vienna University of Technology.
- Katzenbeisser, R. and Kurz, S. (2004). Airborne Laser-Scanning, ein Vergleich mit terrestrischer Vermessung und Photogrammetrie. Photogrammetrie, Fernerkundung, Geoinformation, 3:179–188.
- Koch, B. (2010). Status and future of laser scanning, synthetic aperture radar and hyperspectral remote sensing data for forest biomass assessment. ISPRS Journal of Photogrammetry and Remote Sensing, 65(6):581–590. ISPRS Centenary Celebration Issue.
- Korpela, I., Ørka, H. O., Hyyppä, J., Heikkinen, V., and Tokola, T. (2010). Range and AGC normalization in airborne discrete-return LiDAR intensity data for forest canopies. ISPRS Journal of Photogrammetry and Remote Sensing, 65(4):369–379.

- Kraus, K. and Pfeifer, N. (1998). Determination of terrain models in wooded areas with airborne laser scanner data. ISPRS Journal of Photogrammetry & Remote Sensing, 53(4):193–203.
- Lane, S. N., Richards, K. S., and Chandler, J. H. (2006). Developments in monitoring and modelling small-scale river bed topography. Earth Surface Processes and Landforms, 19(4):349–368.
- Legleiter, C. and Kyriakidis, P. (2008). Spatial prediction of river channel topography by kriging. Earth Surface Processes and Landforms, 33(6):841–867.
- Legleiter, C. J., Roberts, D. A., Marcus, W. A., and Fonstad, M. A. (2004). Passive optical remote sensing of river channel morphology and in-stream habitat: Physical basis and feasibility. Remote Sensing of Environment, 93(4):493–510.
- Lehner, H. and Briese, C. (2010). Radiometric calibration of Full-Waveform Airborne Laser Scanning Data based on natural surfaces. In Wagner, W. and Székely, B., editors, The International Archives of the Photogrammetry, Remote Sensing and Spatial Information Sciences, volume XXXVIII-7B of ISPRS Technical Commission VII Symposium, '100 Years ISPRS - Advancing Remote Sensing Science', pages 360–365, Vienna, Austria,.
- Li, J. and Wong, D. (2010). Effects of DEM sources on hydrologic applications Computers. Environment and Urban Systems, 34(3):251–261.
- Mallet, C. and Bretar, F. (2009). Full-waveform topographic lidar: State-of-the-art. ISPRS Journal of Photogrammetry and Remote Sensing, 64(1):1–16.
- Mallet, C., Bretar, F., and Soerge, I. U. (2008). Analysis of Full-waveform LiDAR Data for Classification of Urban Areas. Photogrammetrie Fernerkundung Geoinformation, 5:337–349.
- Mandlbürger, G. (2006). Topographische Modelle für Anwendungen in Hydraulik und Hydrologie. PhD thesis, Institut für Photogrammetrie und Fernerkundung, TU Wien.
- Mandlbürger, G., Briese, C., Otepka, J., Höfle, B., and Pfeifer, N. (2010a). Verwaltung landesweiter Full Waveform Airborne Laser Scanning Daten. In Kohlhofer, G. and Franzen, M., editors, Dreiländertagung OVG, DGPF und SGPF, 30. Wissenschaftlich-Technische Jahrestagung der DGPF, Wien, 1.–3. Juli 2010, pages 356–365.

- Mandlbürger, G., Briese, C., and Pfeifer, N. (2007). Progress in LiDAR sensor technology - chance and challenge for DTM generation and data administration. In Fritsch, D., editor, Proceedings of the 51th Photogrammetric Week, pages 159–169. Wichmann Verlag.
- Mandlbürger, G., Hauer, C., Höfle, B., Habersack, H., and Pfeifer, N. (2009). Optimisation of LiDAR derived terrain models for river flow modelling. Hydrology and Earth System Sciences, 13:1453–1466.
- Mandlbürger, G., Otepka, J., Karel, W., Wöhrer, B., Wagner, W., and Pfeifer, N. (2010b). OPALS (Orientation and Processing of Airborne Laser Scanning data) - Konzept und Anwendungsbeispiele einer wissenschaftlichen Laserscanning Software. Photogrammetrie, Fernerkundung und Geoinformation, 19(19):376–387.
- Mandlbürger, G., Pfennigbauer, M., Steinbacher, F., and Pfeifer, N. (2011a). Airborne Hydrographic LiDAR Mapping - Potential of a new technique for capturing shallow water bodies. In Modelling and Simulation Society of Australia and New Zealand, 19th International Congress on Modelling and Simulation, pages 2416–2422.
- Mandlbürger, G., Vetter, M., Milenkovic, M., and Pfeifer, N. (2011b). Derivation of a countrywide river network based on Airborne Laser Scanning DEMs - results of a pilot study. In Modelling and Simulation Society of Australia and New Zealand, 19th International Congress on Modelling and Simulation, pages 2423–2429.
- Marcus, W. (2010). Remote sensing of the hydraulic environment in gravel bed rivers. In 7th Gravel-Bed Rivers Conference 2010, Tadoussac, Québec.
- Marcus, W. and Fonstad, M. (2008). Optical remote mapping of rivers at sub-meter resolutions and waters extents. Earth Surface Processes and Landforms, 33(1):4–24.
- Mason, D. C., Schumann, G. J.-P., and Bates, P. D. (2011). Data utilization in flood inundation modelling. In Pender, G. and Faulkner, H., editors, Flood risk science and management, pages 211–233. Wiley-Blackwell.
- Mertes, L. A. K. (2002). Remote sensing of riverine landscapes. Freshwater Biology, 47:799–816.
- Merwade, V. (2009). Effect of spatial trends on interpolation of river bathymetry. Journal of Hydrology, 371(1-4):169–181.

- Merwade, V., Cook, A., and Coonrod, J. (2008). Gis techniques for creating river terrain models for hydrodynamic modeling and flood inundation mapping. Environmental Modelling & Software, 23(10-11):1300–1311.
- Naesset, E., Gobakken, T., Holmgren, J., Hyyppä, H., Hyyppä, J., Maltamo, M., Nilsson, M., Olsson, H., Persson, A., and Soderman, U. (2004). Laser scanning of forest resources: the nordic experience. Scandinavian Journal of Forest Research, 19(6):433–442.
- Naudascher, E. (1992). Hydraulik der Gerinne und Gerinnebauwerke. 2. Springer Verlag, Wien, New York.
- Nordkvist, K., Granholm, A.-H., Holmgren, J., Olsson, H., and Nilsson, M. (2012). Combining optical satellite data and airborne laser scanner data for vegetation classification. Remote Sensing Letters, 3(5):393–401.
- O’Callaghan, J. and Mark, D. (1984). The extraction of drainage networks from digital elevation data. Computer Vision, Graphics and Image Processing, 28:328–344.
- OpenStreetMap (2013). www.openstreetmap.org. 25.04.2013.
- Optech (2008). www.optech.ca. 20.08.2008.
- Passalacqua, P., Belmont, P., and Foufoula-Georgiou, E. (2012). Automatic geomorphic feature extraction from lidar in flat and engineered landscapes. Water Resour. Res., 48(W03528):18.
- Passalacqua, P., Trung, T.-D., Foufoula-Georgiou, E., Sapiro, G., and Dietrich, W. (2010). A geometric framework for channel network extraction from lidar: non-linear diffusion and geodesic paths. Journal of Geophysical Research–Earth Surface, 115(F01002):18.
- Pfeifer, N. and Mandlbürger, G. (2008). Filtering and DTM Generation. In Shan, J. and Toth, C., editors, Topographic Laser Ranging and Scanning: Principles and Processing, pages 307–333. CRC Press.
- Pfeifer, N., Stadler, P., and Briese, C. (2001). Derivation of Digital Terrain Models in the SCOP++ Environment. In Proceedings of OEEPE Workshop on Airborne Laserscanning and Interferometric SAR for Detailed Digital Terrain Models, Stockholm, Sweden.

- Pfennigbauer, M., Mobius, B., Ullrich, A., and Pereira do Carmo, J. (2010). From long range to high precision: pushing the limits of pulsed-time-of-flight measurement. In Proc. SPIE, volume 7684-19.
- Pfennigbauer, M. and Ullrich, A. (2010). Improving quality of laser scanning data acquisition through calibrated amplitude and pulse deviation measurement. In Proc. SPIE, volume 7684-76841F.
- Pfurtscheller, C. and Vetter, M. (2012a). Betriebliche und ökonomische Schäden auf Basis einer Hochwassermodellierung. Internal report (company 1), Österreichische Akademie der Wissenschaften (ÖAW).
- Pfurtscheller, C. and Vetter, M. (2012b). Betriebliche und ökonomische Schäden auf Basis einer Hochwassermodellierung. Internal report (company 2), Österreichische Akademie der Wissenschaften (ÖAW).
- Pfurtscheller, C. and Vetter, M. (2013). Assessing entrepreneurial and regional-economic flood impacts on a globalised production company base on LIDAR data and 2D flood modelling. Journal of Flood Risk Management, January 2013. Submitted in January 2013.
- Python Software Foundation (2012). Python programming language, <http://www.python.org>. 08.2012.
- Quinn, P., Beven, K., Chevallier, P., and Planchon, O. (1991). The prediction of hillslope flow paths for distributed hydrological modelling using digital terrain models. Hydrological Processes, 5:59–79.
- Roncat, A., Dorninger, P., Molnár, G., Székely, B., Zámolyi, A., Melzer, T., Pfeifer, N., and Drexel, P. (2010). Influences of the Acquisition Geometry of different Lidar Techniques in High-Resolution Outlining of microtopographic Landforms. In Fachtagung Computerorientierte Geologie - COGeo 2010, page 17.
- Rudhardt+Gasser and Hunziker, Zarn und Partner (2004). Geschiebe- und Schwebstoffhaushalt der Bregenzerach. Technical report, Bundeswasserbauverwaltung Vorarlberg.
- Rutzinger, M. (2008). Object Detection in Airborne Laser Scanning Data in Urban Environments. PhD thesis, Insitut für Geographie, Universität Innsbruck.
- Rutzinger, M., Höfle, B., Hollaus, M., and Pfeifer, N. (2008). Object-Based Point Cloud Analysis of Full-Waveform Airborne Laser Scanning Data for Urban Vegetation Classification. Sensors, 8(8):4505–4528.

- Rutzinger, M., Höfle, B., and Kringer, K. (2012). Accuracy of automatically extracted geomorphological breaklines from airborne LiDAR curvature images. Geographiska Annaler: Series A, Physical Geography, 94:33–42.
- Rutzinger, M., Höfle, B., Oude Elberink, S., and Vosselman, G. (2011a). Automatic facade extraction from mobile laser scanning data. Photogrammetrie, Fernerkundung und Geoinformation, 3(3):97–107.
- Rutzinger, M., Höfle, B., Vetter, M., and Pfeifer, N. (2011b). Geomorphological Mapping: a professional handbook of techniques and applications, chapter Digital terrain models from airborne laser scanning for the automatic extraction of natural and anthropogenic linear structures, pages 475–488. Elsevier.
- Rutzinger, M., Rüb, B., Höfle, B., and Vetter, M. (2010). Change detection of building footprints from airborne laser scanning acquired in short time intervals. In Wagner, W. and Székely, B., editors, The International Archives of the Photogrammetry, Remote Sensing and Spatial Information Sciences, volume XXXVIII-7B of ISPRS Technical Commission VII Symposium, '100 Years ISPRS - Advancing Remote Sensing Science', pages 475–480, Vienna, Austria.
- Schmidt, A., Rottensteiner, F., and Sörgel, U. (2011). Detection of water surfaces in full-waveform laser scanning data. In International Archives of Photogrammetry, Remote Sensing and Spatial Information Sciences, volume XXXVIII-4/W19, page 6, Hannover.
- Schmitt, T., Mitchell, N. C., and S., R. A. T. (2008). Characterizing uncertainties for quantifying bathymetry change between time-separated multibeam echosounder surveys. Continental Shelf Research, 28(9):1166–1176.
- Schmugge, T. J., Kustas, W. P., Ritchie, J. C., Jackson, T. J., and Rango, A. (2002). Remote sensing in hydrology. Advances in Water Resources, 25(8-12):1367–1385.
- Schumann, G., Hostache, R., Puech, C., Hoffmann, L., Matgen, P., Pappenberger, F., and Pfister, L. (2007). High-Resolution 3-D Flood Information From Radar Imagery for Flood Hazard Management. IEEE Transactions on Geoscience and Remote Sensing, 46(6):1715–1725.
- Sithole, G. and Vosselman, G. (2004). Experimental comparison of filter algorithms for bare-Earth extraction from airborne laser scanning point clouds. ISPRS Journal of Photogrammetry and Remote Sensing, 59(1-2):85–101.

- Sofia, G., Tarolli, P., Cazorzi, F., and Dalla Fontana, G. (2011). An objective approach for feature extraction: distribution analysis and statistical descriptors for scale choice and channel network identification. Hydrology and Earth System Sciences, 15(5):1387–1402.
- Straatsma, M. and Baptist, M. (2008). Floodplain roughness parameterization using airborne laser scanning and spectral remote sensing. Remote Sensing of Environment, 112(3):1062–1080.
- Straatsma, M., Warmink, J., and Middelkoop, H. (2008). Two novel methods for field measurements of hydrodynamic density of floodplain vegetation using terrestrial laser scanning and digital parallel photography. ISPRS Journal of Photogrammetry and Remote Sensing, 29(5):1595–1617.
- Székely, B., Zamolyi, A., Draganits, E., and Briese, C. (2009). Geomorphic expression of neotectonic activity in a low relief area in an Airborne Laser Scanning DTM: A case study of the Little Hungarian Plain (Pannonian Basin). Tectonophysics, 474(1-2):353–366.
- Terrasolid (2012). Users Guide. Technical report, Terrasolid, www.terrasolid.fi (07-08-2012).
- Thiel, K. and Wehr, A. (2004). Performance capabilities of laser scanners – an overview and measurement principle analysis. In Proceedings of the ISPRS working group VIII/2, Laser-Scanners for Forest and Landscape Assessment, volume XXXVI-8/W2, pages 14–18.
- Ustin, S. L. (2004). Remote Sensing for Natural Resources Management and Environmental Monitoring, volume 4 of Manual of Remote Sensing, chapter Rivers and Lakes, pages 345–400. American Society for Photogrammetry and Remote Sensing, 3 edition.
- Vetsch, D., Rousselot, P., and Fäh, R. (2011). Flussgebietsmodellierung mit der Simulationssoftware BASEMENT. Wasser Energie Luft, 103(4):313–319.
- Vetter, M. (2008). Punktwolkenbasierte Ableitung von Wasseroberflächen aus Airborne Laser Scanning Daten - Unter Verwendung von Radiometrie- und Geometriattributen. Master's thesis, Institut für Geographie, Universität Innsbruck.
- Vetter, M., Höfle, B., Hollaus, M., Gschöpf, C., Mandlbürger, G., Pfeifer, N., and Wagner, W. (2011a). Vertical vegetation structure analysis and hydraulic roughness determination using dense ALS point cloud data – a voxel based approach.

- In Lichti, D. and Habib, A., editors, International Archives of Photogrammetry, Remote Sensing and Spatial Information Sciences, volume XXXVIII-5/W12, pages 265–270, Calgary, Canada.
- Vetter, M., Höfle, B., Mandlbürger, G., and Rutzinger, M. (2008). Ableitung von Flusssohlenmodellen aus Flussquerprofilen und Integration in Airborne Laser-scanning Geländemodelle mit GRASS GIS. In Angewandte Geoinformatik 2008, Beiträge zum 20. AGIT-Symposium, pages 382–391, Salzburg.
- Vetter, M., Höfle, B., Pfeifer, N., Rutzinger, M., Sailer, R., Stötter, J., and Geist, T. (2009a). The Hintereisferner - eight years of experience in method development for glacier monitoring with airborne LiDAR. In Geophysical Research Abstracts, volume 11, Vienna, Austria.
- Vetter, M., Höfle, B., and Rutzinger, M. (2009b). Water classification using 3D airborne laser scanning point clouds. Österreichische Zeitschrift für Vermessung & Geoinformation, 97(2):227–238.
- Vetter, M., Höfle, B., Rutzinger, M., and Mandlbürger, G. (2011b). Estimating changes of riverine landscapes and riverbeds by using airborne LiDAR data and river cross-sections. Zeitschrift für Geomorphologie/Annals of Geomorphology, 55(2):51–65.
- Vetter, M., Jochem, A., Franke, M., Werthmann, M., and Schöberl, F. (2009c). Auswirkung der Geländemodellauflösung auf Hochwassermodellierungen. In Angewandte Geoinformatik 2009, Beiträge zum 21. AGIT-Symposium, Salzburg.
- Vetter, M. and Mandlbürger, G. (2013). Conditioning of high resolution airborne laser scanning data for drainage network delineation. Journal of photogrammetry, remote sensing and geoinformation processing, page 10. Submitted in January 2013.
- Vianello, A., Cavalli, M., and Tarolli, P. (2009). Lidar-derived slopes for headwater channel network analysis. CATENA, 76(2):97–106.
- Vosselman, G. (2003). 3-D Reconstruction of Roads and Trees for City Modelling. In International Archives of Photogrammetry, Remote Sensing and Spatial Information Sciences, volume XXXIV-3/W13, pages 231–236, Dresden, Germany.
- Wagner, W. (2010). Radiometric Calibration of Small-Footprint Full-Waveform Airborne Laser Scanner Measurements: Basic Physical Concepts. ISPRS Journal of Photogrammetry and Remote Sensing, 65(6):505–513.

- Wagner, W., Hyypä, J., Ullrich, A., Lehner, H., Briese, C., and Kaasalainen, S. (2008). Radiometric calibration of full-waveform small-footprint airborne laser scanners. In International Archives of Photogrammetry, Remote Sensing and Spatial Information Sciences, volume XXXVII-B1, pages 163–168.
- Wagner, W., Ullrich, A., and Briese, C. (2003). Der Laserstrahl und seine Interaktion mit der Erdoberfläche. Österreichische Zeitschrift für Vermessung & Geoinformation, 91(4):223–235.
- Wagner, W., Ullrich, A., Ducic, V., Melzer, T., and Studnicka, N. (2006). Gaussian decomposition and calibration of a novel small-footprint full-waveform digitising airborne laser scanner. ISPRS Journal of Photogrammetry and Remote Sensing, 60(2):100–112.
- Wagner, W., Ullrich, A., Melzer, T., Briese, C., and Kraus, K. (2004). From Single-Pulse to Full-Waveform airborne laser scanners potential and practical challenges. In International Archives of Photogrammetry, Remote Sensing and Spatial Information Sciences, volume XXXV-B/3, pages 201–206, Istanbul, Turkey.
- Wagner, W., Vetter, M., and Bartsch, A. (2011). Novel Microwave- and Lidar Remote Sensing Techniques for Monitoring of In-Land Water Resources. In acatech Materialien Nr.7, page 42. acatech - Deutsche Akademie der Technikwissenschaften.
- Wehr, A. and Lohr, U. (1999). Airborne laser scanning-an introduction and overview. Photogrammetrie, Fernerkundung und Geoinformation, 54(2-3):68–82.
- Wichmann, V., Rutzinger, M., and Vetter, M. (2008). Digital terrain model generation from airborne laser scanning point data and the effect of grid-cell size on the simulation results of a debris flow model. In Böhner, J., Blaschke, T., and Montanarella, L., editors, SAGA-Second Out, number 19 in Hamburger Beiträge zur Physischen Geographie und Landschaftsökologie, pages 103–113, Hamburg, Germany.
- Wilson, J., Aggett, G., Deng, Y., and Lam, C. (2008). Advances in Digital Terrain Analysis, chapter Water in the landscape: a review of contemporary flow routing algorithms, pages 213–236. Springer.
- Wolfe, W. L. and Zissis, G. J. (1989). The infrared handbook. The Infrared Information Analysis Center. Environmental Research Institute of Michigan.

Wood, J. D. (1996). The geomorphological characterisation of digital elevation models. PhD thesis, University of Leicester, United Kingdom.

Yu, A., Krainak, M., Harding, K., Abshire, J., and Sun, X. (2010). A spaceborne lidar for high-resolution topographic mapping of the Earth's surface. In SPIE Newsroom, page 3.

Curriculum vitae



Michael Vetter

birth	17 th July 1977, Lustenau, Austria
citizenship	Austria
1983–1992	Primary and secondary school in Lustenau
1992–1995	Journeyman’s education and examination in painting, Lustenau
1996–1997	Military service in the military band (drums), Bregenz
1999	Master craftsman’s certificate in painting and management certification, Feldkirch
2001–2003	School leaving examination (Berufsreifeprüfung), Bregenz
2003–2008	Studies of Geography at the University of Innsbruck
2005–2008	Tutor and project staff at the University of Innsbruck
2007–2008	Diploma thesis: ‘Punktwolkenbasierte Ableitung von Wasseroberflächen aus Airborne Laser Scanning Daten – Unter Verwendung von Radiometrie- und Geometrieattributen’, Innsbruck
2008	Graduated as ‘Magister der Naturwissenschaften, (Mag.rer.nat)’
2008–2009	Scientific project staff at the University of Innsbruck
2009–2013	PhD student within the ‘Vienna Doctoral Programme on Water Resource Systems’, Vienna University of Technology, Vienna
2010–2012	Scientific project staff at the Vienna University of Technology